MIT LIBRARIES
3 9080 01585 2020

THERMAL Management of Microelectronic Equipment

Heat Transfer Theory, Analysis Methods, and Design Practices

Lian-Tuu Yeh and Richard C. Chu

ASME Press Book Series on Electronic Packaging
Dereje Agonafer, Editor-in-Chief

SEC et al. v. MRI
SEC Exhibit 1018.0001
IPR2023-00254

Yeh
Chu

Thermal Management of Microelectronic Equipment

Heat Transfer Theory, Analysis Methods, and Design Practices

TK7870
.25
.Y44
2002

SEC et al. v. MRI
SEC Exhibit 1018.0002
IPR2023-00254

TK 7870.25
.Y44
2002

Copyright © 2002
The American Society of Mechanical Engineers
Three Park Ave., New York, NY 10016

All rights reserved. Printed in the United States of America. Except as permitted under the United States Copyright Act of 1976, no part of this publication may be reproduced or distributed in any form or by any means, or stored in a database or retrieval system, without the prior written permission of the publisher.

Statement from By-Laws: *The Society shall not be responsible for statements or opinions advanced in papers . . . or printed in its publications* (B7.1.3)

INFORMATION CONTAINED IN THIS WORK HAS BEEN OBTAINED BY THE AMERICAN SOCIETY OF MECHANICAL ENGINEERS FROM SOURCES BELIEVED TO BE RELIABLE. HOWEVER, NEITHER ASME NOR ITS AUTHORS OR EDITORS GUARANTEE THE ACCURACY OR COMPLETENESS OF ANY INFORMATION PUBLISHED IN THIS WORK. NEITHER ASME NOR ITS AUTHORS AND EDITORS SHALL BE RESPONSIBLE FOR ANY ERRORS, OMISSIONS, OR DAMAGES ARISING OUT OF THE USE OF THIS INFORMATION. THE WORK IS PUBLISHED WITH THE UNDERSTANDING THAT ASME AND ITS AUTHORS AND EDITORS ARE SUPPLYING INFORMATION BUT ARE NOT ATTEMPTING TO RENDER ENGINEERING OR OTHER PROFESSIONAL SERVICES. IF SUCH ENGINEERING OR PROFESSIONAL SERVICES ARE REQUIRED, THE ASSISTANCE OF AN APPROPRIATE PROFESSIONAL SHOULD BE SOUGHT.

For authorization to photocopy material for internal or personal use under circumstances not falling within the fair use provisions of the Copyright Act, contact the Copyright Clearance Center (CCC), 222 Rosewood Drive, Danvers, MA 01923, Tel: 978-750-8400, www.copyright.com.

Library of Congress Cataloging-in-Publication Data

Yeh, L.-T. (Lian-Tuu), 1944-
Thermal management of microelectronic equipment: heat transfer theory, analysis methods, and design practices / L.-T. Yeh and R. C. Chu.
p. cm.
ISBN 0-7918-0168-3
1. Electronic apparatus and appliances – Cooling. 2. Electronic apparatus and appliances – Thermal properties. 3. Heat – Transmission. I. Chu, R. C. (Richard C.), 1933. II. Title.

TK7870.25.Y44 2002
621.381'04 – dc21

2001034086

...I. LIBRARIES
OCT 15 2002
RECEIVED

SEC et al. v. MRI
SEC Exhibit 1018.0003
IPR2023-00254

TABLE OF CONTENTS

List of Figures xi
List of Tables xvii
Nomenclature xix
Foreword xxiii
Preface xxv

Chapter 1 Introduction 1
1.1 Need for Thermal Control 1
1.2 Reliability and Temperature 3
1.3 Levels of Thermal Resistance 4
1.4 Thermal Design Considerations 5
1.5 Optimization and Life-Cycle Cost 6

Chapter 2 Conduction 9
2.1 Fundamental Law of Heat Conduction 9
2.2 General Differential Equations for Conduction 10
2.3 One-Dimensional Heat Conduction 16
2.4 Thermal/Electrical Analogy 17
2.5 Lumped-System Transient Analysis 20
2.6 Heat Conduction with Phase Change 25

SEC et al. v. MRI
SEC Exhibit 1018.0004
IPR2023-00254

Chapter 3 Convection **31**

3.1 Flow and Temperature Fields 31
3.2 Heat Transfer Coefficient 34
3.3 Parameter Effects on Heat Transfer 35
3.4 Pressure Drop and Friction Factor 43
3.5 Thermal Properties of Fluids 46
3.6 Correlations for Heat Transfer and Friction 47

CHAPTER 4 RADIATION **53**

4.1 Stefan-Boltzmann Law 53
4.2 Kirchhoff's Law and Emissivity 54
4.3 Radiation Between Black Isothermal Surfaces 55
4.4 Radiation Between Gray Isothermal Surfaces 58
4.5 Extreme Climatic Conditions 61

Chapter 5 Pool Boiling **67**

5.1 Boiling Curve 67
5.2 Nucleate Boiling 70
5.3 Incipient Boiling at Heating Surfaces 72
5.4 Nucleate Boiling Correlations 76
5.5 Critical Heat Flux Correlations 77
5.6 Minimum Heat Flux Correlations (Leidenforst Point) 79
5.7 Parameters Affecting Pool Boiling 81
5.8 Effect of Gravity on Pool Boiling 87

Chapter 6 Flow Boiling **95**

6.1 Flow Patterns 95
6.2 Heat Transfer Mechanisms 95
6.3 Boiling Crisis 98
6.4 Heat Transfer Equations 99
6.5 Thermal Enhancement 109
6.6 Pressure Drop 109

SEC et al. v. MRI
SEC Exhibit 1018.0005
IPR2023-00254

Chapter 7 Condensation 115

7.1 Modes of Condensation 115
7.2 Heat Transfer in Filmwise Condensation 116
7.3 Improvements Over Nusselt Analysis 121
7.4 Condensation Inside a Horizontal Tube 123
7.5 Noncondensable Gas in a Condenser 127

Chapter 8 Extended Surfaces 131

8.1 Uniform–Cross Section Fins 131
8.2 Fin Efficiency 134
8.3 Selection and Design of Fins 137

Chapter 9 Thermal Interface Resistance 141

9.1 Factors Affecting Thermal Contact Resistance 141
9.2 Joint Thermal Contact Resistance 145
9.3 Methods of Reducing Thermal Contact Resistance 147
9.4 Solder and Epoxy Joints 159
9.5 Practical Design Data 160

Chapter 10 Components and Printed Circuit Boards 169

10.1 Chip Packaging Technology 169
10.2 Chip Package Thermal Resistance 172
10.3 Chip Package Attachment 173
10.4 Board-Cooling Methods 176
10.5 Board Thermal Analysis 177
10.6 Equivalent Thermal Conductivity 178

Chapter 11 Direct Air Cooling and Fans 185

11.1 Previous Work 185
11.2 Heat Transfer Correlations 187
11.3 Pressure Drop Correlations 190
11.4 Heat Transfer Enhancement 194
11.5 Fans and Air-Handling Systems 197

SEC et al. v. MRI
SEC Exhibit 1018.0006
IPR2023-00254

Chapter 12 Natural and Mixed Convection 213

12.1 Parallel Plates 214
12.2 Straight-Fin Arrays 220
12.3 Pin-Fin Arrays 229
12.4 Enclosures 234
12.5 Mixed Convection in Vertical Plates 237

Chapter 13 Heat Exchangers and Cold Plates 243

13.1 Compact Heat Exchangers 243
13.2 Flow Arrangement of Heat Exchangers 244
13.3 Overall Heat Transfer Coefficient 244
13.4 Heat Exchanger Effectiveness 245
13.5 Heat Exchanger Analysis 246
13.6 Heat Transfer and Pressure Drop 248
13.7 Geometric Factors 250
13.8 Cold-Plate Analysis 251
13.9 Correlations 255

Chapter 14 Advanced Cooling Technologies I: Single-Phase Liquid Cooling 261

14.1 Coolant Selection 261
14.2 Natural Convection 265
14.3 Forced Convection 267

Chapter 15 Advanced Cooling Technologies II: Two-Phase Flow Cooling 283

15.1 Figure of Merit 283
15.2 Direct-Immersion Cooling 285
15.3 Enhancement of Pool Boiling 287
15.4 Flow Boiling 300

Chapter 16 Heat Pipes 309

16.1 Operation Principles 309
16.2 Useful Characteristics 309

SEC et al. v. MRI
SEC Exhibit 1018.0007
IPR2023-00254

16.3 Construction 311
16.4 Operation Limits 312
16.5 Materials Compatibility 318
16.6 Operating Temperatures 320
16.7 Operation Methods 321
16.8 Thermal Resistances 323
16.9 Applications 325
16.10 Micro Heat Pipes 330

Chapter 17 Thermoelectric Coolers 335

17.1 Basic Theories of Thermoelectricity 335
17.2 Net Thermoelectric Effect 337
17.3 Figure of Merit 338
17.4 Operation Principles 339
17.5 System Configurations 339
17.6 Performance Analysis 340
17.7 Practical Design Procedure 344

Appendices 349

A. Material Thermal Properties 349
B. Thermal Conductivity of Silicon and Gallium Arsenide 351
C. Properties of Air, Water, and Dielectric Fluids 353
D. Typical Emissivities of Materials 371
E. Solar Absorptivities and Emissivities of Common Surfaces 373
F. Properties of Phase-Change Materials 375
G. Friction Factor Correlations 377
H. Heat Transfer Correlations 381
I. Units Conversion Table 403

Index 405

About the Authors 413

SEC et al. v. MRI
SEC Exhibit 1018.0008
IPR2023-00254

Chapter 1

INTRODUCTION

Electronics are the heart of any modern equipment. Thermal control of electronic equipment has long been one of the major areas of application of heat transfer technologies. Many improvements in reliability, power density, and physical miniaturization of electronic equipment over the years can be attributed in part to improved thermal analysis and design of systems. Improved thermal design has been made possible through advances in heat transfer technologies as well as computational methods and tools.

The primary function of cooling systems for electronic equipment is to provide an acceptable thermal environment in which the equipment can operate. To achieve this goal, it is necessary to maintain a thermal path with a minimum resistance from equipment heat sources to the ultimate heat sink.

1.1 NEED FOR THERMAL CONTROL

Because of advances in circuit and component technologies, electric circuits have become more efficient, and thus heat dissipation from individual devices such as transistors has also become less. Miniaturization of circuits greatly decreases the size of individual devices, however, and increases the number of such devices that can be integrated on a single chip. The net result is that the chip heat flux (heat flow per unit surface area) has significantly increased in recent decades as chip development has moved from small-scale integration (SSI) to very large-scale integration (VLSI), and further to ultra-large-scale integration (ULSI). The chronology of advances in the integrated circuit (IC) is outlined in the following steps, with the trends shown in Figure 1.1.

1960—Small-scale integration (SSI), fewer than 100 devices per chip
1966—Medium-scale integration (MSI), fewer than 1000 devices per chip
1969—Large-scale integration (LSI), fewer than 10,000 devices per chip
1975—Very-large-scale integration (VLSI), fewer than 10^7 devices per chip
1990—Ultra-large-scale integration (ULSI), more than 10^7 devices per chip

Decreasing the temperature of a component increases its performance as well as its reliability. In addition to lowering the junction temperatures within a

SEC et al. v. MRI
SEC Exhibit 1018.0009
IPR2023-00254

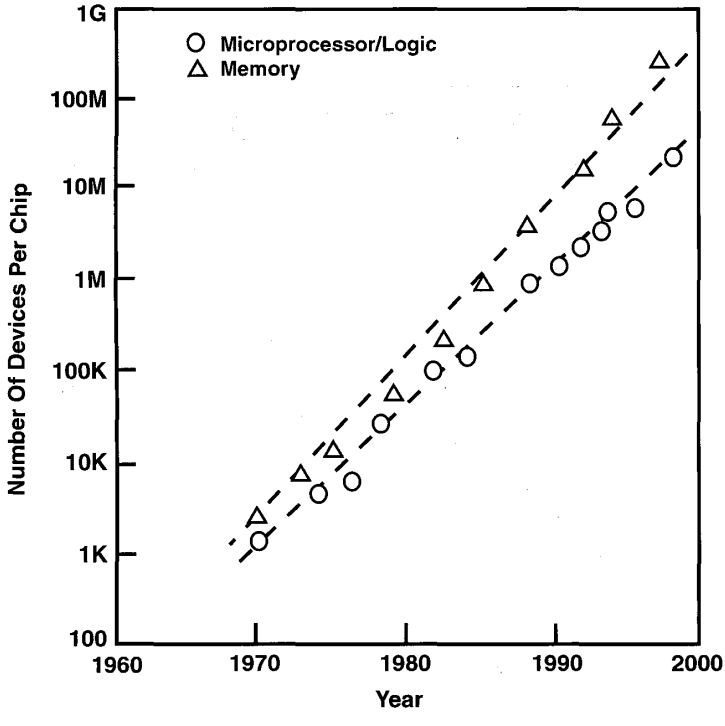

FIGURE 1.1 Increase in circuit complexity.

component, it is sometimes also important to reduce the temperature variation between components that are electronically connected in order to obtain optimum performance. Thermal considerations become an important part of electronic equipment because of increased heat flux.

An increased demand on system performance and reliability also intensifies the need for good thermal management of electronic equipment. Further evidence of the importance of thermal management to electronic systems is shown in Figure 1.2, based on a survey by the U.S. Air Force and indicating that more than 50% of all electronics failures are caused by shortcomings in temperature control [1].

Although a great deal of attention has recently been paid to high-heat-flux systems, the opportunity also exists to improve thermal performance and reliability in low-heat-flux equipment. Therefore, the challenge in the field of thermal management of electronic equipment resides not only with very-high-performance (high-heat-dissipation) devices, but also with intermediate- and

SEC et al. v. MRI
SEC Exhibit 1018.0010
IPR2023-00254

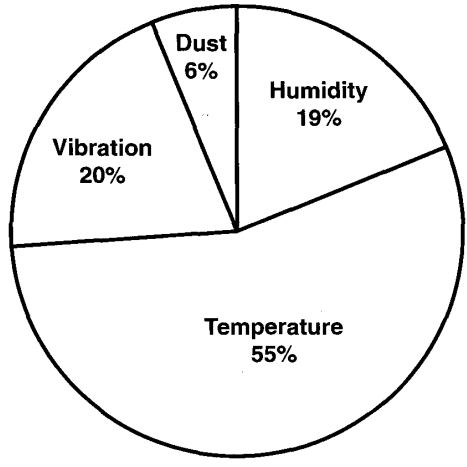

FIGURE 1.2 Major causes of electronics failures [1].

lower-power components where improved reliability objectives require cooler operation of chips.

1.2 RELIABILITY AND TEMPERATURE

Reliability—that is, the reciprocal of the mean time between failures (MTBF)—is described as the statistical probability that a device or system will operate without failure for a specific time period. Each component or device has its failure rate curve. The reliability of a system is determined by combining many individual part failure rates in series and/or parallel. System reliability is also affected by the relative importance of the individual part to the system, and it can be improved by redundancy at the component, packaging, or system level.

Table 1 lists the possible effect of temperature on the part failure under various thermal conditions such as thermal shock, temperature under continuous operation (steady state), and temperature cycling. In the temperature range specific to electronic equipment, it is an established fact that the reliability of electronics is a strongly inverse function (a near exponential dependency) of a component's temperature. The reliability of a silicon chip is decreased by about 10% for every 2°C of temperature rise [2]. A typical temperature limit for a silicon chip is 125°C; however, a much lower design limit is commonly sought to maintain the desired reliability, especially in military products.

The component failure rate is also related to temperature cycling, which results from either device power cycling or cycling of environmental conditions. In a U.S. Navy–sponsored study [3], an eightfold increase in failure rate was

SEC et al. v. MRI
SEC Exhibit 1018.0011
IPR2023-00254

Table 1.1 Effect of Thermal Conditions on Part Failure

Condition	Cause	Effect	Possible failure
Steady-state (hot)	Ambient exposure, equipment-induced	Aging—discoloration Insulation deterioration Oxidation Expansion Viscosity decrease Softening/hardening Evaporation/drying Chemical changes	Alteration of properties Shorting Rust Physical damage, increased wear Loss of lubrication Physical breakdown Dielectric loss
Steady-state (cold)	Ambient exposure, mission-induced	Contraction Viscosity increase Embrittlement Ice formation	Wear, structural failure, binding Loss of lubricity Structural failure, cracked parts Alteration of electric properties Loss of resilience—seal leaks
Thermal cycling	Ambient-induced, mission operation	Temperature gradients Expansion/contraction	Mechanical failure of parts, solder joints, and connections Delimitation of bonding line
Thermal shock	Mission profile	High temperature gradients	Mechanical failure, cracks, rupture

encountered in equipment subjected to a deliberate temperature cycling of more than 20°C.

1.3 LEVELS OF THERMAL RESISTANCE

The *component-level resistance*, which is often referred to as a component's *internal resistance,* is defined as the thermal resistance from the device junction (heat source) to some predetermined reference point on the outside surface of the component or package. In most component assemblies, heat must be transferred through a number of different materials and interfaces. The total thermal resistance is the sum of several individual resistances in series and/or parallel. The primary heat transfer mode inside the component or package is conduction. In well-designed component packaging, the number of interfaces should be minimized, and bonding and sealing operations should also be selected to create the lowest interface resistance. The coefficient of thermal expansion (CTE) is a major concern at the interfaces of all materials laminated together. Any mismatch of the coefficient of thermal expansion would increase the thermal resistance, and even

SEC et al. v. MRI
SEC Exhibit 1018.0012
IPR2023-00254

cause part failure. Note that the thermal designer may have no control over the internal resistance if commercial components are used.

The *packaging-level resistance* is generally defined as the thermal resistance from the aforementioned surface reference point (the terminal point for measuring component-level resistance) to some designated point in a convective stream. For example, this designated point may be the local air temperature over a given component or the local fluid or wall temperature of a cold plate.

The *system-level resistance* is defined as the thermal resistance from the designated terminal point for measuring the packaging-level resistance to the ultimate heat sink of the equipment or system. The ultimate heat sink is the environment in which the system operates. Sometimes, the combined resistance of packaging and system levels is referred to as the *external thermal resistance*.

The foregoing definitions are somewhat arbitrary; however, they give an insight into the contribution of each level of resistance to the total resistance of a system, and thus provide thermal engineers an opportunity to optimize the overall thermal resistance by working at the individual levels.

1.4 THERMAL DESIGN CONSIDERATIONS

Thermal control of electronic equipment may employ several different heat transfer modes simultaneously and may consist of up to three tasks: (1) removing heat from the sources (components), (2) transporting heat to system internal heat sinks, and (3) rejecting heat from the internal heat sinks to the ultimate heat sink, the environment. Sometimes, tasks 2 and 3 are lumped into a single task.

The purpose of a thermal design is to provide equipment that will induce thermal energy to flow properly from heat sources to the ultimate heat sinks. The goal of thermal control is to prevent part failures and also to achieve desired system performance and reliability. Another goal of thermal control is to obtain an optimum design. The optimum system will result from a series of trade-off studies considering several factors:

1. *Performance*. The primary and foremost consideration is that the system must be able to perform its required functions and the specific tasks for which it is designed.
2. *Producibility*. The system under consideration must be producible without involving a very complicated manufacturing process.
3. *Serviceability (or maintainability)*. The equipment under design must be readily and easily accessible for testing, repair, or replacement. The design approach may also be affected by the system maintenance methods—e.g., whether the equipment will be maintained in the field or in the shop.
4. *Compatibility*. The system, including the coolant used, must be compatible with the environment in which it is being used.
5. *Cost*. The final product must be cost-effective. Cost may be the most important factor in product design. In determining the cost of a product, one should consider not only manufacturing but also maintenance costs.

SEC et al. v. MRI
SEC Exhibit 1018.0013
IPR2023-00254

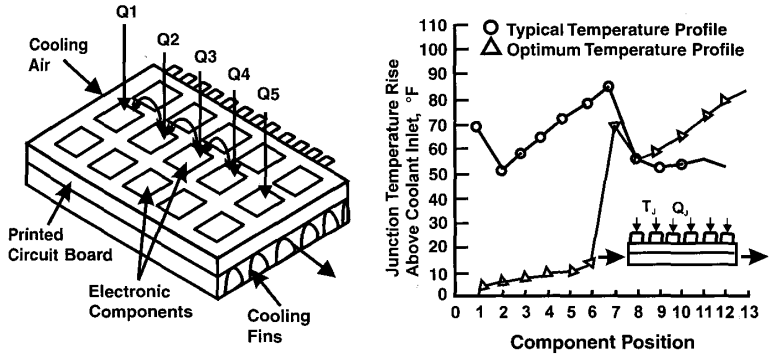

FIGURE 1.3 Effect of part placement on component junction temperature.

The relative importance of these five individual factors is mission-related; for example, the cost may become a secondary issue for some military equipment, where performance and reliability are the major concerns. A concurrent engineering approach must be adopted in the development of a new product. The design philosophy or basic rule is that the best design is the simplest and lowest-cost one that will meet the specified requirements.

1.5 OPTIMIZATION AND LIFE-CYCLE COST

Because of the strong dependence of microelectronic device reliability on temperature, it is important and desirable in the thermal management of electronic systems to pursue temperature distributions that are not merely acceptable but are optimal. Mayer [4] discusses the opportunities for optimization at all packaging levels. These opportunities include (1) optimal thermal placement of electronic components on circuit boards and optimal arrangement of boards within boxes or assemblies, and (2) optimal distribution of thermally conductive layers and optimal distribution of coolant flow rates. As an example of the first type, Figure 1.3 compares junction temperatures with and without optimization at different component positions on a printed circuit board cooled by forced-air convection. The left diagram in the figure is for the purpose of illustration and does not include all components. By switching component locations, a significant improvement in overall temperature (near 40°F reduction for half of the components) is found with optimization, even though the maximum temperature is about the same for both cases. This in turn improves the overall system reliability.

It is important to involve thermal design in the early phase of the equipment design process. The design approach should place emphasis at the system level for optimizing the thermal control unit. However, since for most electronics there

SEC et al. v. MRI
SEC Exhibit 1018.0014
IPR2023-00254

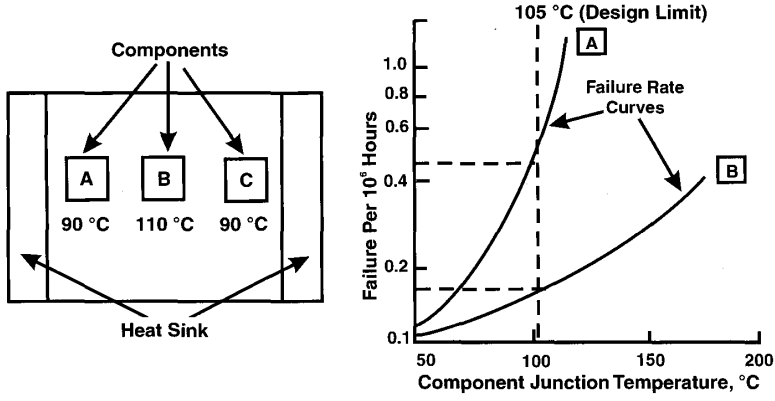

FIGURE 1.4 Example of current thermal design practice.

is a direct relationship between a component's junction temperature and its failure rate, the current design practice is often to establish an upper temperature limit that is below the maximum allowable temperature set by manufacturers, ensuring that no component junction temperatures exceed this temperature limit. Currently, an upper limit of 105°C for semiconductor devices is being used by the U.S. Air Force and Navy [4, 5]. In theory, the actual temperature limit should be determined by the required reliability of each individual piece of equipment.

As pointed out by Berger [6], the problem with this temperature limit design approach stems from the attempt to analyze the reliability of equipment by looking at the individual components in terms of their temperature rather than their actual part failure rate. The goal should not be to minimize component temperatures but to minimize component failure rates that directly impact the reliability of the equipment.

A simplified example given by Berger as shown in Figure 1.4 illustrates the preceding statement. Component B, in the center of the layout diagrammed in the figure, is at 110°C and thus is the hottest component. A redesign is in order, to get the temperature of all parts below 105°C, if that particular standard is to be applied. One of the simplest ways to redesign is just to switch component B with component A at left, thereby placing the hot component close to the heat sink. Acceptable design criteria would be met under the standard if components A and B both turned out to be at 100°C. The graph in the figure reveals, however, that the increase in the failure rate of component A for a 10°C rise outweighs the benefits obtained for a 10°C reduction in temperature for component B. The mandated redesign actually results in a reduction of the overall reliability of the equipment. Any design change, therefore, should not be initiated unless it will be an overall improvement in equipment reliability and the change can also be justified on the basis of a system life-cycle cost (LCC) reduction. In short, the equip-

SEC et al. v. MRI
SEC Exhibit 1018.0015
IPR2023-00254

ment design should be thermally optimized to minimize the LCC and maximize the reliability and operation life of the system.

REFERENCES

1. U.S. Air Force Avionics Integrity Program (AVIP) notes, 1989.
2. A. Bar-Cohen, A. D. Kraus, and S. F. Davidson, "Thermal Frontiers in the Design and Packaging of Microelectronic Equipment," *Mech. Eng.,* June 1983.
3. W. F. Hilbert and F. H. Kube, "Effects on Electronic Equipment Reliability of Temperature Cycling in Equipment," Report No. EC-69-400 (Final Report), Grumman Aircraft Corp., Bethpage, NY, February 1969.
4. A. H. Mayer, "Opportunities for Thermal Optimization in Electronics Packaging," *Proc. 1st Int. Electronics Packaging Soc. Conf.,* 1981.
5. "Thermal Design, Analysis, and Test Procedures for Airborne Electronic Equipment," MIL-STD-2218, 1987.
6. R, L. Berger, "A System Approach—Minimizing Avionics Life-Cycle Cost," SAE Technical Paper Series 831107, *13th Intersociety Conf. on Environmental Systems,* San Francisco, 1983.
7. L. T. Yeh, "Future Thermal Design and Management of Electronic Equipment," in Wei-Jei Yang and Yasuo Mori, eds., *Heat Transfer in High Technology and Power Engineering,* Hemisphere, New York, 1987.
8. A. D. Kraus, *Cooling Electronic Equipment,* Prentice-Hall, Englewood Cliffs, NJ, 1965.
9. J. H. Seely and R. C. Chu, *Heat Transfer in Microelectronic Equipment: A Practical Guide,* Marcel Dekker, New York, 1972.
10. A. W. Scott, *Cooling of Electronic Equipment,* Wiley, New York, 1974.
11. D. S. Steinberg, *Cooling Techniques for Electronic Equipment,* Wiley, New York, 1980.
12. A. D. Kraus and A. Bar-Cohen, *Thermal Analysis and Control of Electronic Equipment,* Hemisphere, New York, 1983.
13. G. N. Ellison, *Thermal Computation for Electronic Equipment,* Van Nostrand Reinhold, New York, 1984.
14. L. T. Yeh, "Review of Heat Transfer Technologies in Electronic Equipment," *J. Electronic Packaging* 117, 1995.
15. M. Pecht, "Why the Traditional Reliability Prediction Models Do Not Work—Is There an Alternative?" *Electronics Cooling* 2(1), 1996.

SEC et al. v. MRI
SEC Exhibit 1018.0016
IPR2023-00254

Chapter 2

CONDUCTION

Heat conduction is a process by which heat flows from a region of higher temperature to a region of lower temperature through a solid, liquid, or gaseous medium, or between different media in intimate contact. Generally, heat conduction is due to movement and interaction of molecules. Therefore, a solid is superior to a liquid in transferring heat by conduction because of its shorter distance between molecules. Similarly, a liquid has better thermal conduction characteristics than a gas. Generally, a good conductor of electricity is also a good conductor of heat.

2.1 FUNDAMENTAL LAW OF HEAT CONDUCTION

The fundamental law of heat conduction is attributed to Fourier [1], who stated that the rate of heat conduction in a medium is proportional to the product of the area normal to the path and the temperature gradient along the path. Mathematically, the Fourier law for the one-dimensional case can be expressed as follows:

$$q \propto -A\frac{dT}{dx} \tag{2.1}$$

where q is the heat transfer rate, A is the area normal to the heat flow path, and dT is the temperature gradient over the distance dx. The negative sign is assigned to allow a positive heat flow when the temperature decreases along the path. With an insertion of a proportionality constant, Equation 2.1 becomes

$$q = -kA\frac{dT}{dx} \tag{2.2}$$

where k is the proportionality constant, also referred to as the *thermal conductivity* of the medium.

Thermal conductivity is a material property. The thermal conductivity of gases is an order of magnitude smaller than that of liquids, and likewise that of liquids is an order of magnitude smaller than that of solids. Thermal conductivity of

SEC et al. v. MRI
SEC Exhibit 1018.0017
IPR2023-00254

materials within a limited temperature range is generally a function of temperature and can be approximately expressed in the form

$$k(T) = k_0(1+\beta T) \tag{2.3}$$

where k_0 is the thermal conductivity of a medium at $T = 0$ °F and β is the temperature coefficient of thermal conductivity. Generally, the value of β is negative for most pure metals and is positive for most alloys, gases, and liquids with an exception in high temperature ranges for some alloys and liquids.

2.2 GENERAL DIFFERENTIAL EQUATIONS FOR CONDUCTION

With the aid of Fourier's law along with the assumption of energy balance on a differential element of a solid, the general differential equations of heat conduction can be developed. Without including the detailed derivations, which are available in most textbooks, we can show the general differential equation for heat conduction as

$$\frac{\partial}{\partial x}\left(k_x \frac{\partial T}{\partial x}\right)+\frac{\partial}{\partial y}\left(k_y \frac{\partial T}{\partial y}\right)+\frac{\partial}{\partial z}\left(k_z \frac{\partial T}{\partial z}\right)+q''' = \rho c \frac{\partial T}{\partial t} \tag{2.4}$$

where the internal heat generation and thermal conductivity can be functions of time, space, and temperature. With proper initial and boundary conditions, the differential equation can be solved analytically or numerically.

For the case with constant thermal properties, Equation 2.4 can be simplified to the form

$$\frac{\partial^2 T}{\partial x^2}+\frac{\partial^2 T}{\partial y^2}+\frac{\partial^2 T}{\partial z^2}+\frac{q'''}{k} = \frac{1}{\alpha}\frac{\partial T}{\partial t} \tag{2.5}$$

where α (= $k/\rho c$) is thermal diffusivity, which represents an approximate measure of the ratio of heat conducted to heat stored.

Equation 2.5 can further be reduced under the following assumptions:

Fourier equation (no internal heat generation):

$$\frac{\partial^2 T}{\partial x^2}+\frac{\partial^2 T}{\partial y^2}+\frac{\partial^2 T}{\partial z^2} = \frac{1}{\alpha}\frac{\partial T}{\partial t} \tag{2.6a}$$

Poisson equation (steady state):

$$\frac{\partial^2 T}{\partial x^2}+\frac{\partial^2 T}{\partial y^2}+\frac{\partial^2 T}{\partial z^2}+\frac{q'''}{k} = 0 \tag{2.6b}$$

SEC et al. v. MRI
SEC Exhibit 1018.0018
IPR2023-00254

Laplace equation (no internal heat generation and steady state):

$$\frac{\partial^2 T}{\partial x^2}+\frac{\partial^2 T}{\partial y^2}+\frac{\partial^2 T}{\partial z^2}=0 \tag{2.6c}$$

The above discussions are limited to the Cartesian coordinate system. Again, without going through the detailed derivations, the final form of the general differential equation for heat conduction in cylindrical or spherical solids can be expressed as follows:

For cylindrical systems:

$$\frac{1}{r}\frac{\partial}{\partial r}\left(rk_r\frac{\partial T}{\partial r}\right)+\frac{1}{r^2}\frac{\partial}{\partial \theta}\left(k_\theta\frac{\partial T}{\partial \theta}\right)+\frac{\partial}{\partial z}\left(k_z\frac{\partial T}{\partial z}\right)+q'''=\rho c\frac{\partial T}{\partial t} \tag{2.7}$$

For spherical systems:

$$\frac{1}{r^2}\frac{\partial}{\partial r}\left(r^2k_r\frac{\partial T}{\partial r}\right)+\frac{1}{r^2\,sin^2\,\theta}\frac{\partial}{\partial \theta}\left(k_\theta\frac{\partial T}{\partial \theta}\right)+\frac{1}{r^2\,sin^2\,\phi}\frac{\partial}{\partial \phi}\left(k_\phi\,sin\,\phi\frac{\partial T}{\partial \phi}\right)+q'''=\rho c\frac{\partial T}{\partial t} \tag{2.8}$$

It should be noted that Equations 2.7 and 2.8 can also be obtained from Equation 2.4 through the following transformations with the coordinates given in Figure 2.1:

Cylindrical systems	Spherical systems
$x = r\cos\theta$	$x = r\sin\phi\cos\theta$
$y = r\sin\theta$	$y = r\sin\phi\sin\theta$
$z = z$	$z = r\cos\phi$

The solution to any three-dimensional heat conduction problem is always complicated, even in the steady-state condition. The problem becomes even more complex where multiple heat sources are applied to the top surface of the multilayer structure to simulate heat conduction in microelectronics. The closed-form solution, which is typically expressed by tediously long infinite series either analytically or approximately, is not practical for engineering applications.

The steady-state solution for the simple case where a single heat source is applied to the top surface of a medium was presented in papers by Lindsted and Surty [2] and Kennedy [3] for rectangular and cylindrical solids, respectively. The maximum temperature occurs at the center of the heat source, and its corresponding temperature rise over the isothermal surface can be determined by

$$\Delta T_m = R_m q \tag{2.9}$$

SEC et al. v. MRI
SEC Exhibit 1018.0019
IPR2023-00254

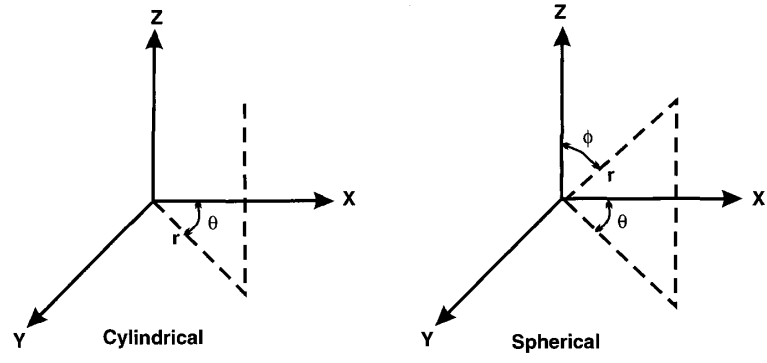

FIGURE 2.1 Cylindrical and spherical coordinates.

where q is heat dissipation and R_m is the maximum thermal resistance. R_m is defined for the two cases as follows:

$$R_m = \begin{cases} \dfrac{\Phi}{k(AB/H)} & \text{rectangular solid} \quad (2.10a) \\ \dfrac{\Phi}{k\pi A} & \text{cylindrical solid} \quad (2.10b) \end{cases}$$

where Φ is the thermal resistance factor, k is the thermal conductivity of the material, and linear dimensions A, B, and H are as listed in Figures 2.2 and 2.3.

Example 2.1

A chip with thermal conductivity of 2 W/(in · °C) dissipates 0.2 W at the junction. The bottom of the chip is assumed to be isothermal. Find the maximum temperature rise in the chip over the isothermal surface for the following cases:

Case I

Chip size: 0.1 by 0.1 by 0.05 in; thus, chip cross-sectional area = 0.01 in^2
Heat source size: 0.005 by 0.005 in; thus, heat input area = 2.5×10^{-5} in^2
Heat source perimeter: 0.02 in, with

- $W = L = 0.1/2 = 0.05$ in
- $A = B = 0.005/2 = 0.0025$ in
- $B/W = 0.0025/0.05 = 0.05$
- $W/H = 0.05/0.05 = 1$
- $A/B = 1$

SEC et al. v. MRI
SEC Exhibit 1018.0020
IPR2023-00254

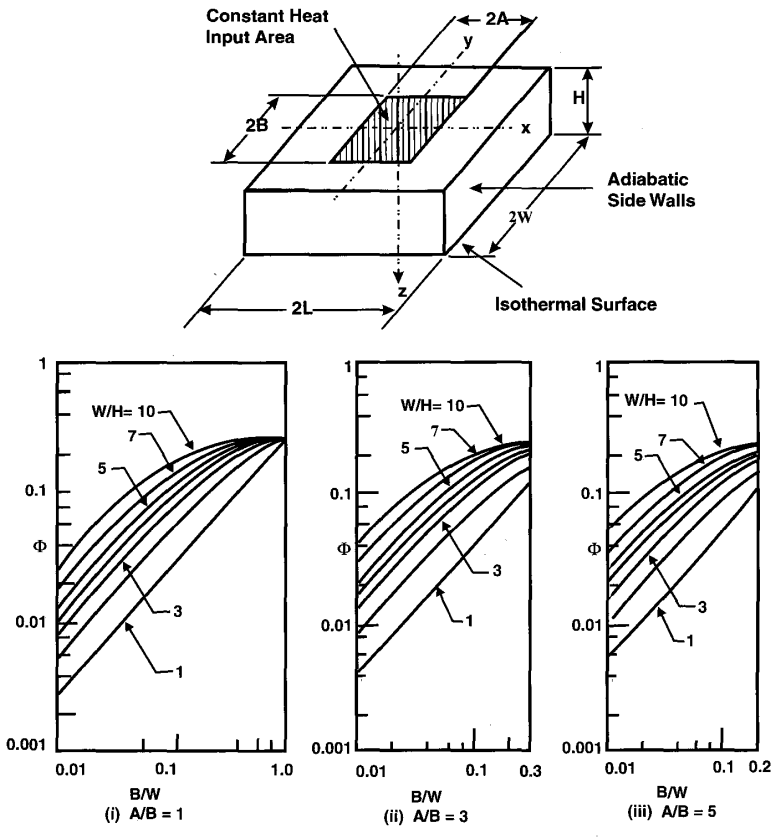

FIGURE 2.2 Thermal resistance factor Φ at heat source center for rectangular solids with *W* = *L*.

From Figure 2.2 with $A/B = 1$, we have

$$\Phi = 0.014$$

From Equation 2.10*a*, one obtains

$$R_m = \frac{0.014}{2(0.0025 \times 0.0025/0.005)} = 56°\text{C/W}$$

SEC et al. v. MRI
SEC Exhibit 1018.0021
IPR2023-00254

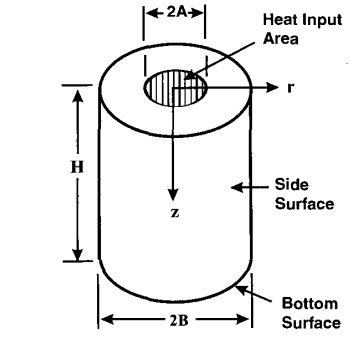

Boundary Conditions	Side Surface (r=B)	Bottom Surface (z=H)
CASE I	ADIABATIC	ISOTHERMAL
CASE II	ISOTHERMAL	ADIABATIC
CASE III	ISOTHERMAL	ADIABATIC

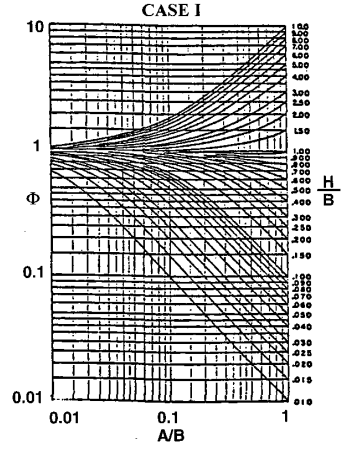

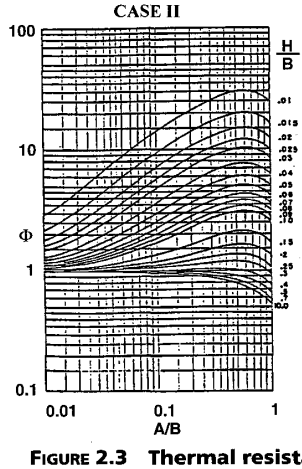

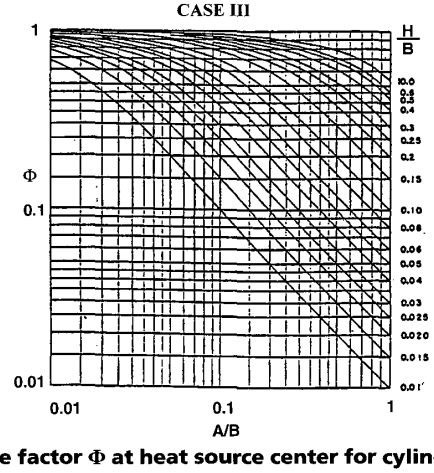

FIGURE 2.3 Thermal resistance factor Φ at heat source center for cylindrical solids.

The maximum temperature rise for the chip can readily be computed according to Equation 2.9:

$$\Delta T_m = 56 \times 0.2 = 11.2°C$$

Case II

Chip size: 0.1 by 0.1 by 0.05 in (chip cross-sectional area = 0.01 in², same as previous case)

SEC et al. v. MRI
SEC Exhibit 1018.0022
IPR2023-00254

Heat source size: 1.18×10^{-2} by 2.236×10^{-3} in (heat input area = 2.5×10^{-5} in^2, same as previous case)

Heat source perimeter: 0.0268 in, with

- $W = L = 0.1/2 = 0.05$ in
- $A = 1.118 \times 10^{-2}/2 = 5.59 \times 10^{-3}$ in
- $B = 2.236 \times 10^{-3}/2 = 1.118 \times 10^{-3}$ in
- $B/W = 1.118 \times 10^{-3}/0.05 = 0.0236$
- $W/H = 0.05/0.05 = 1$
- $A/B = 5$

From Figure 2.2 with $A/B = 5$, we have

$$\Phi = 0.012 \Rightarrow R_m = \frac{0.012}{2\left(5.59\times10^{-3}\times1.118\times10^{-3}/0.05\right)} = 48°\text{C/W}$$

and

$$\Delta T_m = 48 \times 0.2 = 9.6°\text{C}$$

Case III

Cylindrical chip with same cross-sectional areas for chip and heat source as the previous two cases:

Chip diameter (2*B*)*:* 0.11283 in (chip cross-sectional area = 0.01 in^2, same as previous cases)

Heat source diameter (2*A*)*:* 0.0056419 in (heat input area = 2.5×10^{-5} in^2, same as previous cases)

Heat source perimeter: 0.0177 in, with

- $A = 0.0056419/2 = 0.002821$ in
- $B = 0.112838/2 = 0.056419$ in
- $H/B = 0.05/0.0056419 = 8.86$
- $A/B = 0.05$

From Figure 2.3, we have

$$\Phi = 1.5 \Rightarrow R_m = \frac{1.5}{2\pi 0.002821} = 84.6°\text{C/W}$$

and

$$\Delta T_m = 84.6 \times 0.2 = 16.9°\text{C}$$

Comment: The above results clearly indicate that for the same heat source area, the thermal resistance decreases as the perimeter of the heat source increases.

SEC et al. v. MRI
SEC Exhibit 1018.0023
IPR2023-00254

Table 2.1 Equations of Heat Conduction in Various Geometrical Configurations
L = thickness of plane wall or length of cylinder.

Geometry	Temperature profile	Heat flow
Plane wall	$\frac{T-T_1}{T_1-T_2}=-\frac{x}{L}$	$q=\frac{T_1-T_2}{L/kA}$
Hollow cylinder	$\frac{T-T_i}{T_i-T_o}=\frac{\ln(r/r_i)}{\ln(r_i/r_o)}$	$q=\frac{T_i-T_o}{\ln(r_o/r_i)/2\pi kL}$
Hollow sphere	$\frac{T-T_i}{T_i-T_o}=\frac{1/r-1/r_i}{1/r_i-1/r_o}$	$q=\frac{T_i-T_o}{(r_o-r_i)/4\pi kr_ir_o}$

2.3 ONE-DIMENSIONAL HEAT CONDUCTION

Under certain limiting conditions, heat conduction in a three-dimensional system can be approximated by a one-dimensional problem. For example, a one-dimensional heat conduction problem may be assumed if the lateral dimensions of a wall are very large as compared with its thickness. Another case is if thermal resistances in lateral directions are large as compared with the conductive resistance through the thickness of the wall.

2.3.1 Steady-State Condition

For a steady-state condition, the temperature of a medium is independent of the time, and thus the energy entering must be equal to the energy leaving the system. The analysis of Equations 2.4, 2.7, and 2.8 is greatly simplified when heat conduction becomes a one-dimensional steady-state condition. For cases without internal heat generation and with constant thermal properties, the temperature profile and the heat flow for a plane wall, hollow cylinder, and hollow sphere with prescribed wall temperatures can be summarized as in Table 2.1. The temperature profile of a given geometry can easily obtained by a double integration of Equation 2.4, 2.7, or 2.8 with the aid of the boundary conditions, i.e., prescribed temperature at the two surfaces of the wall. Once the temperature profile is known, the heat flux can be determined with Fourier's law.

2.3.2 Transient Condition

For the case with constant properties, the differential equation for one-dimensional heat conduction is

$$\frac{1}{x^{n-1}}\frac{\partial}{\partial x}\left(x^{n-1}\frac{\partial T}{\partial x}\right)+\frac{q'''}{k}=\frac{1}{\alpha}\frac{\partial T}{\partial t} \tag{2.11}$$

SEC et al. v. MRI
SEC Exhibit 1018.0024
IPR2023-00254

where

$$n = \begin{cases} 1 & \text{for slabs} \\ 2 & \text{for cylinders} \\ 3 & \text{for spheres} \end{cases}$$

Again, with proper initial and boundary conditions, Equation 2.11 can be solved either analytically or numerically. Solutions for the above problems are generally available and are often expressed in graphical form for practical applications. For the case without internal heat generation, the charts of Heisler [4] can be applied for a convection boundary condition.

In the case with thermal radiation at the boundary, the problem becomes nonlinear and is typically solved numerically. The labor involved in repeatedly solving these nonlinear problems further warrants the construction of solution charts, which will be of interest to thermal engineers in various fields. The graphical charts of the temperature history are available for a one-dimensional slab [5], cylinder[6], and sphere [7]. Chung and Yeh [8, 9] extended the above solutions by including the internal heat generations for a slab, cylinder, and sphere under heating or cooling conditions. The heating case represents the condition where the environment temperature is higher than the initial temperature of the solid. On the other hand, the cooling case implies that the solid is initially hotter than its environment. Numerical computations reveal that for the same parameters, the sphere cools most rapidly, followed by the cylinder, and finally the slab. The same sequence is found for radiant heating.

2.4 THERMAL/ELECTRICAL ANALOGY

Heat flow within a medium due to a temperature gradient is similar to the case of an electrical system, where the current flows in a circuit according to Ohm's law, which can be stated as

$$\Delta V = IR \tag{2.12}$$

where ΔV is the voltage (electrical potential), I is the current, and R is the electrical resistance. The following relation may express the temperature in a heat transfer process:

$$\Delta T = qR \tag{2.13}$$

where q is the heat transfer rate and R is the thermal resistance, equivalent to the denominators of the heat flow equations in Table 2.1. Analogous quantities between the two kinds of systems are listed in Table 2.2.

The purpose of employing the analogy between electrical and thermal systems is to simplify the calculation procedure for the latter. This approach is often used to develop a general thermal analyzer for analysis and design of a

SEC et al. v. MRI
SEC Exhibit 1018.0025
IPR2023-00254

Table 2.2 Analogous Quantities between Thermal and Electrical Systems

	Thermal system	Electrical system
Potential	ΔT, °K or °R	ΔV, volts
Flow	q, W or Btu/hr	I, amperes
Resistance	R, °K/W or °R/(Btu/hr)	R, ohms
Capacitance	C, kJ/°K or Btu/°R	C, farads

thermal system. For physical systems encountered in practice, one rarely finds a problem that can be solved analytically. A complicated three-dimensional system may be approximated by subdividing it into a large number of small elements or nodes which have no internal temperature gradient. These nodes are then interconnected by thermal paths (thermal resistances) to form a network. Nodes represent discrete quantities of mass that may gain or lose thermal energy from or to neighboring nodes, or may gain energy from internal heat sources.

The thermal resistance for different heat transfer modes may be defined as follows:

$$\textit{Conduction: } R = \frac{L}{kA} \tag{2.14a}$$

where

L = conduction length
A = cross-sectional area normal to heat conduction path

$$\textit{Convection: } R = \frac{1}{hA} \tag{2.14b}$$

where

h = heat transfer coefficient
A = heat transfer surface area (fluid-wall contacting surface)

$$\textit{Radiation: } R = \frac{T_1 - T_2}{\sigma \Im A\left(T_1^4 - T_2^4\right)} \tag{2.14c}$$

where

σ = Stefan-Boltzmann constant
$\Im$ = gray body view factor

As can be seen from Equation 2.14c, the radiation thermal resistance is explicitly expressed as a nonlinear function of the surface temperature that is somewhat

SEC et al. v. MRI
SEC Exhibit 1018.0026
IPR2023-00254

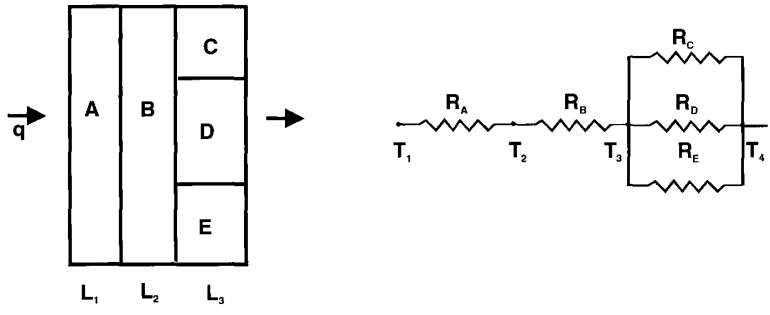

FIGURE 2.4 Thermal network for a multilayer composite wall.

different from the cases of the conduction and convection thermal resistances. The heat transfer coefficient under natural convection is also a nonlinear function of temperature. Convection and radiation heat transfer will be discussed in Chapters 3 and 4, respectively.

As does an electrical network, a thermal network consists of series and parallel paths. For example, the thermal network of a multiple-layer composite wall is shown in Figure 2.4. It should be noted that a two-dimensional heat flow might result if the thermal conductivities of materials *C*, *D*, and *E* are significantly different. Also, the thermal contact resistances at the interfaces are not shown in Figure 2.4. Generally, a thermal resistance exists at the interface when two bodies are in contact. A detailed discussion of the interface thermal contact resistance will be presented in Chapter 9.

Example 2.2

Referring to Figure 2.4, let L_1, L_2, and L_3 be 0.5, 0.8, and 1 ft, respectively. It is assumed the total heat transfer rate, q, is 100 Btu/hr. Other assumptions are listed in the accompanying table. Determine the temperature difference between T_1 and T_4.

	A	*B*	*C*	*D*	*E*
Thermal conductivity, Btu/(h · ft · °F)	50	80	100	100	100
Cross-sectional area, ft²	1	1	0.3	0.4	0.3

Solution:

$$R_A = \frac{L}{kA} = \frac{0.5}{50\times 1} = 0.01 \quad R_B = \frac{0.8}{80\times 1} = 0.01$$

$$R_C = R_E = \frac{1}{100\times 0.3} = 0.033 \quad R_D = \frac{1}{100\times 0.4} = 0.025$$

SEC et al. v. MRI
SEC Exhibit 1018.0027
IPR2023-00254

For parallel paths between T_3 and T_4, the net thermal resistance is

$$R' = \frac{1}{1/R_C + 1/R_D + 1/R_E} = 0.01°\text{F/(Btu/hr)}$$

The total thermal resistance becomes

$$R_t = R_A + R_B + R' = 0.01 + 0.01 + 0.01 = 0.03°\text{F/(Btu/hr)}$$

The temperature difference between T_1 and T_4 is

$$T_1 - T_4 = qR_t = 100 \times 0.03 = 3°\text{F}$$

To facilitate computations, the thermal resistance due to heat conduction for several common geometrical configurations is listed in Table 2.3. By applying proper values of θ and ϕ in Equations 3 and 5 in Table 2.3, one obtains the following equations:

$$R_i = \begin{cases} \dfrac{\ln(r_o/r_i)}{2\pi kL} & \text{hollow cylinder} \quad (2.15a) \\ \dfrac{r_o - r_i}{4\pi k r_i r_o} & \text{hollow sphere} \quad (2.15b) \end{cases}$$

2.5 LUMPED-SYSTEM TRANSIENT ANALYSIS

There is no material with an infinite thermal conductivity. However, many transient problems may be treated approximately as a lumped system by assuming uniform temperature within the system at any instant. This simplification is justified only for the case where the external thermal resistance between the system and its surroundings is so large compared with the internal thermal resistance that the latter can be neglected. The Biot number, hL_c/k, which is the ratio of the internal to the external resistance, is often used to measure the relative importance of the external and internal thermal resistances; h is the average heat transfer coefficient, k is the thermal conductivity of the solid, and L_c is the characteristic length defined as the ratio of the volume of the body to its surface area. For regular-shaped bodies such as plates, cylinders, and spheres, the error induced by the assumption of a uniform internal temperature in the solid is less than 5% if the Biot number is less than 0.1. The following are characteristic lengths for several common geometric shapes:

$$L_c = \begin{cases} \dfrac{(4/3)\pi r^3}{4\pi r^2} = \dfrac{r}{3} & \text{sphere} \quad (2.16a) \\ \dfrac{\pi r^2 L}{2\pi r L} = \dfrac{r}{2} & \text{cylinder} \quad (2.16b) \\ \dfrac{L^3}{6L^2} = \dfrac{L}{6} & \text{cube} \quad (2.16c) \end{cases}$$

SEC et al. v. MRI
SEC Exhibit 1018.0028
IPR2023-00254

Table 2.3 Conduction Thermal Resistance

Geometry	Thermal resistance	
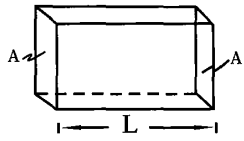	$R = \frac{L}{kA}$	(1)
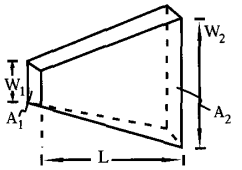	$R = \frac{L\,ln(w_2/w_1)}{k(A_2 - A_1)}$	(2)
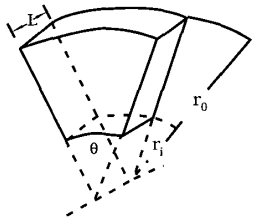	$R_r = \frac{ln(r_o/r_i)}{\theta kL}$	(3)
	$R_\theta = \frac{\theta}{kL\,ln(r_o/r_i)}$	(4)
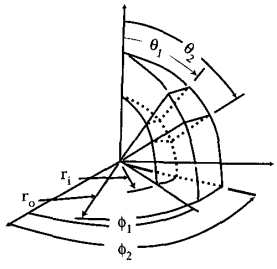	$R_r = \frac{r_o - r_i}{kr_ir_o(\cos\theta_1 - \cos\theta_2)(\phi_2 - \phi_1)}$	(5)
	$R_\theta = \frac{ln\left[\tan(\theta_2/2)/\tan(\theta_1/2)\right]}{k(r_o - r_i)(\phi_2 - \phi_1)}$	(6)
	$R_\phi = \frac{\phi_2 - \phi_1}{k(r_o - r_i)ln\left[\tan(\theta_2/2)/\tan(\theta_1/2)\right]}$	(7)
	where θ_1, θ_2, ϕ_1, and ϕ_2 are angles in radians	

To understand the solution to the lumped-system transient, let us consider a solid body with an internal heat generation, q. The body is initially at a uniform temperature of T_i and is suddenly exposed to an airstream at a temperature of T_a. The heat transfer coefficient is assumed to be relatively small compared with the thermal conductivity of the body, so that the Biot number is less than 0.1. From the energy balance equation, we have

$$c\rho V\frac{dT}{dt} = q - hA(T - T_a) \tag{2.17}$$

SEC et al. v. MRI
SEC Exhibit 1018.0029
IPR2023-00254

with the following initial boundary condition:

$$T = T_i \quad \text{at} \quad t = 0 \tag{2.18}$$

where c is the specific heat, ρ is the density, and V is the volume of the body.

Equation 2.17 can be rewritten as follows:

$$\frac{dT}{T - T_\infty} = \frac{dT}{\tau} \tag{2.19}$$

where

$$T_\infty = \frac{q}{hA} + T_a \tag{2.20}$$

and

$$\tau = \frac{c\rho V}{hA} \tag{2.21}$$

Let us assume that T_∞ and τ are constant. The solution of Equations 2.19 to 2.21 becomes

$$T - T_\infty = (T_i - T_\infty)e^{-t/\tau} \tag{2.22}$$

where τ is usually referred to as the time constant.

Equation 2.22 indicates that the transient response decreases when τ increases. In other words, the rate of the temperature change is slow when the body heat capacitance is large or the product of the heat transfer coefficient and the surface area is small.

A similar solution can be obtained for a more complicated case which includes multiple heat transfer paths from the body to various heat sinks at different temperatures. The basic energy equation takes the form

$$c\rho V \frac{dT}{dt} = q - \sum h_i A_i \left(T - T_{a,i}\right) \quad i = 1, 2, 3, \ldots, n \tag{2.23}$$

and the solution is identical to that of Equation 2.22, with T_∞ and τ modified as follows:

$$T_\infty = \frac{q + \sum h_i A_i T_{a,i}}{\sum h_i A_i} \tag{2.24}$$

and

$$\tau = \frac{c\rho V}{\sum h_i A_i} \tag{2.25}$$

SEC et al. v. MRI
SEC Exhibit 1018.0030
IPR2023-00254

Lumped-system analysis is very handy in making a quick estimate of the transient response of a body or an electronic component. The following example will illustrate the usefulness of the approach.

Example 2.3

A relay whose weight is 0.5 oz is mounted on a printed circuit board at 185°F. The relay is initially at 170°F and is suddenly exposed to an airstream at 140°F. It is assumed that the heat transfer coefficient h_1 between the relay and the airstream is 5 Btu/(hr · ft² · °F) and the conductance h_2 from the relay to the printed circuit board, including conduction from leads to the board, is 50 Btu/(hr · ft² · °F). The specific heat and heat dissipation of the relay are 0.2 Btu/(lb_m · °F) and 20 Btu/hr, respectively. It is further assumed that the heat transfer surface area for h_1 and h_2 is 0.003 ft² (neglecting the convection from the sides of the relay because components are close-packed). Determine the relay temperature at the end of 1 minute.

Solution:

From Equations 2.23 and 2.24, we have

$$T_\infty = \frac{q + \sum h_i A_i T_{a,i}}{\sum h_i A_i}$$

$$= \frac{20 + 5 \times 140 \times 0.003 + 50 \times 185 \times 0.003}{5 \times 0.003 + 50 \times 0.003}$$

$$= 302.1°\text{F}$$

$$\tau = \frac{c\rho V}{\sum h_i A_i}$$

$$= \frac{(0.5/16) \times 0.2}{5 \times 0.003 + 50 \times 0.003}$$

$$= 0.0379 \text{ hr}$$

At the end of 1 minute, t = 1/60 = 0.0167 hr. The corresponding temperature is obtained from Equation 2.22 as follows:

$$T - T_\infty = (T_i - T_a)e^{-t/\tau}$$

$$T - 302.1 = (170 - 302.1)e^{-(0.0167/0.0379)}$$

$$T = 217°\text{F}$$

It should be noted that the value of 217°F represents the case temperature of the relay (not a junction temperature).

A more general equation for a system in the process of heating or cooling down can be expressed as follows:

$$c\rho V \frac{dT}{dt} = q + \alpha_a q'' A - \sum h_i A_i (T - T_{a,i}) - \sum \sigma \varepsilon F A_i (T^4 - T_{e,i}^4) \quad i = 1, 2, 3, \ldots, n \tag{2.26}$$

SEC et al. v. MRI
SEC Exhibit 1018.0031
IPR2023-00254

where

F = radiation view factor
q″ = external heat flux, e.g., solar flux
α_a = solar absorptivity of surfaces

Equation 2.26 can be rewritten in the form

$$\frac{dT}{dt} = f(t,T) \tag{2.27}$$

where

$$f(t,T) = \frac{q + \alpha_a q'' A - \sum h_i A_i (T - T_{a,i}) - \sum \sigma \varepsilon F A_i (T^4 - T_{e,i}^4)}{c\rho V} \tag{2.28}$$

Since Equation 2.27 is a nonlinear problem, it can be solved numerically, e.g., by the fourth-order Runge-Kutta method described as follows:

$$k_1 = Hf(t, T_{\text{old}}) \tag{2.29a}$$

$$k_2 = Hf\left(t + \frac{H}{2}, T_{\text{old}} + \frac{k_1}{2}\right) \tag{2.29b}$$

$$k_3 = Hf\left(t + \frac{H}{2}, T_{\text{old}} + \frac{k_2}{2}\right) \tag{2.29c}$$

$$k_4 = Hf\left(t + \frac{H}{2}, T_{\text{old}} + \frac{k_3}{2}\right) \tag{2.29d}$$

and

$$T_{\text{new}} = T_{\text{old}} + \frac{k_1 + 2k_2 + 2k_3 + k_4}{6} \tag{2.30}$$

where H is a small time increment.

The calculation begins by setting T_{old} equal to the initial temperature of the system. A new temperature is then obtained at the end of the time step, and this process is repeated until the specified time is reached.

The thermal conductivities of silicon (Si) and gallium arsenide (GaAs) are a strong function of temperature. Generally, the thermal conductivity of a pure single-crystal silicon material is zero at 0 K and rises approximately exponentially to a maximum value near 20 K, then falls somewhat faster than $1/T$ to about 500 K, and then varies approximately as $1/T$ to the melting point. Virtually all semiconductor materials—materials of the same family as Si—exhibit this general trend of thermal conductivity as a function of temperature.

SEC et al. v. MRI
SEC Exhibit 1018.0032
IPR2023-00254

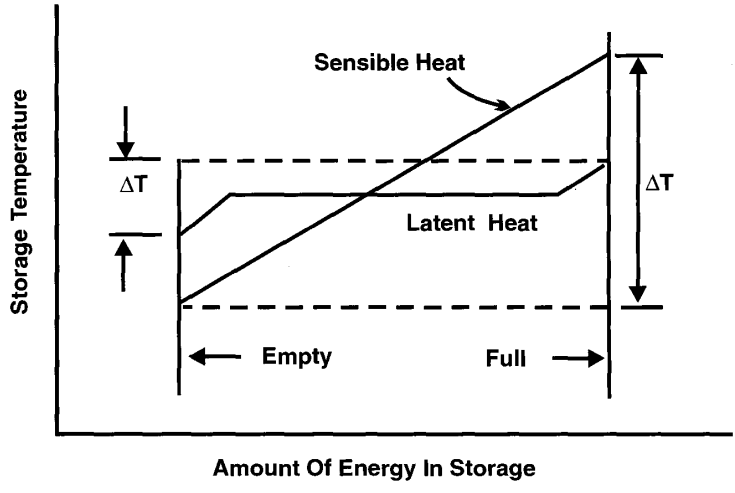

FIGURE 2.5 Temperature profile in a thermal-energy storage system.

2.6 HEAT CONDUCTION WITH PHASE CHANGE

Heat transfer involving melting and solidification has many engineering applications. One of the most noticeable applications is in thermal-energy storage (TES) systems. Compared with sensible-energy storage systems, using a phase-change material (PCM) for energy storage has some advantages:

1. Larger heat capacity in the storage system (the latent heat is much larger than the specific heat)
2. Lower temperature gradient in the storage system, as shown in Figure 2.5 (theoretically, phase change takes place at a constant temperature)

Heat transfer involving melting and solidification is a complex problem because of its moving boundary condition. Figure 2.6 shows the moving boundary condition at the interface between the solid and liquid. Mathematically, the boundary condition at the interface can be described in the following equation by assuming no energy storage at the interface:

$$q_s'' - q_1'' = m\rho L \frac{ds(t)}{dt} \tag{2.31}$$

SEC et al. v. MRI
SEC Exhibit 1018.0033
IPR2023-00254

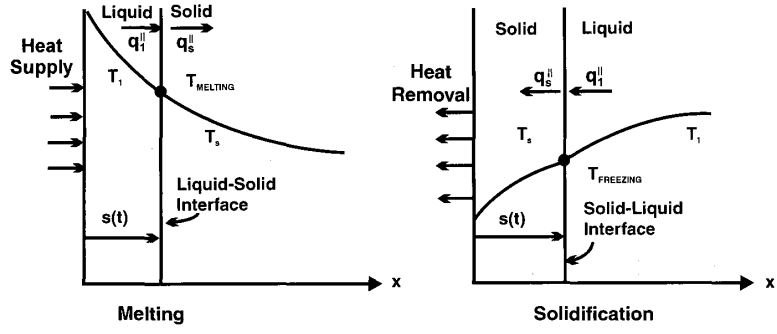

FIGURE 2.6 Moving solid-liquid interface for melting and solidification.

where

L = latent heat

ρ = density (assuming the same value for the solid and the liquid)

$$m = \begin{cases} -1 & \text{for melting} \\ 1 & \text{for solidification} \end{cases}$$

In addition, q_s'' and q_1'' are heat fluxes, respectively, at the solid and liquid sides of the interface pointing in the direction of the cooled surface as shown in Figure 2.6. The location of the solid-liquid interface measured from the origin is given by s and is a function of time. Basically, the left-hand side of Equation 2.31 represents the net energy removed from (or supplied to) the interface per unit area and per unit time in the direction of the cooled surface. The right-hand side of the equation corresponds to the energy released (or gained) at the interface per unit area and per unit time as a result of release of the latent heat during solidification (or melting). Equation 2.31 can be rewritten as follows:

$$\left(k_s \frac{\partial T_s}{\partial x} - k_1 \frac{\partial T_1}{\partial s}\right)_{x=s(t)} = m\rho L \frac{ds(t)}{dt} \tag{2.32}$$

Another boundary condition at the interface is the continuity of temperature where the interface temperature is equal to the melting or freezing temperature, i.e., $T_s = T_1$ at $x = s$.

To simplify the problem, solutions are often obtained by assuming no natural convection in the liquid region. Even with this assumption, the problem of transient heat conduction involving melting and freezing, which was first studied by Stefan [10], is still complex. Therefore, exact solutions are limited to only a few very simple cases [10, 11]. Approximate and numerical methods become very

SEC et al. v. MRI
SEC Exhibit 1018.0034
IPR2023-00254

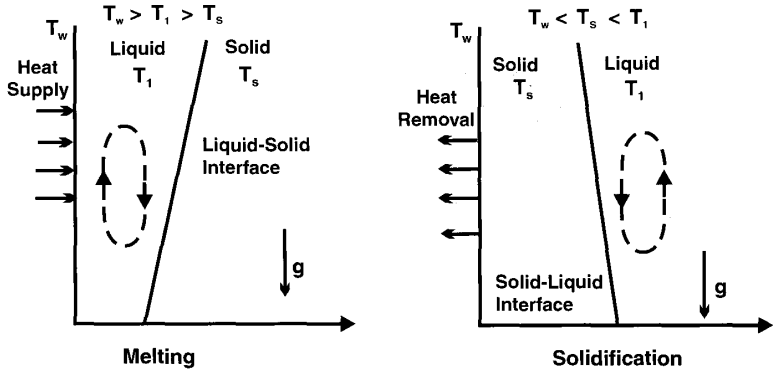

FIGURE 2.7 Temperature profile with natural convection in liquid region.

important and practical. Due to extensive studies on this subject, there are too many published papers to be listed here; however, some basic information can be found in Stefan's paper [10] and in works of Carslaw and Jaeger [11] and Ozisik [12]. The temperature profile for the case including natural convection in the liquid region is illustrated schematically in Figure 2.7. Representative papers in this area have been written by Sparrow and others [13, 14].

Because of their ability to absorb a relatively large amount of heat with a small temperature gradient, phase-change materials have been used in thermal control of electronics. Examples of this application are given in Estes [15] and Pal and Yoshi [16]. Various types of paraffin wax are commonly used because of their low cost and chemical stability during thermal cycling. Some thermophysical properties of a representative type (P116 paraffin wax) are as shown here [17]:

Specific heat of solid	2.95 kJ/(kg · °C)
Specific heat of liquid	2.51 kJ/(kg · °C)
Density of solid	818 kg/m^3
Density of liquid	760 kg/m^3
Thermal conductivity of solid	0.24 W/(m · °C)
Thermal conductivity of liquid	0.24 W/(m · °C)
Heat of fusion (latent heat)	262 kJ/kg
Melting point	44°C

A common characteristic of most phase-change materials is low thermal conductivity in both liquid and solid phases. To enhance the heat transfer rate, an extended surface such as plate or honeycomb-type fins which extend from the heat exchange surface through the phase-change material is often applied.

Recently, a microencapsulation of PCMs has been developed to enhance heat transport in liquid [18]. Figure 2.8 shows a single micro-PCM particle. Particle

SEC et al. v. MRI
SEC Exhibit 1018.0035
IPR2023-00254

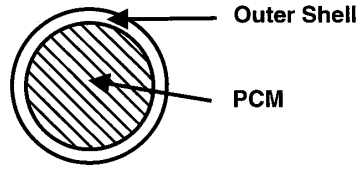

FIGURE 2.8 Cross section of microencapsulated phase-change material particle.

diameters can range from one to several hundred microns. The core PCM constitutes approximately 80 to 85% of the total weight, and the thickness of shell is typically less than one micron. When it is heated, the PCM inside the shell is changed from solid to liquid. The particle flexible wall can accommodate the volumetric expansion (less than 15%).

Another type of phase-change is *ablation,* or the change of a material from solid to gas. The process is similar to the melting process except that the liquid phase as shown in Figure 2.6 no longer exists and the heat supply, $q(t)$, is always applied to the solid-gas interface. To reflect this change, Equation 2.32 is rewritten as follows:

$$q(t) + k_s \left(\frac{\partial T_s}{\partial x} \right)_{x=s(t)} = \rho L \frac{ds(t)}{dt} \tag{2.33}$$

The assumption that the boundary surface is completely free from the ablated material is not always correct. This is because a porous charred layer may be formed on the heating surface during the ablation of many materials consisting of organic substances such as plastic or resins. Heat transfer with ablation is commonly employed in thermal protection systems. For example, a thin insulation layer is frequently applied to the external surface of a high-speed object such as a missile to protect the internal structures from aerodynamic heating on the missile skin.

REFERENCES

1. J. B. J. Fourier, *The Analytical Theory of Heat,* Dover, New York, 1955.
2. R. D. Lindsted and R. J. Surty, "Steady State Junction Temperature of Semiconductor Chips," *IEEE Trans. Electron Devices* 19(1), 1972.
3. D. P. Kennedy, "Spreading Resistance in Cylindrical Semiconductor Devices," *J. Appl. Phys.* 31(8), 1960
4. M. P. Heisler, "Temperature Charts for Induction and Constant-Temperature Heating," *Trans. ASME* 26, 1947.

SEC et al. v. MRI
SEC Exhibit 1018.0036
IPR2023-00254

5. R. D. Zerkle and J. E. Sunderland, "The Transient Temperature Distribution in a Slab Subject to Thermal Radiation," *J. Heat Transfer* 87, 1965.
6. D. L. Ayers, "The Transient Temperature Distribution in a Radiating Cylinder," ASME Paper No. 67-HT-71, 1967.
7. D. L. Ayers, "Transient Cooling of a Sphere in Space," *J. Heat Transfer* 92, 1970.
8. B. T. F. Chung and L. T. Yeh, "Heat Conduction in Slabs with Uniform Heat Sources and Radiative Boundary Conditions," *J. Spacecraft and Rockets* 10, 1973.
9. B. T. F. Chung and L. T. Yeh, "Temperature Distribution in Radiating Cylinders and Spheres with Uniform Heat Generation," ASME Paper No. 73-WA/HT-2, 1973.
10. J. Stefan, "Über die Theorie der Eisbildung, insbesondere über die Eisbildung im Polarmeere," Ann. Phys. Chem. N.S. 42, 1891.
11. H. S. Carslaw and J. C. Jaeger, *Conduction of Heat in Solids,* Oxford University Press, London, 1947.
12. M. N. Ozisik, *Boundary Value Problems of Heat Conduction,* International Textbook, Scranton, PA, 1968.
13. E. M. Sparrow, S. V. Patankar, and S. Ramadhyani, "Analysis of Melting in the Presence of Natural Convection in the Melt Region," *J. Heat Transfer* 99, 1977.
14. E. M. Sparrow and P. Souza Mendes, "Natural Convection Heat Transfer Coefficients Measured in Experiments on Freezing," *Int. J. Heat Mass Transfer* 25, 1982.
15. R. C. Estes, "The Effect of Thermal Capacitance and Phase Change on Outside Plant Electronic Enclosures," *IEEE Trans. Components, Hybrid and Manufacturing Technol.* 5, 1992.
16. D. Pal and Y. K. Joshi, "Transient Thermal Management of an Avionics Module Using Solid-Liquid Phase Change Materials (PCMs)," 7, *ASME Proc. 31st Nat. Heat Transfer Conf.,* ASME HTD-329, 1996.
17. A. Haji-Sheikh, J. Eftekhar, and D. Y. S. Lou, "Some Thermophysical Properties of Paraffin Wax as a Thermal Storage Medium," in P. E. Bauer and H. E. Collicott, eds., *Spacecraft Thermal Control, Design, and Operations,* Vol. 86 of *Progress in Astronautics and Aeronautics,* AIAA, New York, NY, 1983.
18. C. P. Colvin, J. C. Mulligan, and Y. G. Bryant, "Enhanced Heat Transport in Environmental Systems Using Microencapsulated Phase Change Materials," *22nd Int. Conf. on Environmental Systems,* Seattle, July 13–16, 1992.

SEC et al. v. MRI
SEC Exhibit 1018.0037
IPR2023-00254

Chapter 3

CONVECTION

Convection is a heat transport process in a fluid involving the combined action of heat conduction and energy storage when the fluid is undergoing a mixing motion. Since convection heat transfer is closely related to fluid motion, prior knowledge of the flow field is prerequisite before the mechanism of heat transfer in the fluid can be investigated. Generally, the motion of a fluid, either a gas or a liquid, can be divided into two basic flow conditions, namely, laminar and turbulent.

In laminar flow, the fluid particles follow smooth and continuous paths in an orderly fashion. The fluid particles in any one layer do not move across layers, and particles remain in an orderly sequence within each layer without passing one another. Therefore, heat is transferred purely by molecular conduction among the particles through direct contact. Heat is also exchanged through the interface between the fluid and the surface of the walls. On the other hand, turbulent flow is irregular, and the fluid velocity components are random, varying with time and space. Turbulent eddies of the fluid move across the streamlines. Energy is transferred by mixing the fluid particles in motion. Thus, increasing the mixing rate will increase the heat transfer rate.

Convection heat transfer can be classified into forced and free (or natural) convection. In the former process, the fluid motion is induced by some external means such as a pump, blower, fan, or wind. In the latter process, the fluid motion is generated from the density difference caused by a temperature variation in the fluid.

3.1 FLOW AND TEMPERATURE FIELDS

Due to the viscous effect, the velocity boundary layer of an internal flow begins forming at the inlet when a fluid with a uniform velocity enters a duct. The hydrodynamic boundary-layer thickness increases along the flow path as shown in Figure 3.1. For a symmetrical tube flow, the edge of the boundary layer coincides with the axis at some distance from the entrance, and this distance is often referred to as the *hydrodynamic entry length*. The flow continues to develop throughout the entire hydrodynamic entry length. After the boundary layer merges, the flow becomes fully developed hydrodynamically, which implies that the velocity profile is invariant with the axial distance.

SEC et al. v. MRI
SEC Exhibit 1018.0038
IPR2023-00254

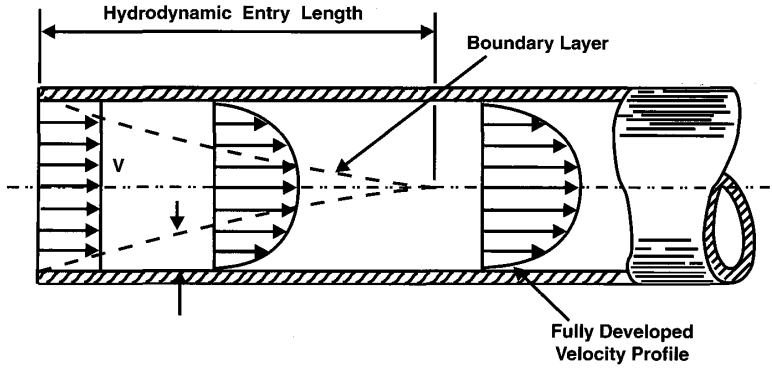

FIGURE 3.1 Boundary-layer development for fluid in a tube.

Similar trends are found for the temperature field in a heat transfer process. The boundary layer is now referred to as the *thermal* boundary layer, and the distance for the thermal boundary layer to develop is called the thermal entrance length. In a thermally developed flow, the temperature profile of the fluid is invariant with the axial distance.

The ratio of the tube length x to the diameter D_h is often adopted as an indicator to express the flow condition, i.e., fully developed or developing flow. This ratio is sometimes misleading. A better way to indicate the flow regime is to use the respective dimensionless parameters x^* [$= x/(\text{Re Pr } D_h)$] thermally and x^+ [$= x/(\text{Re } D_h)$] hydrodynamically. The hydraulic diameter D_h is equal to 4 times the hydraulic radius, which is defined as the ratio of the cross-section area to the perimeter of a tube. Re and Pr are the Reynolds and Prandtl numbers, respectively. Both these dimensionless parameters take into account the tube geometry (x and D_h), whereas Pr takes into account the fluid property and Re the flow condition. A small value of x^* or x^+ represents a developing flow, while a large value of x^* or x^+, on the other hand, corresponds to a fully developed flow.

The problem of fluids flowing over or across solids in the case of an external flow has also frequently occurred in many engineering applications. Figure 3.2 shows one of the simple cases where fluid flows over a flat plate. There is a significant difference between the internal and the external flow cases in the development of the boundary layer. As shown in Figure 3.2, the hydrodynamic boundary layer continues to grow over the plate. Additionally, the flow may separate from the wall of a nonslender body.

The following are the major differences between flow over a bluff body and flow over a flat plate or a streamlined body:

1. As noted in Figure 3.3, the velocity outside the boundary layer, u_∞, which is different from the upstream or approaching velocity V, depends on the distance x from the stagnation point. The velocities of u_∞ and V are identical in the case of flow over a flat plate.

SEC et al. v. MRI
SEC Exhibit 1018.0039
IPR2023-00254

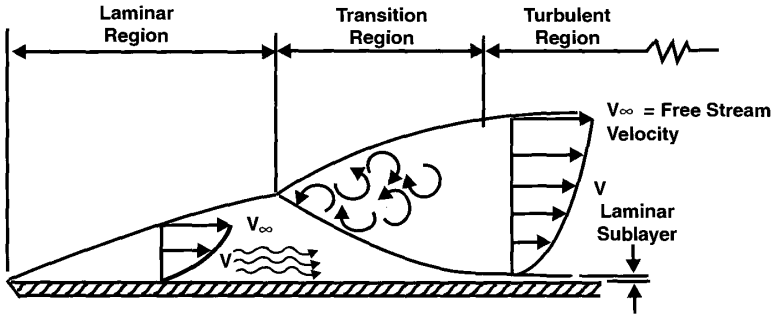

FIGURE 3.2 Flow regimes for flow over a flat plate.

2. The most important difference between these two cases lies in the behavior of the boundary layer. For a streamlined body, the flow separation from the solid wall, if it happens at all, occurs nears the rear. For a bluff body, on the other hand, the point of flow separation often takes place not far from the leading edge. The separation as indicated in Figure 3.4 is a condition in which the boundary detaches from the surface of a solid and a wake is then formed in the downstream. At the separation point, the velocity gradient at the wall surface becomes zero.
3. In the case of flow over a streamlined body, the pressure drop is mainly caused by the boundary-layer surface shear stress, i.e., skin friction drag. For a bluff body, however, the skin friction drag is small

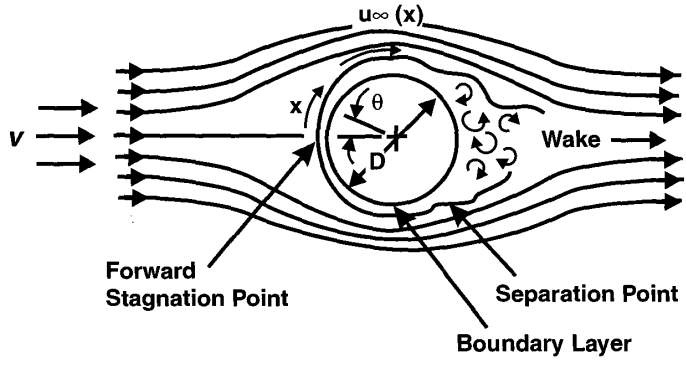

FIGURE 3.3 Boundary-layer formation and separation on a circular cylinder in crossflow.

SEC et al. v. MRI
SEC Exhibit 1018.0040
IPR2023-00254

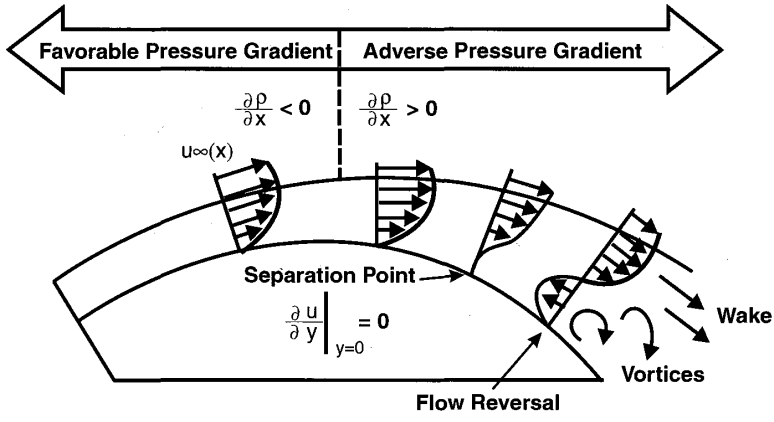

FIGURE 3.4 Velocity profile and flow separation for a circular cylinder in crossflow.

compared with the form drag. The form or pressure drag arises from the separation of the flow, which induces a low-pressure region in the rear of a solid body. A pressure difference is generated in the flow direction when the pressure over the rear of the body is lower than that over the front.

3.2 HEAT TRANSFER COEFFICIENT

The practical concern in heat transfer by convection is to determine the heat transfer coefficient. The governing equation for convection can be expressed as follows:

$$q = hA(T_w - T_{\text{ref}}) \tag{3.1}$$

where

q = heat transfer rate
h = heat transfer coefficient
A = heat transfer surface area
T_w = wall temperature
T_{ref} = reference temperature of fluid

The heat transfer coefficient is a proportional constant and does not have any physical meaning by itself. However, it is a function of the fluid flow, fluid properties, and the geometry of the system. Note that in defining the heat transfer

SEC et al. v. MRI
SEC Exhibit 1018.0041
IPR2023-00254

coefficient, the reference temperature can be the bulk fluid temperature or the inlet fluid temperature for an internal flow, and the free stream temperature for an external flow. Therefore, one should apply the heat transfer coefficient according to its definition.

The heat transfer coefficient is frequently expressed in a dimensionless form called the Nusselt number, $\text{Nu} = hL_c/k$, which is, in turn, a function of various dimensionless groups as follows:

For forced convection:

$$\text{Nu} = F_1(\text{Re})F_2(\text{Pr}) \tag{3.2}$$

For free or natural convection:

$$\text{Nu} = F_3(\text{Gr})F_4(\text{Pr}) \tag{3.3}$$

where

Re = Reynolds number
Pr = Prandtl number
Gr = Grashof number

The details of each dimensionless group will be discussed later. The characteristic length, L_c, used to define the Nusselt number can have different meanings under various physical conditions. For example, it can be the hydraulic diameter for a duct flow or it can be the height of a vertical plate in natural convection.

The heat transfer coefficient can be obtained either mathematically or experimentally; however, neither approach is generally enough to cover all possible physical problems. Mathematically, the heat transfer coefficient can be obtained by knowing the fluid temperature distribution that is determined by solving a set of differential equations involving conservation of mass, momentum, and energy. Analytical solutions are confined to some very simple cases. For a more complex problem, numerical solutions are needed. The accuracy and validity of numerical solutions depend on both the mathematical model used to describe the physical problem and numerical methods used in the analysis. The computer simulations of computational fluid dynamics (CFD), therefore, cannot replace experiments totally because physical phenomena still cannot be modeled accurately and completely, such as the turbulent flow. It should be noted that all empirical correlations should be applied only to the conditions under which the tests were conducted.

3.3 PARAMETER EFFECTS ON HEAT TRANSFER

Since there is no simple way to predict heat transfer coefficients under various thermal and physical conditions, the following discussions place emphasis on understanding the physical phenomena in convection heat transfer and the effects of various parameters on the heat transfer coefficient.

SEC et al. v. MRI
SEC Exhibit 1018.0042
IPR2023-00254

3.3.1 Effects of the Reynolds Number

In the case of forced convection, the Nusselt number depends on the flow conditions, which can be characterized by the Reynolds number Re, defined as follows:

$$\mathrm{Re} = \frac{\rho V L_c}{\mu} \tag{3.4}$$

where

ρ = density of fluid
V = velocity of fluid
L_c = characteristic length
μ = viscosity of fluid

The Reynolds number also represents the ratio of the inertia force to the friction (or viscous) force. In laminar flow, which corresponds to the case with small Reynolds numbers, there is no mixing in fluid particles, and heat transfer takes place only by molecular conduction due to contact between fluid particles. Since all fluids (with the exception of liquid metals) have a small thermal conductivity, the heat transfer coefficients in laminar flow are relatively small. As the Reynolds number (or velocity) increases, the flow regime is changed gradually from laminar to transition flow, in which a certain amount of mixing takes place between the fluid particles. The mixing motion, even on a small scale, accelerates the heat transfer rate considerably.

As the Reynolds number is further increased, the flow becomes fully turbulent except for a very thin layer of fluid immediately adjacent to the wall. In this thin layer, which is called the laminar sublayer, the viscous force predominates near the wall surface, and heat transfer takes place mainly by conduction. In the turbulent core, the mixing due to eddies is so efficient that heat is transferred very rapidly between the edge of the laminar sublayer and the turbulent core of the fluid. Although the thermal resistance of the laminar sublayer controls the rate of heat transfer, the overall heat transfer in turbulent flow is still much higher than that in laminar flow. This phenomenon results from the small thickness of the laminar sublayer as compared with the thickness of the entire thermal boundary layer in laminar flow. It is found that increasing the Reynolds number decreases the thickness of the laminar sublayer and at the same time increases the eddy mixing in the turbulent core. The net result is that the heat transfer rate goes up with the Reynolds number.

3.3.2 Effect of the Prandtl Number

The Prandtl number is defined as the ratio of the kinematic viscosity of the fluid to the thermal diffusivity of the fluid; that is,

$$\begin{aligned} \mathrm{Pr} &= \frac{\nu}{\alpha} \\ &= \frac{\mu c_p}{k} \end{aligned} \tag{3.5}$$

SEC et al. v. MRI
SEC Exhibit 1018.0043
IPR2023-00254

where

c_p = specific heat of fluid
k = thermal conductivity of fluid

The kinematic viscosity, $\nu = \mu/\rho$, is often referred to as the *molecular diffusivity of momentum* because it is a measure of the rate of momentum transfer between the molecules. On the other hand, the thermal diffusivity $\alpha = k/\rho c_p$ of a fluid usually is called the *molecular diffusivity of heat,* which is a measure of the ratio of the heat transmission and energy storage capacities of the molecules. The heat and momentum are diffused through the fluid at the same rate if the Prandtl number is unity (1). If the Prandtl number is greater than 1, the velocity profile will develop more rapidly than the temperature profile, whereas the opposite trends are found in a fluid with Prandtl number less than 1.

It should be noted that the temperature profile starts to develop at the point where the heat transfer between the fluid and wall actually takes place. If the Prandtl number is greater than 5, the velocity profile generally will develop much faster than the temperature profile, so that a solution based on a fully developed velocity profile will apply quite accurately, even without accounting for the hydrodynamic starting length. Such a condition frequently prevails in the dielectric fluids that are widely used for electronic equipment, because the Prandtl number for most dielectric fluids is, in general, greater than 20 at room temperatures. On the other hand, for the case of $\text{Pr} \to 0$, the velocity profile never actually develops, while the temperature profile does develop. A uniform velocity profile (slug flow), therefore, can be assumed over the entire thermal boundary layer.

At very low Prandtl numbers, such as for liquid metals, the thermal resistance is distributed over the entire fluid. The temperature profile for a fluid with a low Prandtl number is similar to that in laminar flow. In addition, the thermal entry length and the thermal response of the fluid to axial changes in surface temperature are slow and are similar to those characteristics of laminar behavior. For fluids with high Prandtl numbers, very short thermal entry length and quick thermal response to axial surface temperature changes are found. Both are attributed to the concentration of the thermal resistance in the thin laminar sublayer near the wall and the rapid transfer of heat from the edge of the sublayer over the entire fluid because of effective mixing of fluid particles in the turbulent core.

3.3.3 Effect of the Grashof Number

The Grashof number represents the ratio of buoyant to viscous forces and is defined as follows:

$$\text{Gr} = \frac{g\rho\beta\,\Delta T\,L_c^3}{\mu^2} = B\,\Delta T\,L_c^3 \tag{3.6}$$

SEC et al. v. MRI
SEC Exhibit 1018.0044
IPR2023-00254

where

g = gravitational constant
β = fluid thermal expansion coefficient
ΔT = temperature difference between wall and ambient
B = property parameter
$= \dfrac{g\rho^2\beta}{\mu^2}$

As the Reynolds number characterizes the flow condition in forced convection, the flow condition—i.e., laminar or turbulent flow—in free or natural convection can be characterized by the Grashof number, or sometimes by the Rayleigh number, defined as

$$\text{Ra} = \text{Gr Pr} \tag{3.7}$$

In natural convection, flow can be laminar or turbulent, depending on the value of the Grashof or Rayleigh number. For example, the flow over a vertical plate becomes turbulent as $\text{Ra} \geq 10^9$.

Figure 3.5 shows the velocity profile over a vertical plate in natural convection. The velocity profile is different from that in forced convection. At the wall, the velocity is zero because of the nonslip condition. The velocity increases to a maximum value and then decreases to zero again at the edge of the boundary layer because of the stationary air that exists outside the velocity boundary layer in the natural convection.

Natural convection is not a very effective heat transfer process; it tends to give a low heat transfer coefficient. The effect of radiation is important in many cases of natural convection and should not be neglected. This situation is especially true for natural convection occurring in high altitudes, where the air density is low.

3.3.4 Effect of Boundary Conditions

In laminar flow or for fluids with a Prandtl number less than 1, the heat transfer coefficient depends on the thermal boundary conditions. The reason for this dependency is that the heat transfer mechanism is primarily due to molecular diffusion. Thus, the thermal resistance is distributed over the entire thermal boundary-layer thickness, and different boundary conditions or different shapes of the tube cross section simply generate different temperature profiles. For high–Prandtl number fluids or turbulent flow, the thermal resistance is mainly in the laminar sublayer near the wall, which yields a square temperature profile in a tube or a very flat temperature profile over the wall in an external flow case.

The above discussion suggests that the Nusselt number for a high Prandtl number or for any fluids in turbulent flow is relatively insensitive to variations of the wall surface temperature or heat flux in the flow direction. On the other

SEC et al. v. MRI
SEC Exhibit 1018.0045
IPR2023-00254

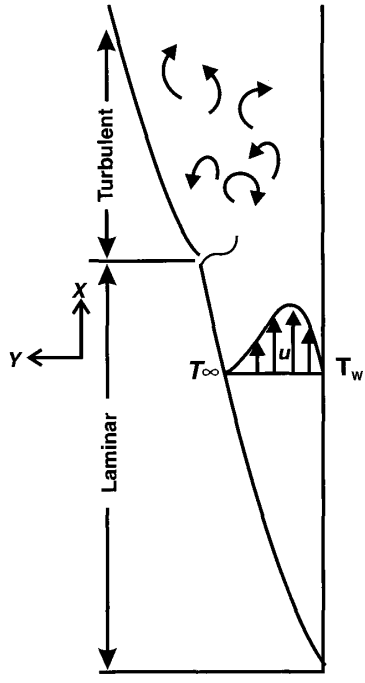

FIGURE 3.5 Boundary layer over a vertical plate in natural convection.

hand, the Nusselt number for a low–Prandtl number fluid or any fluid in laminar flow is strongly dependent on the axial variations of the wall surface temperature and/or heat flux. As pointed out in a 1984 paper by Yeh [1], based on the subject discussed here, it is concluded that the heat transfer correlations for a given shaped tube cannot be applied to other shaped tubes in laminar flow or to low–Prandtl number fluids.

The two basic thermal boundary conditions are constant axial wall temperature (T condition)and constant axial wall heat flux (H condition) Both are realized in many practical applications—the former in condensers and evaporators with high liquid flow rates, and the latter in electrical heating as well as in a counterflow heat exchanger with equal thermal capacity rates. It should be noted that, in both cases, the wall temperature around the periphery of a duct is also uniform. In laminar flow, the heat transfer coefficients for constant axial wall heat flux and constant axial wall temperature conditions represent the upper and the lower limits, respectively. In other words, bounded between the heat transfer coefficient in laminar flow for other boundary conditions are these two limits.

SEC et al. v. MRI
SEC Exhibit 1018.0046
IPR2023-00254

For symmetrically heated noncircular tubes (with corners or variable peripheral curvature), two common cases are:

1. H_1 condition: constant axial wall heat flux with uniform peripheral wall temperature (variable peripheral heat flux). This is identical to the above-mentioned H condition.
2. H_2 condition: constant axial and peripheral wall heat fluxes (variable peripheral wall temperature).

The H_1 condition is a good approximation for a tube with very highly conductive materials (e.g., copper or aluminum) or with a very thick wall. On the other hand, the H_2 condition is an approximation for a tube with very poorly conductive materials or a very thin wall. It should be noted that the H_1 and H_2 conditions are identical for circular tubes or parallel plates, but the heat transfer coefficient for the H_2 condition is generally less than that of the H_1 condition for noncircular tubes.

Like the heat transfer process, the friction factor in laminar flow or for fluids with a low Prandtl number also depends on the shape of the tube. Excellent information about heat transfer and flow friction for fluids in laminar flow with various shaped tubes is presented in Shah and London [2].

It is a common mistake to use the round-tube heat transfer (or friction) correlation for rectangular ducts in laminar flow. Table 3.1 illustrates the dependence of the Nusselt number and friction factor on the shape of duct and on thermal boundary conditions. Information contained in Table 3.1 is primarily from Shah and London [2]. The aspect ratio α is defined as the ratio of the small to large sides of a rectangular tube. The aspect ratio is bounded by 1 (representing a square duct) and 0 (representing parallel plates).

The Reynolds and Nusselt numbers are based on the hydraulic diameter. The values listed in the table are valid only for the case with all sides heated uniformly.

Example 3.1

Compare the heat transfer coefficients h of circular and square tubes carrying the same fluid under the fully developed laminar flow condition. Assume that the diameter of the round tube is D and that this is also the length of each side of the square tube.

Solution

The hydraulic diameter for the square tube is determined as follows:

$$D_s = \frac{4D^2}{2(D+D)} = D$$

Since both tubes have the same hydraulic diameter, the ratio of the heat transfer coefficients is equal to the ratio of the Nusselt numbers (assuming thermal conductivity k is constant). From Table 3.1, we have:

SEC et al. v. MRI
SEC Exhibit 1018.0047
IPR2023-00254

Table 3.1 Nusselt Number and Friction Factor in Fully Developed Laminar Flow

Tube shape	$f \cdot \mathrm{Re}$	Nu_T	Nu_{H1}	Nu_{H2}
Rectangular tube				
Aspect ratio $\alpha = 2a/2b$:				
1	14.227	2.976	3.608	3.091
0.9	14.261	—	3.620	—
0.8	14.378	—	3.664	—
0.714	14.565	3.077	3.734	—
0.667	14.712	3.117	3.790	—
0.6	14.980	—	3.895	—
0.5	15.548	3.391	4.123	3.020
0.4	16.368	—	4.472	—
0.333	17.090	3.956	4.795	2.970
0.3	17.512	—	4.990	—
0.25	18.233	4.439	5.331	2.940
0.2	19.071	—	5.738	2.930
0.167	19.702	5.137	6.049	2.930
0.125	20.585	5.597	6.490	2.940
0.1	21.169	—	6.785	2.950
0.05	22.477	—	7.451	—
0	24.000	7.541	8.235	8.235
Circular tube	16.000	3.657	4.364	4.364
Triangle tube (equilateral)	13.333	2.470	3.110	1.892

T *condition:*

$$\frac{h_r(\text{round tube})}{h_s(\text{square tube})} = \frac{\mathrm{Nu}_r}{\mathrm{Nu}_s} = \frac{3.657}{2.976} = 1.23$$

H1 *condition:*

$$\frac{h_r(\text{round tube})}{h_s(\text{square tube})} = \frac{\mathrm{Nu}_r}{\mathrm{Nu}_s} = \frac{4.364}{3.608} = 1.21$$

The above results clearly indicate that the heat transfer coefficient for a round tube is different from that of a square one, and an improper use of the correlation will result in a significant error.

Rectangular tubes have been used extensively in cooling of electronics, especially in cold-plate cooling. Tables 3.2 and 3.3 present the Nusselt number with one or more walls transferring heat under constant-wall temperature and constant-wall heat flux conditions, respectively [2].

SEC et al. v. MRI
SEC Exhibit 1018.0048
IPR2023-00254

Table 3.2 Nusselt Number Nu_T for Rectangular Tubes in Fully Developed Laminar Flow at *T* Condition

Dimensions:

Adiabatic wall:

Heat transfer wall:

	Nu_T for wall configuration				
2b/2a			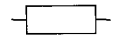		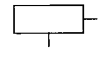
0.0	7.541	7.541	7.541	0.0	4.861
0.1	5.858	6.091	6.399	0.457	3.823
0.2	4.803	5.195	5.703	0.833	3.330
0.3	4.114	4.579	5.224	1.148	2.996
0.4	3.670	4.153	4.884	1.416	2.768
0.5	3.383	3.842	4.619	1.647	2.613
0.7	3.083	3.408	4.192	2.023	2.443
1.0	2.970	3.018	3.703	2.437	2.375
2.0	3.383	2.602	2.657	3.185	2.613
2.5	3.670	2.603	2.333	3.390	2.768
3.33	4.114	2.703	1.946	3.626	2.996
5.0	4.803	2.982	1.467	3.909	3.330
10.0	5.858	3.590	0.843	4.270	3.823
∞	7.541	4.861	0.0	4.861	4.861

3.3.5 Other Effects

Another factor that can influence heat transfer and friction considerably is the variation of physical properties with temperature. In general, the properties of most fluids are temperature-dependent and will vary through the boundary layer or over the flow cross section of a tube. Further, if the viscosity of fluids varies significantly, the velocity profile can be altered, which, in turn, changes the heat transfer characteristics.

As stated by Kays [3], the specific heat of a gas varies only slightly with temperature, but the viscosity and thermal conductivity are a strong function of temperature to about the 0.8 power of the absolute temperature while the density varies inversely with the first power of the absolute temperature. The Prandtl number, however, is nearly independent of temperature. On the other hand, the specific heat and thermal conductivity of most liquids are relatively insensitive to temperature variation, but the viscosity decreases very significantly as the temperature increases. Thus, the Prandtl number varies with temperature in the same manner as the viscosity. The density of liquids varies little with temperature.

In most cases, a constant-property assumption is reasonably acceptable for general engineering calculations. The effects of physical property variations

SEC et al. v. MRI
SEC Exhibit 1018.0049
IPR2023-00254

Table 3.3 Nusselt Number Nu_{H1} for Rectangular Tubes in Fully Developed Laminar Flow at H_1 Condition

Dimensions:

Adiabatic wall:
Heat transfer wall:

	Nu_T for wall configuration				
2b/2a					
0.0	8.235	8.235	8.235	0.0	5.385
0.1	6.700	6.939	7.248	0.538	4.410
0.2	5.704	6.072	6.561	0.964	3.914
0.3	4.969	5.393	5.997	1.712	3.538
0.4	4.457	4.885	5.555	1.004	3.279
0.5	4.111	4.505	5.203	1.854	3.104
0.7	3.740	3.991	4.662	2.263	2.911
1.0	3.599	3.556	4.094	2.712	2.836
2.0	4.111	3.146	2.947	3.539	3.104
2.5	4.457	3.159	2.598	3.777	3.279
3.33	4.969	3.306	2.182	4.060	3.538
5.0	4.704	4.636	1.664	4.441	2.914
10.0	6.700	4.252	0.975	4.851	4.410
∞	8.235	5.385	0.0	5.385	5.385

become important when the temperature difference between the fluid and the solid surface is large. Two possible ways are commonly applied to correct the constant-property results. One is called the *reference temperature approach,* and another is referred to as the *property ratio method.* The former chooses a reference temperature to evaluate all properties. This reference temperature can be the wall temperature, the bulk temperature, or the film temperature. The film temperature, which is an average of the wall and bulk temperatures, is most commonly used in empirical correlation of heat transfer and friction data.

In the property ratio approach, all properties are computed at the free-stream temperature or the mixed mean temperature. Then all of the variable-property effects are lumped into a function of the ratio of some pertinent property evaluated at the surface to that property determined at the free-stream or mixed mean temperature.

3.4 PRESSURE DROP AND FRICTION FACTOR

In addition to the heat transfer coefficient, the friction factor is also needed in computing the pressure drop in a system. The general relation for pressure drop in a duct can be expressed as follows:

SEC et al. v. MRI
SEC Exhibit 1018.0050
IPR2023-00254

$$\Delta P_t = \Delta P_f + \Delta P_s + \Delta P_a \pm \Delta P_g \tag{3.8}$$

where

ΔP_t = total pressure drop

ΔP_f = pressure drop due to friction

$$= 4f \frac{L}{D_h} \frac{G^2}{2\rho_m g_c}$$

ΔP_s = pressure drop due to additional losses such as entrance, exit, bends, fittings, valves, etc.

$$= \Sigma K \frac{G^2}{2\rho_m g_c}$$

ΔP_a = pressure drop due to flow acceleration (or momentum changes)

$$= \left(\frac{1}{\rho_2} - \frac{1}{\rho_1} \right) \frac{G^2}{2g_c}$$

ΔP_g = pressure drop (+, for upward flow) or gain (–, for downward flow) due to gravity in a vertical flow

and where

D_h = hydraulic diameter

f = Fanning friction factor

G = mass velocity

$= \rho V$ (V is velocity)

g = gravitational acceleration

g_c = conversion factor

$= 32.1739\ \mathrm{lb_m \cdot ft/(lb_f \cdot s^2)} = 4.17 \times 10^8\ \mathrm{lb_m \cdot ft/(lb_f \cdot hr^2)}$

H = tube vertical height

K = loss coefficient

For a single-phase fluid and incompressible flow, ΔP_a is very small and can be neglected. As is the heat transfer coefficient in the thermal entrance region, the friction factor in a hydrodynamically developing flow is much higher than that of the fully developed flow. In addition, rough surface in a tube will increase the pressure drop in turbulent flow. On the other hand, the roughness will also increase the heat transfer coefficient.

In addition to the Reynolds number, the friction factor in turbulent flow also depends on the surface roughness of a tube. Typically, the effect of roughness is expressed by the relative roughness ε/D, where ε is the absolute (average) surface roughness and D is the tube inner diameter. A simplified Moody chart for friction factor [4] is shown in Figure 3.6. The absolute surface roughness for pipes of different materials included in the same reference is presented in Table 3.4

SEC et al. v. MRI
SEC Exhibit 1018.0051
IPR2023-00254

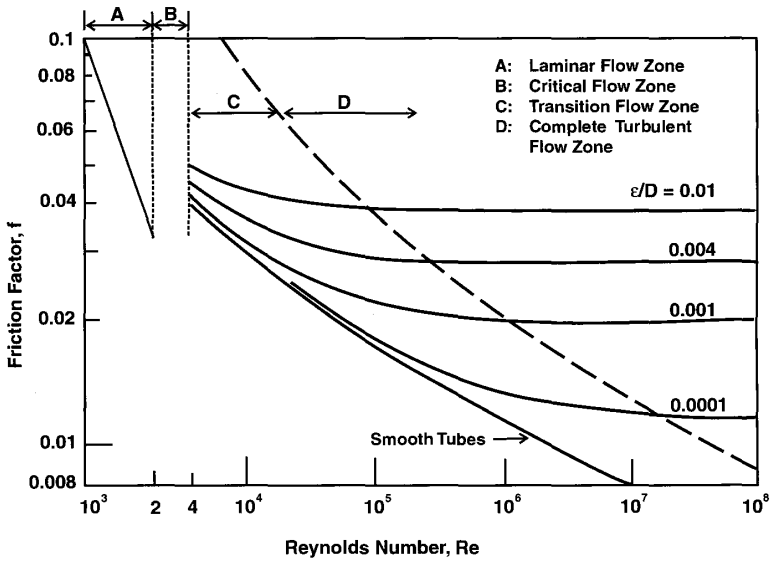

FIGURE 3.6 Friction factor versus Reynolds number for round tubes.

The turbulent flow in the Moody chart is further divided into transition and complete turbulent flow zones. The friction factor for the former is a complicated function of the Reynolds number and the relative roughness, while the friction factor for the latter is nearly independent of the Reynolds number, depending only on the relative surface roughness of the tube.

In summary, the heat transfer coefficient (or Nusselt number) for laminar flow or for low–Prandtl number fluids in a tube depends not only on the fluid property

Table 3.4 Absolute Surface Roughness

Material	ε, ft
Riveted steel	0.003–0.03
Concrete	0.001–0.01
Wood stave	0.0006–0.003
Cast iron	0.00085
Galvanized iron	0.0005
Asphalted cast iron	0.0004
Commercial steel or wrought iron	0.00015
Drawn tubing	0.000005

SEC et al. v. MRI
SEC Exhibit 1018.0052
IPR2023-00254

and the flow condition but also on the shape of the cross section and the thermal boundary conditions. The adoption of the heat transfer correlations for a round tube via the concept of the hydraulic diameter to other shaped tubes may, therefore, result in a significant error. There is only a weak influence of the duct shape on the heat transfer and friction in turbulent flow or for high–Prandtl number fluids. Consequently, for turbulent flow in a noncircular tube, the round-tube correlations for heat transfer coefficient and friction factor, in general, will yield accurate results if the hydraulic diameter is used as a characteristic dimension and if the Prandtl number of the fluids is not very small. The same conclusion can also be applied to the use of the friction factor correlations.

From Table 3.1, one can clearly see that the Nusselt number is constant. This result implies that the heat transfer coefficient h depends only on thermal conductivity k and hydraulic diameter D_h and is independent of the other fluid properties and velocity. This unique feature results from the fact that in fully developed laminar flow heat transfer occurs as purely molecular conduction. Similarly, the friction factor is a linear function of the Reynolds number. It should be noted that any methods used to enhance the heat transfer would generally also increase the pressure drop of the system.

3.5 THERMAL PROPERTIES OF FLUIDS

Before all heat transfer and flow friction calculations, the properties of the fluids involved must be known. Air and water are the most popular working fluids used in industry. The former is a primary coolant in much electronic equipment while the latter is probably the most effective and cheap liquid coolant. Some dielectric fluids—such as silicate ester fluids marketed as Coolanols by Exxon, Fluorinert chemicals (FC-xx) made by 3M, and synthetic fluids with a polyalphaolefin (PAO) base made by Chevron, Mobile, Dow Corning, and others—are often used to cool high-heat-dissipation electronics. Silicate ester–based fluids such as Coolanol-25R are most widely used in the cooling of electronics by the U.S. Navy and Air Force. A decade ago, these fluids were found to cause significant and sometimes catastrophic problems under consistent high-temperature use and in high-voltage electronics fields. These problems are due to the fluids' hygroscopic nature and subsequent formation of flammable alcohol and silica gel. Efforts have been made by the U.S. military to replace Coolanol-25R with PAO since 1989.

Electronic equipment is often required to operate at high altitudes without conditioned cooling air. At high altitudes, the air density is low. The mass flow rate of cooling air for a given volumetric flow rate under forced convection may be reduced sharply; hence the equipment may be damaged as a result of overheating. A reduction of air density in high altitudes also has a great effect on free convection; therefore, accurate prediction of the air density is required. For engineering application purposes, air can be treated approximately as an ideal gas, and its density can be obtained from the ideal gas law in the form

$$\rho = \frac{P}{RT} \tag{3.9}$$

SEC et al. v. MRI
SEC Exhibit 1018.0053
IPR2023-00254

where

ρ = air density, lb_m/ft^3
P = air pressure, lb_f/ft^2
R = gas constant
$= 53.34\ ft \cdot lb_f/lb_m \cdot °R$
T = air (absolute) temperature, °R

As the altitude changes, the atmospheric pressure will vary accordingly. Based on the tabular values presented in Reference 5, the correlations for atmospheric pressure as a function of altitude are obtained as follows:

$$P = \begin{cases} 2116.2 - 0.091H & H \le 0 \quad (3.10a) \\ 2116.2 - 0.071H & 0 \le H \le 5000 \quad (3.10b) \end{cases}$$

and

$$\log_{10}(P) = -0.19036A^4 + 2.20331A^3 - 8.56533A^2 + 11.14878A + 3.32556 \qquad H \ge 5000 \quad (3.10c)$$

where

P = atmosphere pressure, lb_f/ft^2 (or psf)
H = altitude, ft
$A = \log_{10}(H)$

According to the ideal gas assumption, the properties of gases (except the density) are a function of temperature only. In other words, all air properties except the density are independent of the altitude.

For liquids, the properties given in Appendix C are limited to saturated conditions. If a fluid is not at the saturated state, the effect of pressure on its properties is very significant; therefore, it cannot be neglected. For example, the properties of water at a superheated or subcooled condition are functions of temperature and pressure. In addition, all correlations developed are valid within certain temperature ranges (generally between the freezing and boiling points of liquids) as listed in the same appendix. To simplify calculations for the Grashof number, the B parameter defined in Equation 3.6 is also included in the property tables of Appendix C.

3.6 CORRELATIONS FOR HEAT TRANSFER AND FRICTION

Some of the friction factors in fully developed laminar flow have been included in Table 3.1 The friction factor correlations for various configurations under fully developed flow conditions are summarized in Appendix G.

SEC et al. v. MRI
SEC Exhibit 1018.0054
IPR2023-00254

On the basis of an extensive review and evaluation of the available literature in the field of convection heat transfer, the authors have prepared a comprehensive convection heat transfer catalog for practical applications. This catalog presents the correlations for both forced and free convention under various physical and thermal constraints. The correlation for flow parallel to or across a tube bank is also included. This convective heat transfer catalog, presented in Appendix H, includes the following tables:

Table H.1: Common Correlations for External Forced Convection
Table H.2: Common Correlations for Internal Forced Convection
Table H.3: Common Correlations for External Free Convection
Table H.4: Common Correlations for Free Convection in Enclosures or Vertical Parallel Plates
Table H.5: Common Correlations for Forced Convection in Tube Banks

Example 3.2

An airstream with a mass flow rate of m = 400 lb_m/hr flows through an uninsulated metal tube with diameter D = 0.4 ft. The inlet and outlet air temperatures are 210 and 170°F, respectively. The tube, with a length L = 20 ft, is located in a still-air environment at 40°F. Determine the heat flux and the tube surface temperature at the end of the tube ($x = L$).

Assumptions made in the analysis are as follows:

1. Steady-state conditions
2. Uniform and constant free convection coefficient at the outer surface of the tube
3. Tube-wall conduction having no bearing and therefore ignored
4. Fully developed flow inside the tube

Solution

As a first step, determine the inside convection heat transfer coefficient h_i for forced convection in a tube, on the basis of the following:

$$A = \frac{\pi D^2}{4} = 3.14159 \times \frac{0.4^2}{4} = 0.1257 \text{ ft}^2$$

$$G = \frac{\dot{m}}{A} = \frac{400}{0.1257} = 3183.1 \text{ lb}_m/(\text{ft}^2 \cdot \text{hr})$$

$$T_{ave} = \frac{210 + 170}{2} = 190°\text{F}$$

$$\mu = 0.0517 \text{ lb}_m/(\text{hr} \cdot \text{ft}); \; k = 0.0174 \text{ Btu}/(\text{hr} \cdot \text{ft} \cdot °\text{F}); \; \text{Pr} = 0.714$$

$$\text{Re} = \frac{GD}{\mu} = \frac{3183.1 \times 0.4}{0.0517} = 24{,}628 > 2300 \quad \text{(turbulent flow)}$$

From index 6 of Table H.2 in Appendix H (table of correlations for internal forced convection),

SEC et al. v. MRI
SEC Exhibit 1018.0055
IPR2023-00254

$$\begin{aligned}\mathrm{Nu}_L &= 5+0.012\mathrm{Re}^{0.83}(\mathrm{Pr}+0.29)\\ &= 5+0.012(24{,}628)^{0.83}(0.714+0.29)\\ &= 58.19\\ h_i &= \mathrm{Nu}\frac{k}{D} = \frac{58.19\times 0.0174}{0.4} = 2.53\ \mathrm{Btu/(hr\cdot ft^2\cdot °F)}\end{aligned}$$

The internal thermal resistance per unit area becomes

$$R_I = \frac{1}{h_i} = \frac{1}{2.53} = 0.395$$

The next step is to determine the outside convection heat transfer coefficient h_e for free convection over a tube. In order to determine the free convection coefficient, we need a value for the tube-wall temperature T_w. Let T_w = 120°F. Then:

$$\begin{aligned}T_{\mathrm{ave}} &= \frac{T_w+T_{a,e}}{2} = \frac{120+40}{2} = 80°\mathrm{F}\\ K &= 0.015\ \mathrm{Btu/(hr\cdot ft\cdot °F)} \qquad \mathrm{Pr} = 0.718\\ \rho &= 0.743\ \mathrm{lb_m/ft^3} \qquad \mu = 0.045\ \mathrm{lb_m/(hr\cdot ft)}\\ \beta &= 0.001866\ (°\mathrm{F})^{-1} \qquad B = 0.2125\times 10^7\end{aligned}$$

From Equation 3.6,

$$\begin{aligned}\mathrm{Gr} &= \frac{g\rho^2\beta\Delta T L_c^3}{\mu^2}\\ &= B\Delta T L_c^3\\ &= 0.2125\times 10^7\times(120-40)0.4^3\\ &= 1.088\times 10^7\end{aligned}$$

and

$$\begin{aligned}\mathrm{Ra} &= \mathrm{GrPr} = 1.088\times 10^{7}\times 0.718\\ &= 7.8118\times 10^6 < 10^9 \qquad \text{(laminar flow)}\end{aligned}$$

At the constant–surface temperature condition, from index 7 of Table H.3 in Appendix H, we have

$$\begin{aligned}\mathrm{Nu}_T &= 0.36+\frac{0.518\mathrm{Ra}^{1/4}}{[1+(0.559/\mathrm{Pr})^{9/16}]^{4/9}}\\ &= 0.36+\frac{0.518(7.8118\times 10^6)^{1/4}}{[1+(0.559/0.718)^{9/16}]^{4/9}}\\ &= 21.1\end{aligned}$$

SEC et al. v. MRI
SEC Exhibit 1018.0056
IPR2023-00254

or

$$h_T = \mathrm{Nu}_T \frac{k}{D} = 21.1 \times \frac{0.015}{0.4} = 0.79 \text{ Btu/(hr} \cdot \text{ft}^2 \cdot \text{°F)}$$

On the other hand, at the constant–heat flux condition, from index 8 of Table H.3 in Appendix H, we have

$$\begin{aligned} \mathrm{Nu}_H &= 0.36 + \frac{0.579\,\mathrm{Ra}^{1/4}}{[1+(0.442/\mathrm{Pr})^{9/16}]^{4/9}} \\ &= 0.36 + \frac{0.579(7.8118 \times 10^6)^{1/4}}{[1+(0.442/0.718)^{9/16}]^{4/9}} \\ &= 24.16 \end{aligned}$$

or

$$h_H = \mathrm{Nu}_H \frac{k}{D} = 24.16 \times \frac{0.015}{0.4} = 0.906 \text{ Btu/(hr} \cdot \text{ft}^2 \cdot \text{°F)}$$

Since the problem is characterized by neither the constant surface nor the constant heat flux condition, an average value is adopted, i.e.,

$$h_e = \frac{0.79 + 0.906}{2} = 0.848 \text{ Btu/(hr} \cdot \text{ft}^2 \cdot \text{°F)}$$

The external thermal resistance per unit area is

$$R_e = \frac{1}{h_e} = \frac{1}{0.848} = 1.179$$

Based on the assumption of no thermal resistance across the tube wall, the heat flux q'' at $x = L$ can be expressed in the following form:

$$q'' = \frac{\Delta T}{R_i + R_e}$$

where

$$\begin{aligned} \Delta T &= T_{a,i} - T_{a,e} = 170 - 40 = 130\text{°F} \\ \Sigma R &= R_i + R_e = 0.395 + 1.179 = 1.575 \end{aligned}$$

From the above equation, the heat flux q'' is calculated to be 82.5 Btu/hr·ft^2.

SEC et al. v. MRI
SEC Exhibit 1018.0057
IPR2023-00254

Since it is at the steady state, the heat flux at $x = L$ can also expressed in terms of the tube-wall temperature as follows:

$$q'' = \frac{T_{a,i} - T_w}{1/h_i} = \frac{T_w - T_{a,e}}{1/h_e}$$

T_w can be computed from the above equation by knowing either the internal or the external air temperature as follows:

$$T_w = 170 - 82.5 \times 0.395 = 170 - 32.6 = 137.4°F$$

or

$$T_w = 40 + 82.5 \times 1.179 = 40 + 97.3 = 137.3°F$$

Since the calculated T_w is different from the assumed value (T_w was assumed to be 120°F), additional iterations are required to obtain the final solution.

REFERENCES

1. L. T. Yeh, "Validity of One Heat Transfer Correlation to Various Shaped Ducts via Hydraulic Diameter Concept," *Proc. 4th Int. Electronics Packaging Conf.*, Baltimore, 1984.
2. R. K. Shah and A. L. London, "Laminar Flow Forced Convection in Ducts," *Advances in Heat Transfer, Supplement 1,* Academic Press, New York, 1978.
3. W. M. Kays, *Convective Heat and Mass Transfer,* McGraw-Hill, New York, 1966.
4. L. F. Moody, "Friction Factors for Pipe Flow," *Trans. ASME* 66, 1944.
5. F. Kreith, *Principles of Heat Transfer,* International Textbook, Scranton, PA, 1965.

SEC et al. v. MRI
SEC Exhibit 1018.0058
IPR2023-00254

Chapter 10

COMPONENTS AND PRINTED CIRCUIT BOARDS

Since the invention of the integrated circuit (IC) in the latter part of the 1950s, the development of new integrated circuits of greater complexity as shown in Figure 1.1 (Chapter 1) has progressed very rapidly. Along with greater numbers of components per integrated circuit have come greater challenges in cooling of electronic equipment. Generally, heat is generated from metallized areas on a small, thin, and fragile silicon die or chip inside a package. The heat transfer engineer must address the issue of cooling of electronics at all levels of packaging.

The chip package that is the housing for the silicon die is the most fundamental level of packaging for solid-state electronic equipment; it serves to protect the chip from the environment and to facilitate handling during manufacturing as well as chip interconnection. The next higher level of packaging is the circuit board. The printed circuit board (PCB), which is also often referred to as the printed wiring board (PWB), is a major element of any electronic equipment. It serves as a mounting surface for most of the basic components (chip packages) and provides wiring channels that act as conduits for chip-to-chip connections. The PCB is also frequently considered the primary field-replaceable unit and provides a test bed of accessible points for making circuit checks.

10.1 CHIP PACKAGING TECHNOLOGY

There are two major categories of chip package: first, the single-chip package (SCP), and second, the multichip module (MCM), or multichip package (MCP). In the SCP, each chip is in a self-contained unit. In MCMs, in contrast, all chips are packaged inside a single housing. Individual chips in an MCM are not encapsulated or enclosed for mechanical protection. In addition, it is typical to use a common substrate or thermal spreader for the entire multichip package. Figure 10.1 [1] gives a quantitative comparison in scale of a typical SCP—which may be a dual in-line package (DIP) or a pin-grid array (PGA)—and a typical MCM.

Various MCMs and their benefits and drawbacks can be classified as follows, according to type of process and substrate material:

1. MCM-C: Ceramic substrate (alumina) with thick film
   - Moderate cost
   - Mature technology

SEC et al. v. MRI
SEC Exhibit 1018.0059
IPR2023-00254

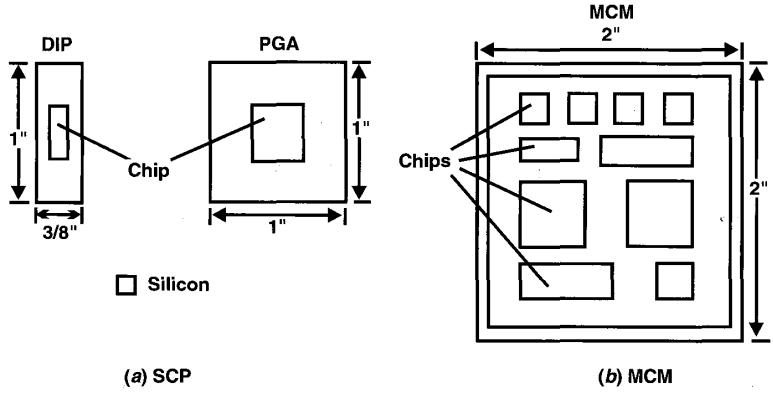

FIGURE 10.1 Scale comparison of MCM and SCP. (*a*) Two basic single-chip packages, the dual in-line package (DIP) and the pin-grid array. (*b*) MCM containing various types of individual chips.

2. MCM-D: Organic thin film deposited on a silicon, ceramic, or metal substrate
   - Most expensive
   - High interconnection density
3. MCM-L: Organic substrate (e.g., FR-4 and polyimide) with laminated copper
   - Poor thermal and electrical characteristics
   - Very inexpensive

From a construction point of view, the package can also be classified as plastic (nonhermetic) or ceramic (hermetic). The latter costs more and is often used in demanding environments where reliability is a major concern. To the contrary, the plastic package offers lower cost but is less reliable, having a higher package thermal resistance.

Another difference between plastic and ceramic packages is in the heat transfer path. In the ceramic package, the silicon die is typically placed in a cavity and is bonded to a substrate. Heat flows from the chip or die through the bonding material to the substrate and finally to the housing or case. Meanwhile, some of the heat is transferred from the leads to the printed circuit board. High thermal conductivities of substrate and die bond are a major thermal consideration. A good match in coefficient of thermal expansion between substrate and die is equally important. In the plastic package, on the other hand, most of the heat is transferred from the chip through the plastic molding compound—which has a relatively low thermal conductivity—to the case. The desired thermal properties are high thermal conductivities of the plastic molding compound and lead frames.

SEC et al. v. MRI
SEC Exhibit 1018.0060
IPR2023-00254

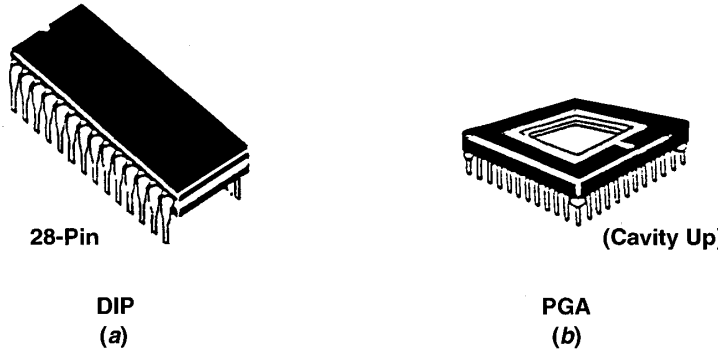

FIGURE 10.2 Drawings of common packages: (*a*) DIP; (*b*) PGA.

Figure 10.2 shows two of the most popular packages, the dual in-line package (DIP) and the pin-grid array (PGA). The pins that provide input and output (I/O) functions for a DIP are arranged along the long sides of the rectangular package. The typical center-to-center distance between pins for a standard DIP is 100 mils (0.254 cm), which severely limits the I/O count. The maximum I/O count for a standard DIP is therefore 64. A PGA is much larger than a DIP, and its silicon die is usually located in a cavity. Although a PGA package has a large number of pins, none of them is directly under the silicon chip. Because of the much greater number of pins it allows, the PGA is the package design used for the ASIC (application-specific integrated circuit).

The main drawbacks of PGAs are high cost of pin materials such as Alloy 42 and Copper, and mounting technology of having through-holes on the PCB which is not compatible to the surface mount technology. To overcome the problems, a new package, Ball Grid Array (BGA), was recently developed by replacing the pins of PGAs with small solder balls. Solder balls are generally cheaper than Alloy 42 (or Copper) pins and are also easier to attach to the bottom of the package. Through solder balls, the BGA is then attached to the copper pads on the PCB. The mounting approach is compatible to the surface mount technology. Unlike a PGA where there is no pin under the die area, the solder balls are spreading over the entire bottom of the BGA package.

The interconnection between pins of a DIP or PGA and the PCB is illustrated in Figure 10.3. Because of manufacturing tolerances, the space between the bottom of the chip package (or component) and the top surface of the printed circuit board can vary from 0.015 to 0.060 in for a DIP and 0.033 to 0.068 in for a PGA. This space will sometimes create a thermal problem for a conduction-cooled board. The varying gap sizes under components will also cause an additional complication in the manufacturing process when a heat sink or thermal spreader is required to fill up the gaps between the board and components.

SEC et al. v. MRI
SEC Exhibit 1018.0061
IPR2023-00254

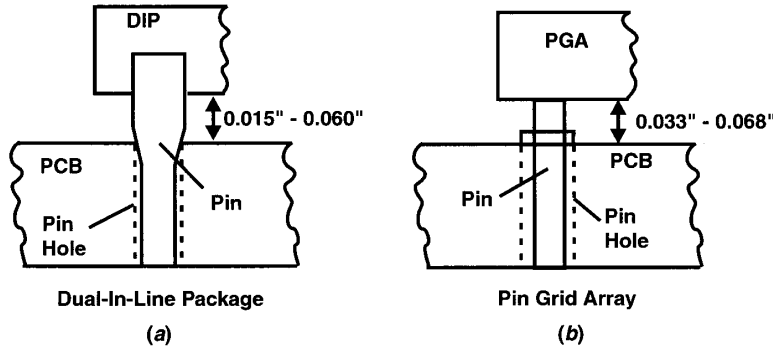

FIGURE 10.3 Interconnection between pin and board: (*a*) DIP; (*b*) PGA.

10.2 CHIP PACKAGE THERMAL RESISTANCE

The chip package or component thermal resistance $\theta_{j\text{-}c}$, which is often also referred to as internal resistance, is defined as the thermal resistance between the junction (metallized area) on the silicon die and some reference point on the outside of the chip package or component case. The value of $\theta_{j\text{-}c}$ can vary if different reference points are used. Therefore, caution must be taken to use this value in a correct way. In most component assemblies, heat must be transferred through a number of different materials and interfaces, and the total component thermal resistance is the net value of several individual thermal resistances in series or parallel. Once $\theta_{j\text{-}c}$ is known, the temperature rise from the case to the device junction can be determined as follows:

$$\Delta T_{j\text{-}c} = q\theta_{j\text{-}c} \tag{10.1}$$

where q is component heat dissipation. A typical unit for $\theta_{j\text{-}c}$ is °C/W.

In the thermal analysis, the component case temperature is usually computed and Equation 10.1 is then used to predict the component junction temperature. A direct modeling of a chip package is possible if the materials and internal structures of the package are known. The important thermal design considerations in a chip package are as follows:

1. Spreading in die or chip:
   a. Die material: silicon or gallium arsenide (GaAs).
   b. Heat source:
      - Uniform versus nonuniform heat source: high thermal resistance for nonuniform heat sources.
      - Shape of heat source: low thermal resistance for a heat source with a larger perimeter.

SEC et al. v. MRI
SEC Exhibit 1018.0062
IPR2023-00254

2. Die bond: The thermal resistance of the die bond is especially important for hermetic packages, where heat from the die is first transferred through the die bond to the substrate and then to the housing or case.
   a. Cracks: Caused by excessive mechanical stresses between the chip and substrate, or metallurgical fatigue during temperature cycling.
   b. Voids: Created either during the chip attachment process, or during cooling down, or in storage. The thermal resistance is affected by the size, shape, and distribution of the voids. For a fixed void fraction in the die bond, a few large, contiguous voids give a higher thermal resistance. Both cracks and voids increase the thermal resistance across the die bond materials.
3. Spreading in substrate and plastic molding:
   a. High–thermal conductivity materials.
   b. Good match in coefficient of thermal expansion between materials.

10.3 CHIP PACKAGE ATTACHMENT

Packages can also be divided according to the method of chip attachment, into through-hole and surface-mount packages (or components). DIPs and PGAs are typically mounted to the printed circuit board using the through-hole technology. The disadvantages of this approach are poor area efficiency and limited I/O counts. The surface-mount technology can significantly increase the pin count and board area efficiency, and improve the package density as well as electrical performance, because of the component size (surface-mount components are several times smaller in size than DIP equivalents). This approach also allows the components to be mounted on both sides of a printed circuit board. There are some challenges, as follows, involved in the use of surface-mount components:

1. Thermal expansion matching: The coefficient of thermal expansion (CTE) of the chip, substrate, and board may be quite different.
2. Thermal management: As component density increases, the heat load on the printed circuit board increases. The problem becomes even worse when components are mounted on both sides of the board.
3. Mechanical rigidity: The board must be very flat, without any warpage or twist, because the solder joints are the only mechanical attachment medium for surface-mounted components. The board must also be very rigid to resist flexing during handling or under vibration or shock conditions in order to prevent stress cracking in the solder joints.
4. Dimensional stability: The board must be able to withstand high assembly temperatures without any deformation, delamination, or via plating fracture.

The thermal conductivity and the coefficient of thermal expansion are probably the most important properties for surface-mount technology. Figure 10.4 shows both properties for various materials. For a PCB, multilayer dielectric materials may be adhesively bonded to a metal core using copper-invar (Cu-Inv). The Cu-Inv can provide the mechanical rigidity required for a typical PCB, and it

SEC et al. v. MRI
SEC Exhibit 1018.0063
IPR2023-00254

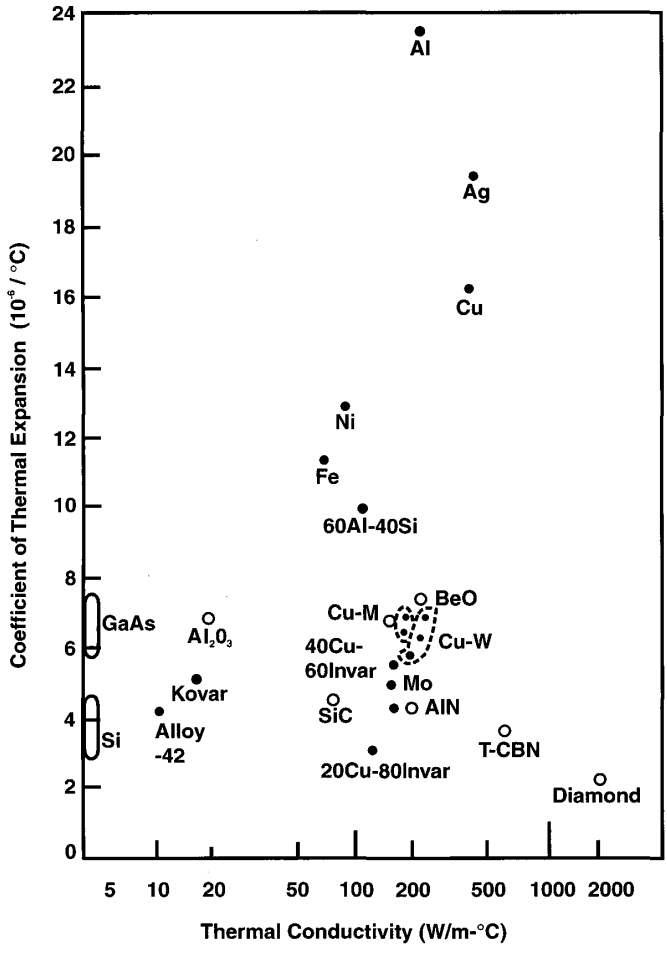

FIGURE 10.4 Thermal conductivity and CTE of various materials.

also enables achieving the proper value of the coefficient of thermal expansion by adjusting the percent of invar involved. Cu-Inv-Cu is a metallurgically bonded trilayer consisting of a core of invar (36% nickel/64% iron alloy) bonded on both sides with equal thicknesses of oxygen-free copper. This material has been made in thicknesses from 5 to 52 mils and in width up to 24 in. Figure 10.5 [2, 3] shows the lateral thermal conductivity and the coefficient of thermal expansion for various percents of copper involved.

SEC et al. v. MRI
SEC Exhibit 1018.0064
IPR2023-00254

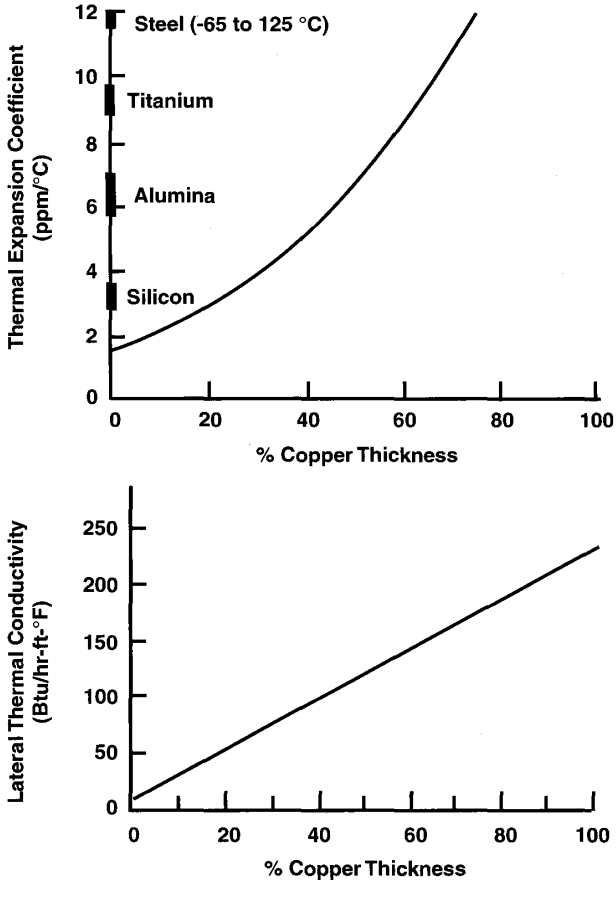

FIGURE 10.5 Thermal conductivity and CTE of copper-invar.

The following equations can be used to determine the thermal conductivity in the *xy* plane and *z* direction for Co-Inv combinations. For the xy plane (lateral):

$$K_{xy} = ak_{\text{Cu}} + (1 - a)k_{\text{inv}} \tag{10.2a}$$

For the *z* direction:

$$K_z = \left(\frac{a}{k_{\text{Cu}}} + \frac{1-a}{k_{\text{inv}}} \right)^{-1} \tag{10.2b}$$

SEC et al. v. MRI
SEC Exhibit 1018.0065
IPR2023-00254

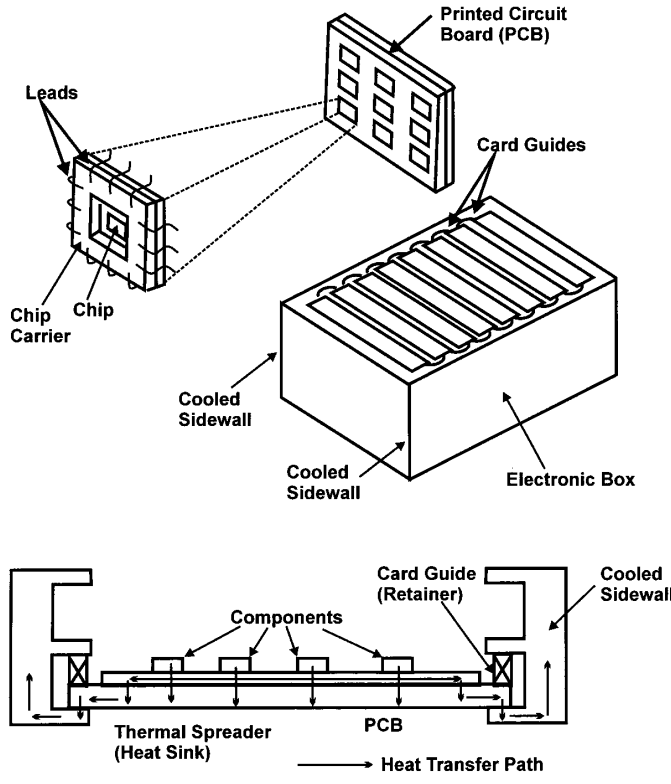

FIGURE 10.6 Thermal path for a common board in an electronic box.

where a is the fraction of copper involved and k_{Cu} and k_{inv} are thermal conductivities of copper and invar, respectively.

10.4 BOARD-COOLING METHODS

Board-level thermal analysis includes conduction cooling and direct air cooling of components. The board and components are cooled by air through convection for the latter case, which will be discussed in the next chapter. On the other hand, heat generated from components, for the former case, is conducted through the PCB and is then transferred to the chassis at the edges of the board as illustrated in Figure 10.6. Typically, the board is attached to the chassis by a card retainer. The card retainer provides a better thermal path by

SEC et al. v. MRI
SEC Exhibit 1018.0066
IPR2023-00254

forcing the board into contact with the chassis. A parametric study of a conduction-cooled board is provided in Laderman et al. [4]. The parameters in the study include PCB construction, chip carrier material, lead count, chip size, and thermal via density.

To improve board thermal performance, a thermal spreader or plane (often also called a heat sink) is added to the board. For surface-mount components, the thermal spreader is generally added to the back side (opposite side from the components) of the board; however, the thermal spreader is usually added to the component side of the board for through-hole components such as DIPs and PGAs. In this case, many cutouts on the thermal spreader must be made for component leads.

10.5 BOARD THERMAL ANALYSIS

A typical printed circuit board consists of a multilayer of dielectric material and copper film. The copper layers are used to provide the chip-to-chip connections for transmitting signals, for power supply, and for grounding. The basic concern in thermal analysis is how to model the board accurately. Although the majority of the material of a PCB (probably over 95% by volume) is insulation materials, which have a very low thermal conductivity, one can never omit the contribution due to the copper layers in the thermal analysis. Any omission of the copper layer in the analysis will result in excessively high component temperatures, especially for the case of conduction-cooled PCBs. The high temperature is due to lack of heat conduction spreading because of the low thermal conductivity of the board.

The thermal conductivities of the basic materials used to construct a PCB are listed in Table 10.1. The terminology typically used to describe the thickness of a copper layer is expressed as "x-oz," which represents the weight in ounces of a copper layer with 1 ft^2 surface area. For example, the thickness of a 1-oz copper layer is about 0.00135 in.

In theory, one can include every layer of a given PCB in the thermal model, but this approach is time-consuming, and above all, it is not practical. This is because the construction of a PCB is very complex. As shown in Figure 10.7, a typical PCB frequently has more than 10 layers of each type of material (dielectric material and copper) laminated together, with the total thickness of the board less than 0.1 in. In addition, the coverage of the copper layers is not always 100%. There are often many cutouts over a copper layer, and sometimes only traces of the copper exist on some given layers.

Table 10.1 Thermal Conductivity of Basic PCB Materials

Material	W/(m·°C)	Btu/(hr·ft·°F)
Copper layer	386.00	223.180
Dielectric layer:		
G10	0.30	0.173
FR-4	0.35	0.202
Polyimide	0.52	0.301

SEC et al. v. MRI
SEC Exhibit 1018.0067
IPR2023-00254

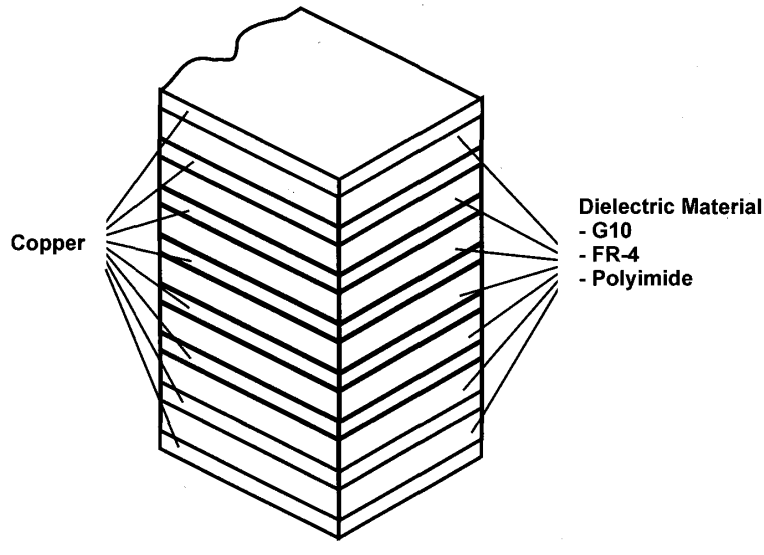

FIGURE 10.7 Typical PCB construction.

The practical approach in the thermal analysis is to use the so-called equivalent thermal conductivities for the *xy* plane and the *z* direction (across the thickness) of the board. The basic treatment is to assume that the PCB consists of a single layer of material with equivalent thermal conductivities of K_{xy} and K_z.

10.6 EQUIVALENT THERMAL CONDUCTIVITY

As noted in the previous section, the two equivalent thermal conductivities of a printed circuit board (PCB) are the planar (lateral) thermal conductivity K_{xy} and the normal thermal conductivity (in the *z* direction). These can be determined through the respective methods described in the rest of this section.

10.6.1 Planar Thermal Conductivity K_{xy}

The laminated layers are considered as parallel paths in calculation of the equivalent thermal conductivity. For a parallel network, the total resistance is

$$\frac{1}{R_{xy}} = \frac{1}{R_1} + \frac{1}{R_2} + \frac{1}{R_3} + \ldots \tag{10.3}$$

SEC et al. v. MRI
SEC Exhibit 1018.0068
IPR2023-00254

where

R_i = thermal resistance for the i^{th} layer, $i = 1, 2, 3, \ldots$
$= \dfrac{L_i}{k_i A_i c_i}$
L_i = length of i^{th} layer
A_i = cross-sectional area of i^{th} layer (normal to heat flow)
k_i = thermal conductivity of i^{th} layer
c_i = fraction of total coverage for i^{th} layer
(e.g., 0.8 if the cutout for a given layer is 20%)

Rearranging Equation 10.3, we have

$$\frac{K_{xy}A}{L} = \Sigma\left(\frac{c_i k_i A_i}{L_i}\right)_{in} + \Sigma\left(\frac{c_i k_i A_i}{L_i}\right)_{Cu} \tag{10.4}$$

where the subscripts "in" and "Cu" represent the dielectric insulation material and the copper, respectively. A is the total cross-sectional area over the thickness of a PCB; i.e., $A = t$ (thickness) times w (width). Since $L = L_1 = L_2 = L_3 = \ldots$, Equation 10.4 can be rewritten as follows:

$$K_{xy} = \Sigma\left(\frac{c_i k_i A_i}{A}\right)_{in} + \Sigma\left(\frac{c_i k_i A_i}{A}\right)_{Cu} \tag{10.5}$$

Assuming there is 100% coverage on each layer ($c_i = 1$), Equation 10.5 can be reduced to the following form:

$$K_{xy} = k_{in}\left(\frac{t_{in}}{t_{PCB}}\right) + k_{Cu}\left(\frac{t_{Cu}}{t_{PCB}}\right) \tag{10.6}$$

where

t_{in} = total thickness of dielectric material
t_{Cu} = total thickness of copper film
t_{PCB} = total thickness of printed circuit board
$= t_{in} + t_{Cu}$

10.6.2 Normal Thermal Conductivity K_z

In considering the heat flow normal to each layer, it is assumed that the resistances are in series, as follows:

$$R_z = R_1 + R_2 + R_3 + \ldots \tag{10.7}$$

or

SEC et al. v. MRI
SEC Exhibit 1018.0069
IPR2023-00254

$$\frac{t_{\text{PCB}}}{K_z A_z} = \Sigma\left(\frac{t_i}{c_i k_i A_i}\right)_{\text{in}} + \Sigma\left(\frac{t_i}{c_i k_i A_i}\right)_{\text{Cu}} \tag{10.8}$$

Since $A_z = A_i$, the equivalent thermal conductivity in the z direction is

$$K_z = \frac{t_{\text{PCB}}}{\Sigma(t_i/c_i k_i)_{\text{in}} + \Sigma(t_i/c_i k_i)_{\text{Cu}}} \tag{10.9}$$

Again, if $c_i = 1$ (100% coverage on each layer), we have

$$K_z = \frac{t_{\text{PCB}}}{t_{\text{in}}/k_{\text{in}} + t_{\text{Cu}}/k_{\text{Cu}}} \tag{10.10}$$

For $c_i = 1$, Equations 10.5 and 10.9 are also reduced to those presented in Guenin [5].

Example 10.1

A PCB with thickness 0.1 in consists of 12 layers of $^1/_2$-oz copper and polyimide. Determine the equivalent thermal conductivities K_{xy} and K_z.

Solution

Assuming each layer has 100% coverage,

$$t_{\text{Cu}} = 12 \times \frac{0.00135}{2} = 0.0081 \text{ in} \qquad \text{and} \qquad t_{\text{in}} = 0.1 - 0.0081 = 0.0919 \text{ in}$$

From Table 10.1, we have

$$k_{\text{Cu}} = 386 \text{ W/(m·°C)} = 9.66 \text{ W/(in·°C)}$$

and

$$k_{\text{in}} = 0.52 \text{ W/(m·°C)} = 0.0132 \text{ W/(in·°C)}$$

From Equation 10.6,

$$K_{xy} = 0.0919\left(\frac{0.0132}{0.1}\right) + 0.0081\left(\frac{9.66}{0.1}\right) = 0.794 \text{ W/(in·°C)}$$

and from Equation 10.10,

$$K_z = \frac{0.1}{0.0919/0.0132 + 0.0081/9.66} = 0.0144 \text{ W/(in·°C)}$$

SEC et al. v. MRI
SEC Exhibit 1018.0070
IPR2023-00254

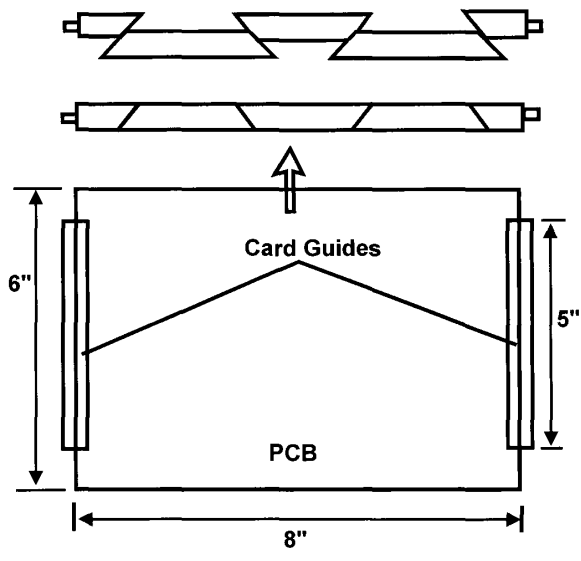

FIGURE 10.8 Dimensions of board and card guides for Example 10.2.

Comments:

1. The present example is relatively simple because each layer has 100% coverage.
2. Units such as W/(in·°C) for thermal conductivity and W/(in²·°C) for heat transfer coefficient are often used in the electronics industry for convenience because the heat dissipation is typically expressed in watts while drawing dimensions are frequently given in inches.
3. For printed circuit board analysis, one can consider the present PCB a single, homogeneous layer with equivalent thermal conductivities K_{xy} and K_z.

Example 10.2

The board of Example 10.1 is clamped into a chassis similar to that shown in Figure 10.6. The board dimensions and the length of the card guide (or retainer) are given in Figure 10.8. Determine the temperature rise from the center of the board to the chassis if 12 W of heat is uniformly distributed over the board.

Solution

Because of the symmetry, the analysis can be performed on half the configuration:

SEC et al. v. MRI
SEC Exhibit 1018.0071
IPR2023-00254

$$q = \frac{12}{2} = 6 \text{ W}$$

$$L = \frac{8/2}{2} = 2 \text{ in}$$

$$A = 6 \times 0.1 = 0.6 \text{ in}^2$$

$$R_{\text{pcb}} = \frac{L}{K_{xy}A} = \frac{2}{0.794 \times 0.6} = 4.2°\text{C/W}$$

The temperature rise from the center to the edge of the board is

$$\Delta T_1 = qR_{\text{PCB}} = 6 \times 4.2 = 25.2°\text{C}$$

Assume the thermal resistance of the card guide is 2.5°C·in/W. (This is a very typical value.) Then

$$R_{\text{guide}} = \frac{2.5}{5} = 0.5°\text{C/W}$$

The temperature rise from the board to the chassis is

$$\Delta T_2 = qR_{\text{guide}} = 6 \times 0.5 = 3°\text{C}$$

Therefore, the total temperature rise is

$$\Delta T = \Delta T_1 + \Delta T_2 = 25.2 + 3 = 28.2°\text{C}$$

Comments:

1. The actual thermal resistance of the card guide depends on the construction of the card guide, and the value can be obtained from the manufacturer's data sheet.
2. The suggested card guide thermal resistance from the manufacturer should be applied only to the region directly covered by the card guide because the contact pressure will decrease in the region outside the range (length) of the card guide.

REFERENCES

1. C. Maxfield and D. Kuk, "A Multichip Module Primer," *Printed Circuit Des.*, June 1992.
2. F. J. Dance, "Can PWB's Meet the Surface Mount Challenge?" Part 1, *Electronics*, May 1983.
3. F. J. Dance, "Can PWB's Meet the Surface Mount Challenge?" Part 2, *Electronics*, June 1983.
4. A. J. Laderman, D. B. Osborn, R. M. Grabow, and M. C. Bury, "Parametric Study of Conduction Cooling for High Power Density Electronics," *Proc. Int. Symp. Cooling Technology for Electronic Equipment*, Honolulu, March 17–21, 1987.

SEC et al. v. MRI
SEC Exhibit 1018.0072
IPR2023-00254

5. B. M. Guenin, "Conduction Heat Transfer in a Printed Circuit Board," *Electronic Cooling Mag.* 4(2), 1998.
6. R. J. Hannemann, "Physical Technology and the Air Cooling and Interconnection Limits for Mini- and Microcomputers," Chapter 1 in A. Bar-Cohen and A. D. Kraus, eds., *Advances in Thermal Modeling of Electronic Components and Systems,* Vol. 2, ASME Press, New York, 1990.
7. J. W. Dally, *Packaging of Electronic Systems: A Mechanical Engineering Approach,* McGraw-Hill, New York, 1990.

SEC et al. v. MRI
SEC Exhibit 1018.0073
IPR2023-00254

Chapter 11

DIRECT AIR COOLING AND FANS

Simplicity and easy maintenance make direct air cooling a most attractive approach in cooling of electronics. Direct air cooling can take an active form, represented by forced convection; or a passive form, as free or natural convection. Passive cooling has always been the preferred choice. However, it is generally limited to systems with very low heat dissipation because of the poor heat transfer coefficients being characteristic of free convection.

Forced-air cooling over printed circuit boards (PCBs) is often encountered in electronic equipment. Variations in component size and spacing, cause flow separation over components and recirculation between components. Analysis of the flow field is a fully three-dimensional (3D) problem and extremely complex. Heat transfer involves convection from components and the PCB to the airstream, conduction from components to the PCB, and heat spreading along the PCB, and also radiation exchange among components and from components to surroundings.

Theoretically, the only possible way to analyze components over a PCB is by means of a 3D computational fluid dynamics (CFD) program. The thermal model with this approach may become very large, because of the large number of components involved in a typical board. The number of components on a PCB can be over one hundred. A simple analysis approach, utilizing a general-purpose thermal analyzer, is sometimes used to analyze the entire board. The most difficult task in using such a program is estimating the heat transfer coefficients over the components and the board, which are required as input, because of the complicated flow field.

11.1 PREVIOUS WORK

Heat transfer involving flow over solid objects has a great engineering application. Because of its importance, many efforts have been made to examine this type of problem. Most experimental studies idealize the integrated circuit (IC) components as rectangular blocks as shown in Figure 11.1. In the simplest case [1], the board is fully populated with components in an array with all of equal height t and equal spacing s, whereas in the more general case, the components are of varying heights and there are some "missing" modules [1–4]. The basic findings from References 1 through 4 can be summarized as follows:

SEC et al. v. MRI
SEC Exhibit 1018.0074
IPR2023-00254

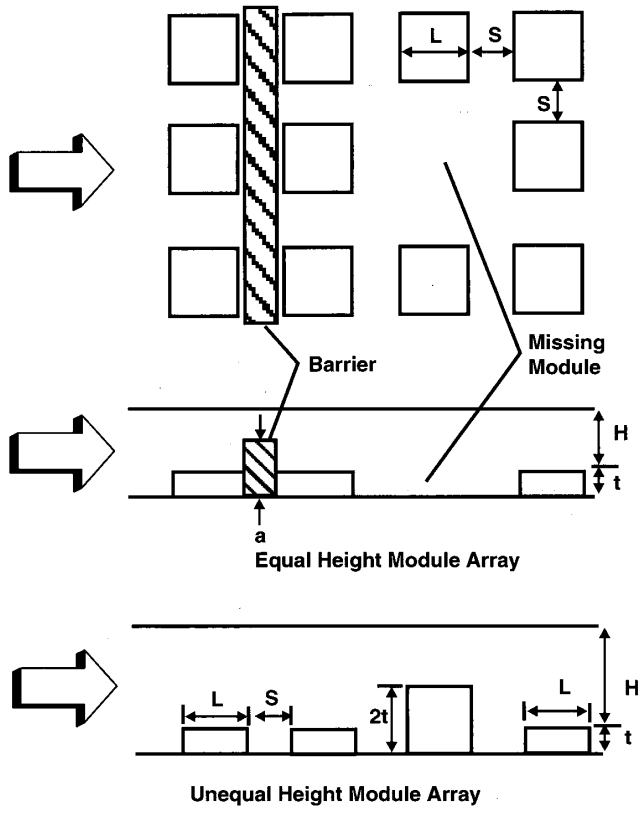

FIGURE 11.1 Array of rectangular modules in a channel.

1. Within an array of equal-height components, fully developed flow occurs at about the fifth row.
2. The heat transfer coefficient at neighboring modules is increased when there is a missing module in the array. The greatest enhancement of about 40% takes place on the module located immediately downstream of the missing module. The effect gradually decreases for the further downstream modules.
3. The enhancement of heat transfer coefficient due to the missing module is greater for flow at low Reynolds numbers, because the flow at a low Reynolds number penetrates the cavity created by the missing module while a high–Reynolds number flow tends to skim over the cavity.

SEC et al. v. MRI
SEC Exhibit 1018.0075
IPR2023-00254

4. A missing module located at the side and downstream of the monitored module generates only a modest enhancement.
5. The application of a barrier in an array increases the heat transfer coefficient. The greatest improvement, which is about a factor of 2, occurs at the second row downstream of the barrier.
6. The heat transfer coefficient at a monitored module is increased when the monitored module is either taller or shorter than other modules in the array. Enhancement at a taller module is caused by direct impingement of the airflow on the portions of the module protruding above other modules. On the other hand, the improvement at the shorter module results from the recirculation zone in the cavity created by the gap in height in the array. The enhancement (up to 80%) for a taller module increases as the module height increases. The enhancement for a shorter module is less pronounced (up to 26%) and is increased as the Reynolds number increases.
7. The largest enhancement (up to 50%) of the heat transfer coefficient due to a taller module over the array occurs on the modules by the side of the taller module, and the second best location is just downstream of the taller module.8.
8. The entry region for a regular array with equal-height modules is generally characterized by higher heat transfer coefficients than is the developed-flow region. In an array containing a tall module, on the other hand, the heat transfer coefficient becomes relatively higher downstream as the tall module is moved along streamwise locations.
9. Any enhancement of the heat transfer coefficient also increases the pressure drop.

The preceding discussions provide an in-depth understanding of the physical phenomena associated with direct air–cooled components on a PCB. Furthermore, this information can be used as a guideline for placing components on a board so as to improve thermal performance.

11.2 HEAT TRANSFER CORRELATIONS

For an array of equal-height modules, the Nusselt number for fully developed flow can be represented as follows [1]:

$$\mathrm{Nu}_L = 0.0935\mathrm{Re}_H^{0.72} \tag{11.1}$$

where

$$\mathrm{Nu}_L = \frac{hL}{k}$$

$$\mathrm{Re}_H = \frac{\rho VH}{\mu}$$

H = height of flow passage (above module)

SEC et al. v. MRI
SEC Exhibit 1018.0076
IPR2023-00254

h = heat transfer coefficient
L = side dimension of square module
V = mean velocity based on flow cross section above module
k = thermal conductivity
ρ = density
μ = viscosity

Another correlation can be expressed as follows [4]:

$$\mathrm{Nu}_t = 0.075\mathrm{Re}_t^{0.653}\left(\frac{H}{t}\right)^{-0.543}\left(\frac{L}{t}\right)^{1.48} \tag{11.2}$$

where

$$\mathrm{Nu}_t = \frac{ht}{k}$$

$$\mathrm{Re}_t = \frac{\rho Vt}{\mu}$$

t = module height

Equation 11.1 was obtained from experiments with the following parameters: $t/L = {}^3/_8$, $s/L = {}^1/_4$, and $(H + t)/L = 1$. On the other hand, the module and array configurations for Equation 11.2 are $(H + t)/L = 10/20$ and $5/30$, $s/L = 8/20$ and $12/30$, and $H/t = 5/10$ and $12.8/5$. The heat transfer coefficient h computed from Equation 11.1 increases when the module length L decreases, while the opposite trends are found from Equation 11.2 if other parameters remain constant.

Re_H (= $\rho VH/\mu$) defined in Equation 11.1 can be rewritten as mw/μ, where m is the mass flow rate and w is the spanwise width. The Reynolds number becomes independent of the gap height H. Therefore, the Nusselt number or the heat transfer coefficient in Equation 11.1 is also independent of the gap height. For a given flow rate and channel width w, the velocity of the airflow increases when the gap height decreases. The heat transfer coefficient should also increase as the velocity increases. In other words, the heat transfer coefficient depends indirectly on the gap height for a given flow rate; however, the effect due to the gap height cannot be found in the present form of Equation 11.1.

A large number of thermal tests were conducted by the Cranfield Institute of Research in England on ceramic dual in-line packages (DIPs) soldered onto PCBs in a variety of array configurations. Based on the test data, the following correlations [5] were obtained for air velocities ranging from 0 to 8 m/s:

- For PCBs fitted into card guides,

$$h = 5.3\left(\frac{b}{d}\right) + \frac{6.2(\rho V)^{0.8}[(d/b)-1]^{0.13}}{(nd)^{0.36}} \tag{11.3}$$

where

SEC et al. v. MRI
SEC Exhibit 1018.0077
IPR2023-00254

b = streamwise dimension of component, m
d = streamwise component pitch, m
n = streamwise component location (numbered from PCB leading edge)
V = mean velocity based on minimum free flow area between PCBs, m/s

The units for the heat transfer coefficient and air density are W/(m^2·°C) and kg/m^3, respectively.

- Without card guides at the PCB leading edges, the heat transfer coefficients are as follows:

$$h = 5.3\left(\frac{b}{d}\right) + \frac{7.6(\rho V)^{0.8}[(d/b)-1]^{0.13}}{(nd)^{0.2}} \tag{11.4}$$

For convenience, Equation 11.3 can also be rewritten in terms of English units and it becomes [6]:

$$h = 0.93\left(\frac{b}{d}\right) + \frac{0.225(\rho V)^{0.8}[(d/b)-1]^{0.13}}{(nd)^{0.36}} \tag{11.5}$$

where the units of b and d are ft and V is in ft/min. The product ρV is often referred to as the mass velocity G. The units for the density and the heat transfer coefficient are lb_m/ft^3 and Btu/(hr·ft^2·°F), respectively.

If only the high–velocity range data are considered, Equation 11.3 can be replaced by the following dimensionless equation:

$$\mathrm{Nu} = 0.19\,\mathrm{Re}^{0.7}\left(\frac{d}{b}-1\right)^{0.13}\mathrm{Pr}^{1/3} \tag{11.6}$$

The characteristic length used to define the Nusselt and Reynolds numbers is the distance from the PCB leading edge, x. Pr is the Prandtl number. Equation 11.6 yields values of the heat transfer coefficient typically twice those obtained from the usual relationship for turbulent flow over a flat plate.

For plated through-hole (PTH) mounting technology, electronic components are typically mounted on one side of a PCB with the leads going through the holes and extending to the opposite (back) side of the PCB for soldering. Therefore, some of the heat dissipated from the components is conducted through the leads to the back side of the PCB and is convected to the airstream over the back side. This situation is especially true when there are a large number of copper circuit runs on the back side of the PCB to spread heat. In this case, the following heat transfer correlations for the parallel plates with uniform but different heat flux on each wall [7, 8] may be used:

- For fully developed laminar flow, use

SEC et al. v. MRI
SEC Exhibit 1018.0078
IPR2023-00254

$$\mathrm{Nu}_i = \frac{5.385}{1 - 0.346(q_j''/q_i'')} \tag{11.7}$$

- For fully developed turbulent flow, use

$$\mathrm{Nu}_i = \frac{0.0334\,\mathrm{Re}^{0.755}}{1 - 0.49\,\mathrm{Re}^{-0.1}(q_j''/q_i'')} \tag{11.8}$$

where the quantities q_i'' and q_j'' are the heat fluxes on walls i and j, respectively. The Nusselt and Reynolds numbers are based on the hydraulic diameter. For parallel plates where the plate width is much larger than the gap, the hydraulic diameter is equal to twice the distance between the plates. If components are packaged close together, a new surface can be considered to form over the top of the components; therefore, the hydraulic diameter is equal to $2H$.

11.3 PRESSURE DROP CORRELATIONS

Some pressure drop data are provided in references 1 and 3 for regular arrays with and without a tall module as well as with or without a barrier. For the case without a tall module or barrier, the correlations for parallel plates at fully turbulent flow under-predict the pressure drop over the array by just over 10%. In this case, the spacing between two plates is the distance H from the top of the modules to the upper plate, as defined following Equation 11.1, and the hydraulic diameter used to compute the friction factor is $2H$.

On the basis of experiments on ceramic DIPs, Wills [5] presented an empirical correlation for the pressure drop in the form

$$\Delta P = \rho V^2 \left(\frac{0.033L}{s^{1.3} V^{0.3}} + 1.9 \Sigma K \right) \tag{11.9}$$

where

ΔP = pressure drop, N/m^2
K = loss coefficients
L = PCB streamwise length, m
s = PCB pitch, m
V = mean velocity based on minimum free flow area, m/s
ρ = air density, kg/m^3

The loss factor for a card guide or turbulator is approximately as follows:

$$K = \left(\frac{y}{s - y} \right)^2 \tag{11.10}$$

where y is the height of the protuberance (e.g., card guide width).

SEC et al. v. MRI
SEC Exhibit 1018.0079
IPR2023-00254

Equation 11.9 predicts a much higher pressure drop (about 4 times) than those obtained from the equations for parallel plates or the results of references 1 and 3 for the cases of an array with equal-height modules. This is because Equation 11.9 is obtained from tests with actual DIPs on the PCB. The leads of DIPs may cause additional turbulence and disturbance in the flow.

Example 11.1

DIPs, size 0.3 in × 1.2 in, are mounted on a PCB as shown in Figure 11.2 aligned in 17 columns pitched at 0.35 in and 5 rows pitched at 1.25 in. The DIPs protrude 0.2 in from the PCB. The dimensions of the PCB are 6 in × 6 in × 0.1 in, and the spacing between PCBs is 0.8 in. Air entering the PCBs at 120°F with a mass flow rate of 51 lb_m/h flows normal to the 1.2-in side of the DIPs. Determine the maximum and minimum heat transfer coefficients.

Solution

Equation 11.5 will be used in the following calculations. The free flow area is defined as follows:

$$A = (0.8 - 0.1) \times 6 - 5(0.2 \times 1.2) = 3 \text{ in}^2$$

The mass flow velocity is:

$$\rho V = G = \frac{m}{A} = \frac{51}{3/144} = 2448 \text{ lb}_m/(\text{ft}^2 \cdot \text{hr}) = 40.8 \text{ lb}_m/(\text{ft}^2 \cdot \text{min})$$

From the dimensions in Figure 11.2,

$$\left(\frac{d}{b} - 1\right)^{0.13} = \left(\frac{0.35}{0.3} - 1\right)^{0.13} = 0.792 \quad \text{and} \quad \frac{b}{d} = \frac{0.3}{0.35} = 0.85$$

From Equation 11.5, the heat transfer coefficient is

$$h = 0.93\left(\frac{b}{d}\right) + \frac{0.225(\rho V)^{0.8}[(d/b) - 1]^{0.13}}{(nd)^{0.36}}$$

The maximum heat transfer coefficient occurs at the first column (n = 1):

$$h_1 = 0.93 \times 0.857 + \frac{0.225 \times (40.8)^{0.8} \times 0.792}{(1 \times 0.35/12)^{0.36}}$$
$$= 13.164 \text{ Btu}/(\text{hr} \cdot \text{ft}^2 \cdot °\text{F})$$

The minimum heat transfer coefficient occurs at the 17th column (n = 17):

SEC et al. v. MRI
SEC Exhibit 1018.0080
IPR2023-00254

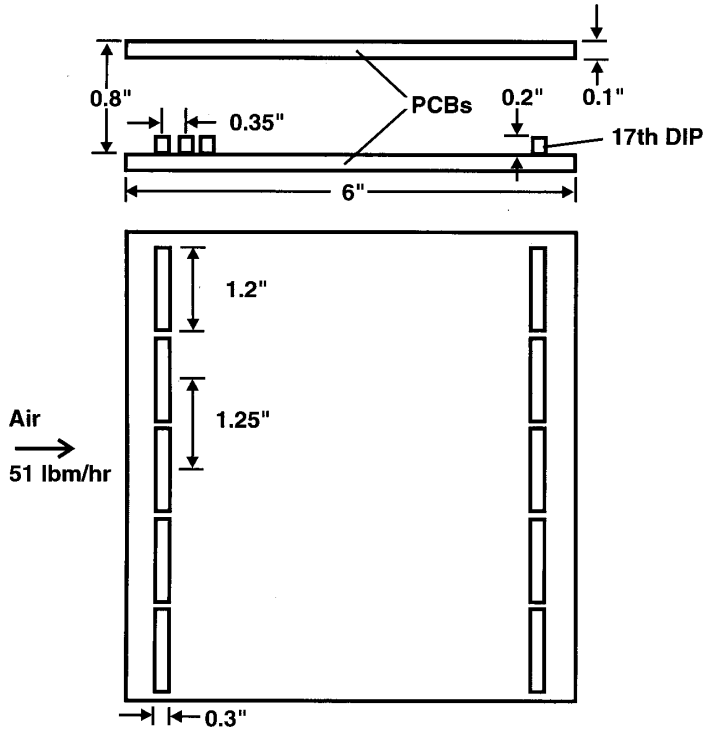

FIGURE 11.2 Airflow over the PCB of Example 11.1.

$$h_{17} = 0.93 \times 0.857 + \frac{0.225 \times (40.8)^{0.8} \times 0.792}{(17 \times 0.35/12)^{0.36}}$$
$$= 5.26 \text{ Btu/(hr} \cdot \text{ft}^2 \cdot {}^\circ\text{F)}$$

If the nondimensional Equation 11.6 is used, the maximum and minimum heat transfer coefficients occur at x_1 and x_{17}, respectively.

At the center of the first column, or $x_1 = 0.3/2 = 0.15$ in $= 0.0125$ ft,

$$(\text{Re}_x)_1 = \frac{Gx_1}{\mu} = \frac{2448 \times 0.0125}{0.048} = 637.5$$

$$\frac{hx}{k} = \text{Nu} = 0.19\text{Re}^{0.7}\left(\frac{d}{b} - 1\right)^{0.13} \text{Pr}^{1/3}$$
$$= 0.19 \times 91.862 \times 0.792 \times 0.892 = 12.33$$

SEC et al. v. MRI
SEC Exhibit 1018.0081
IPR2023-00254

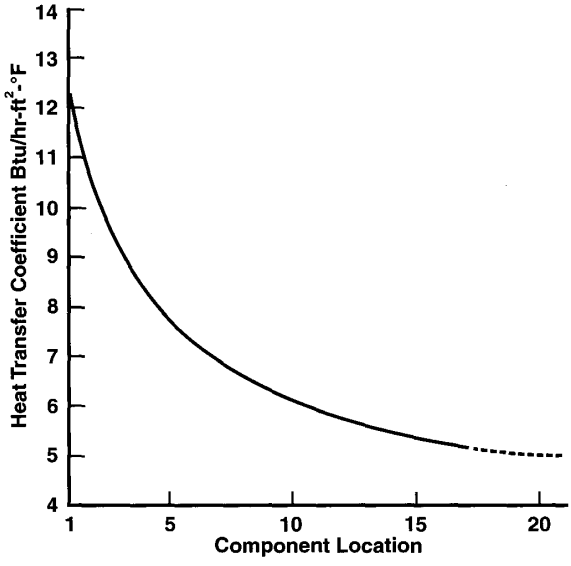

Figure 11.3 Local heat transfer coefficient over the DIPs of Example 11.1.

$$h_1 = 12.33 \times \frac{0.016}{0.0125} = 15.78 \text{ Btu/(hr} \cdot \text{ft}^2 \cdot \text{°F)}$$

where Pr = 0.715 and k = 0.016 Btu/(hr·ft²·°F). At the center of the 17th column, or x_{17} = 16 × 0.35 + 0.3/2 = 5.75 in = 0.479 ft,

$$(\text{Re}_x)_{17} = \frac{2448 \times 0.479}{0.048} = 24437.5$$

$$\text{Nu} = 0.19 \times 1179.342 \times 0.792 \times 0.892 = 158.3$$

$$h_{17} = 158.3 \times \frac{0.016}{0.479} = 5.28 \text{ Btu/(hr} \cdot \text{ft}^2 \cdot \text{°F)}$$

The results clearly indicate that Equation 11.5 and Equation 11.6 are in excellent agreement for the region with high Reynolds numbers. The local heat transfer coefficients based on Equation 11.5 are plotted in Figure 11.3. It appears that fully developed flow would begin at about the 20th column and the heat transfer coefficient at this condition would be 5 Btu/(hr·ft²·°F).

It is of interest to compare the present results with those obtained from the correlation for parallel plates. Since the components are so closely packaged, a

SEC et al. v. MRI
SEC Exhibit 1018.0082
IPR2023-00254

new surface is formed at the top of the components. The new spacing between plates becomes

$$H = 0.8 - 0.1 - 0.2 = 0.5 \text{ in}$$

The free flow area is

$$A = (0.8 - 0.1 - 0.2) \times 6 = 3 \text{ in}^2$$

and the mass velocity is

$$G = \frac{m}{A} = \frac{51}{3/144} = 2448 \text{ lb}_m/(\text{ft}^2 \cdot \text{hr})$$

The hydraulic diameter for parallel plates is twice the distance between the plates, or $D_h = 2 \times 0.5 = 1$ in. Thus,

$$\text{Re} = \frac{GD_h}{\mu} = \frac{2448 \times \frac{1}{12}}{0.048} = 4250 > 2300 \Rightarrow \text{turbulent flow}$$

For fully developed turbulent flow, Equation 11.8 can be applied. Assuming that only the bottom wall is heated,

$$\text{Nu} = 0.0334 \text{ Re}^{0.755} = 0.0334(4250)^{0.755} = 18.331$$

and

$$h = 18.331 \times \frac{0.016}{1/12} = 3.52 \text{ Btu}/(\text{hr} \cdot \text{ft}^2 \cdot {}^\circ\text{F})$$

The results (h = 3.52 versus h = 5) clearly demonstrate that using the parallel plate assumption is too conservative.

11.4 HEAT TRANSFER ENHANCEMENT

To enhance thermal performance, individual small heat sinks are frequently added to hot components to maintain the component temperature at the desired limit. Three typical heat sinks used with PGAs are shown in Figure 11.4. Of these, the straight-finned heat sinks are also often applied to DIPs. The enhancement gained from most heat sinks is primarily due to the increased surface area for heat transfer.

One way to increase the heat transfer area of a heat sink is to increase its number of fins. This action, however, reduces the spacing between fins and increases the flow resistance. The net result for a given fan or pump is to reduce the available flow through the heat sink, in turn decreasing the heat transfer coefficient.

SEC et al. v. MRI
SEC Exhibit 1018.0083
IPR2023-00254

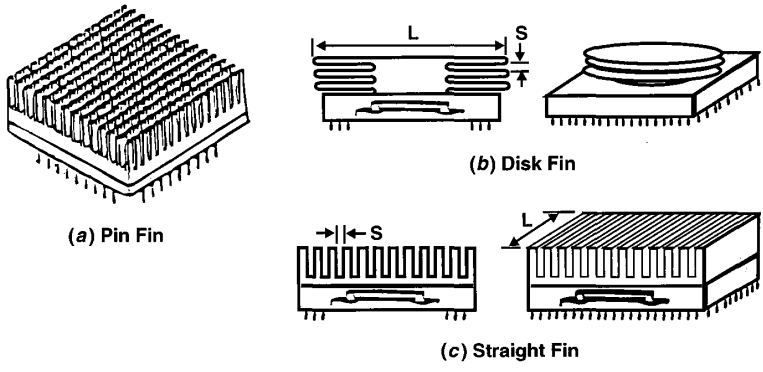

FIGURE 11.4 Diagrams of heat sinks applied to PGAs: (*a*) pin-fin, (*b*) disk-fin, and (*c*) straight-fin heat sinks.

Just as with flow over a solid, a boundary layer will develop in the space between fins. A general rule is that the fin spacing must be large enough to prevent boundary-layer interference at the lowest expected velocity. In other words, the space between fins must be greater than twice the boundary-layer thickness at the exit of the heat sink to avoid excessive flow resistance. The boundary-layer thickness over a flat plate is as follows:

$$\delta = \frac{5x}{\mathrm{Re}_x^{0.5}} = 5\left(\frac{\mu x}{\rho V}\right)^{0.5} \tag{11.11}$$

where ρ and μ are density and viscosity of the fluid, V is the free-stream velocity, and x is the distance from the leading edge. To define the minimum fin spacing, x is set equal to the length of the heat sink in the flow direction. Figure 11.5 [9] illustrates the effect of the fin spacing on the flow pattern for heat sinks. The flow will be pushed away from the heat sink if boundary-layer interference occurs as shown in Figure 11.5*c*.

A third surface, the fin base, must be accounted for in the analysis of any heat sink, complicating the examination of boundary-layer interference. Hannemann et al. [9] experimentally determined the critical space between fins as follows:

$$s = 3.41\left(\frac{\mu L}{\rho V}\right)^{0.5} \tag{11.12}$$

where L is the length of the heat sink in the flow direction, and where s and L are in meters, V is in m/s, μ is in kg·m/s, and ρ is in kg/m^3. For a given heat sink with

SEC et al. v. MRI
SEC Exhibit 1018.0084
IPR2023-00254

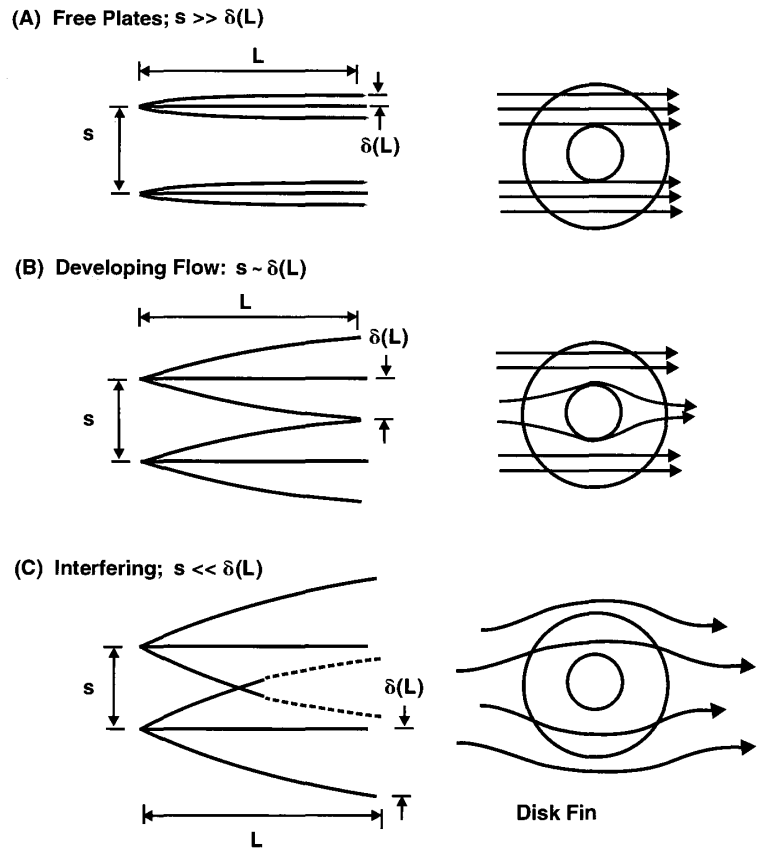

FIGURE 11.5 Flow patterns in a heat sink: (*a*) free plates, $s >> \delta(L)$; (*b*)developing flow, $s \approx \delta(L)$; (*c*) interfering, $s << \delta(L)$.

fixed dimensions, Equation 11.12 can be used to determine the critical velocity V_c required to avoid boundary-layer interference. The mean heat transfer coefficient experimentally determined over the total heat sink area is

$$h = 4.37\left(\frac{V}{L}\right)^{0.5} \quad \text{for} \quad \frac{A_f}{A} \geq 0.85 \tag{11.13}$$

where the units for h are W/(m²·°C), V is in m/s, and L is meters. A_f/A is the ratio of the fin area to the total area of a heat sink. The above correlations

SEC et al. v. MRI
SEC Exhibit 1018.0085
IPR2023-00254

are based on tests conducted for disk and straight fins with the following configurations:

Number of fins: 2–38
Fin length L: 1.52–8.38 cm
Fin spacing s: 0.089–0.330 cm
Velocity V_c: 0.5–11.3 m/s

A reduction in fin spacing decreases the flow through the heat sink, resulting in a decrease in the heat transfer coefficient. On the other hand, the number of fins on the heat sink is increased, and so is the total heat transfer surface. In optimizing thermal design, one should never focus on the heat transfer coefficient alone. The most important factor to consider is the product of the heat transfer coefficient, the heat transfer area, and the fin efficiency.

In addition to the fin spacing, several factors such as the tip and side (lateral) clearances of a heat sink have a direct impact on the available flow through the heat sink. This bypass phenomenon of airflow over a heat sink is one of the most important factors affecting thermal performance. The larger the clearance, the less flow is available to the heat sink. This result follows because the fluid always flows through the least resistant path. The result of airflow bypass is to reduce the heat transfer coefficient. The subject of flow bypass has been discussed in detail [10–12].

The thermal resistance of a heat sink is defined as follows:

$$\theta = \frac{T_w - T_{a,i}}{q} \tag{11.14}$$

where q is the component heat dissipation, T_w is the average heat sink base temperature, and $T_{a,i}$ is the bulk fluid temperature at the inlet of the heat sink. Equation 11.14 can be rewritten in the following form:

$$\theta = \theta_c + \theta_h$$

$$= \frac{T_{a,o} - T_{a,i}}{q} + \frac{T_w - T_{a,o}}{q} \tag{11.15}$$

$$= \frac{1}{mc_p} + \frac{1}{\eta_o hA} \tag{11.16}$$

where $T_{a,o}$ is the bulk fluid temperature at the exit of the heat sink, m is the mass flow rate and c_p specific heat, η_o is the overall surface efficiency, h is the heat transfer coefficient, and A is the total heat transfer area.

11.5 FANS AND AIR-HANDLING SYSTEMS

The fan is the heart of any forced-air system. The fan propeller converts torque from the motor to increase the static pressure across the rotor of the fan and to energize the air particles. A fan is frequently employed in electronic equipment to

SEC et al. v. MRI
SEC Exhibit 1018.0086
IPR2023-00254

provide the airflow required for cooling. Direct air cooling is a primary example of using a fan for thermal control of electronic systems.

11.5.1 Fan Types

Fans are generally classified into two types, namely, centrifugal (blower) and axial fans. The properties of the two categories are as follows:

1. Centrifugal fans
   - Receive air at their axis of rotation and exhaust air at their periphery in a direction normal to the rotation axis
   - Produce pressure from two sources: (1) centrifugal force created by the rotating air column, and (2) kinetic energy imparted to air as it leaves the impeller
   - Create a low flow rate against a high resistance (pressure)
2. Axial fans
   - Deliver air in a direction parallel to the fan blade axis
   - Produce pressure from the change in velocity passing through the impeller
   - Provide a high airflow rate but tend to work against low pressure

The axial fan can further be divided into three categories as follows:

1. Propeller fans are the simplest type and are designed to move large volumes of air at low velocity and develop low static pressure.
2. Tube axial fans are similar to the propeller fan but provide a higher total pressure capability than propeller fans.
3. Vane axial fans are the same as the tube axial fan but have vanes to straighten the swirling flow created as the air is accelerated, resulting in improved efficiency and noise characteristics.

Basically, tube axial and vane axial fans fill the gap for performance between centrifugal and propeller fans.

11.5.2 Fan Performance and System Resistance

The fan performance or characteristic curve as given in Figure 11.6 is generated through a series of tests. The fan is tested from shutoff conditions to nearly free delivery conditions. At the shutoff point, the duct connected to the fan outlet is completely blocked. On the other hand, the outlet resistance of the duct is reduced to zero at the free delivery point. Additional test points between these two limiting conditions are obtained when various flow restrictions are placed at the end of the duct to simulate various fan operating conditions.

Fans designed to be used with a duct are generally tested with a length of duct between the fan and the measurement station. The purpose of this length of duct is to smooth out the flow as it exits the fan and to provide stable and uniform

SEC et al. v. MRI
SEC Exhibit 1018.0087
IPR2023-00254

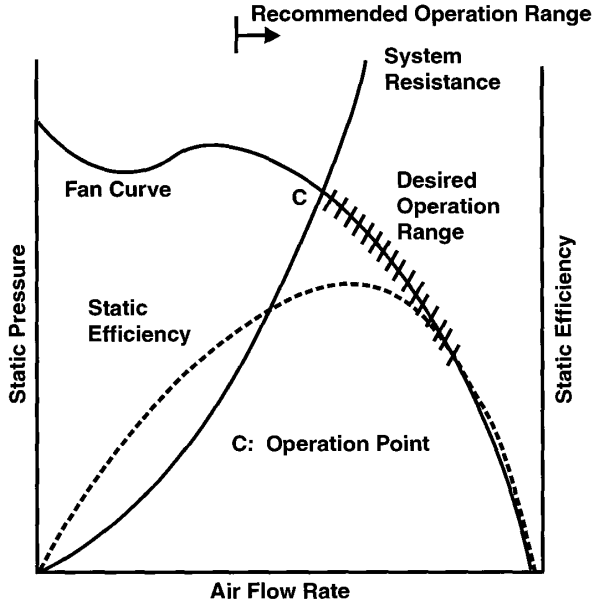

FIGURE 11.6 Typical fan curves and system operation point.

flow conditions at the measurement station. The measured pressures are then corrected back to the fan outlet conditions. Fans designed to be used without a duct are tested without the duct.

As air moves through a system, the pressure is decreased because of pressure losses due to expansions, contractions, bends, other structure blockages, and friction. For a system under consideration, the pressure drop is a function of the flow rate; therefore, a system resistance curve can be generated. The intersection of the fan performance and system resistance curves is the operation point of the system, as illustrated in Figure 11.6

Figure 11.6 also shows the static efficiency η (= Qp/hp), which is defined as the ratio of the static-pressure power to the input power (in horsepower) of a fan. The maximum static efficiency identifies the ideal combination of the flow rate and pressure of the fan. Fans should be operated as close to this point as possible if they are to achieve optimum results as given in the figure.

The fan laws relate the performance variables for any dynamically similar series of fans. The variables involved are fan size D, rotational speed N, gas density ρ, volumetric flow rate Q, pressure p, power (hp), and efficiency η. The relationships among the variables are as follows:

$$Q = \varphi N D^3 \tag{11.17a}$$

SEC et al. v. MRI
SEC Exhibit 1018.0088
IPR2023-00254

$$p = \psi\rho N^2 D^2 \tag{11.17b}$$
$$\text{hp} = \lambda\rho N^3 D^5 \tag{11.17c}$$

where φ, ψ, and λ are the constants for geometrically and dynamically similar operation and are also referred to as the flow coefficient, pressure coefficient, and power coefficient, respectively.

The specific speed N_s is often used to determine the type of fan that is best suited for a given application, one with the highest efficiency. The specific speed is a dimensionless parameter created by combining the flow and pressure coefficients to eliminate the characteristic dimension D:

$$N_s = \frac{\varphi^a}{\psi^b} = Q^a N^{2b-a} \left(\frac{p}{\rho}\right)^b D^{2b-3a} \tag{11.18}$$

In order to eliminate D,

$$2b - 3a = 0 \tag{11.19}$$

Also, for simplicity and convenience of calculation, let N be raised to the first power, i.e.,

$$2b - a = 1 \tag{11.20}$$

Combining Equations 11.19 and 11.20, we have

$$N_s = \frac{NQ^{0.5}}{(p/\rho)^{0.75}} \tag{11.21}$$

where N is angular speed (rpm), Q is in cfm (ft^3/min), and (p/ρ) is in inches of water. These are the units most commonly used by major fan manufacturers. Figure 11.7 gives the range of specific speeds for each basic type of fan.

Unless otherwise identified, fan performance data are based on dry air at standard conditions of 14.696 psia and 70°F with a density of 0.075 lb_m/ft^3. Since most fans operate at a constant speed and provide a constant volumetric flow rate, one must be cautious about the operation of a fan at high altitudes or reduced density conditions. The electronic equipment may be overheated because the mass flow rate ($m = \rho Q$) is reduced at the above-mentioned conditions. The effect of density (or altitude) on fan performance is illustrated in Figure 11.8. Because of the reduction in air density at high altitudes, both fan performance and the system resistance curves are lowered.

Sometimes, several fans are used simultaneously in a system. For two fans in series (push and pull), there is usually one fan at the inlet and another at the exit. The new fan characteristic curve for two fans in series is constructed by adding the values of *pressure* of individual fans at a given flow rate. Adding the *flow rates*

SEC et al. v. MRI
SEC Exhibit 1018.0089
IPR2023-00254

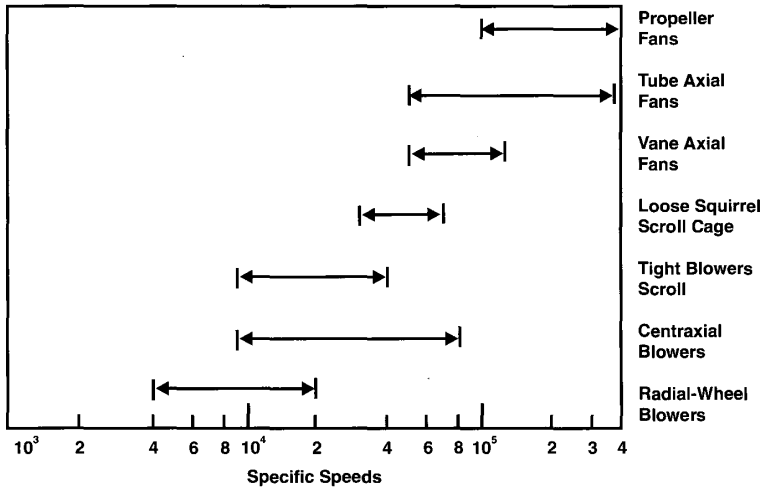

FIGURE 11.7 Range of specific speed for various types of fan.

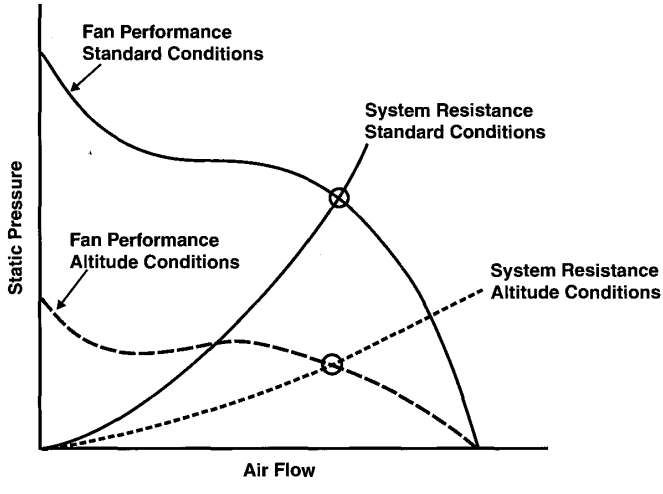

FIGURE 11.8 Effect of altitude or air density on system operation point.

SEC et al. v. MRI
SEC Exhibit 1018.0090
IPR2023-00254

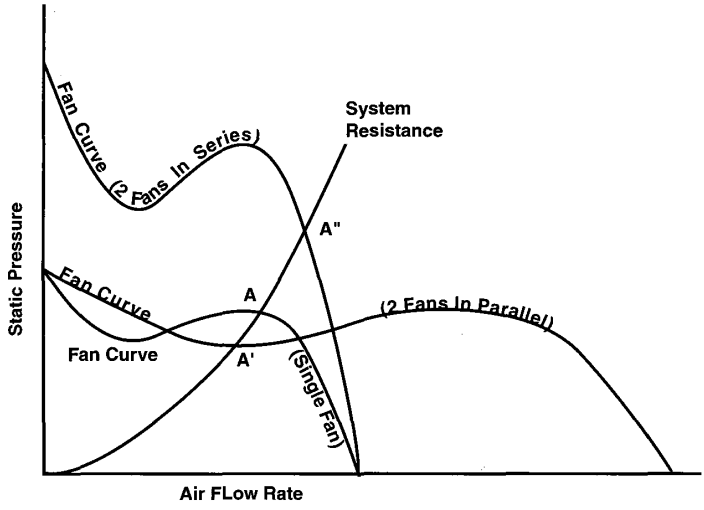

FIGURE 11.9 Performance of fans in series or parallel.

of individual fans at a given pressure yields the new characteristic curve for two fans in parallel. As compared with a single fan, two fans in series always increase the flow rate. In theory, however, it may not necessarily be true that two fans in parallel increase the flow rate. Figure 11.9 illustrates the performance of two fans in action.

Thermally, the location of a fan in a system is also an important factor to consider. The fan located at the exit of a system is usually referred to as an *exhaust fan;* it draws air through the system. This type of installation reduces the internal system pressure (to less than the ambient pressure) and possibly draws dust or dirt into the system. The advantage of this method is that no heat from the fan motor is added to the system, and therefore there is no increase in the inlet air temperature. On the other hand, a *blowing* fan, which is located at the inlet of the system, creates a higher internal system pressure and keeps dust or dirt out of the system; however, the inlet air is heated by the heat dissipation from the fan motor, and thus the air temperature is increased prior to entering the system. An exhaust fan is generally less reliable because it operates at a higher air temperature.

11.5.3 Air-Delivery Systems

The system resistance is the sum of various pressure drops in the air-delivery system. The basic equations for the pressure drop as described in Chapter 3 are still applicable. In addition to the friction loss, the system pressure drop is caused by other losses such as inlet, exit, change of cross section (expansion and

SEC et al. v. MRI
SEC Exhibit 1018.0091
IPR2023-00254

contraction), turns, and elbows. The pressure loss in the above items is typically expressed by the velocity head in the following form:

$$\Delta p = \frac{k\rho V^2}{2g_c} \tag{11.22}$$

where k is the loss coefficient and can often be found in the *Applied Fluid Dynamics Handbook* [13] and where g_c is 32.2 $lb_m \cdot ft/(lb_f \cdot s^2)$.

Frequently, the pressure drop in an airflow system is expressed in inches of water. For air at standard conditions, Equation 11.22 can be simplified as follows:

$$\Delta p = k\left(\frac{V}{4005}\right)^2 \tag{11.23}$$

where Δp is in inches of water and V is in ft/min.

The loss coefficients for various physical configurations are given in Table 11.1 [13].

A sharp bend in the tube is generally said to exist where the ratio of the radius of curvature to tube diameter is less than 2 and the bend angle is greater than 45°. A low-pressure region is created as illustrated in Figure 11.10 for turbulent flow over a sharp bend in the tube because of the flow separation from the inner wall. The flow separation and the low-pressure region along with the associated contraction of the axial flow beyond the bend are responsible for the high pressure loss in a sharp bend.

Rounding the inner corner can significantly reduce the pressure drop in the bend by attenuating the separation zone, but the improvement is limited by rounding the outer corner of a bend. The existing test data suggest that the pressure loss for turbulent flow in a sharp bend is relatively independent of Reynolds numbers if the Reynolds number is greater than 2×10^5. For smaller Reynolds numbers, the pressure loss varies approximately as $(\mathrm{Re})^a$, where a is between –0.17 and –0.2.

Vanes are often installed in sharp bends as shown in Figure 11.11, to reduce pressure loss and provide more uniform flow at the exit from the bends. For sharp bends of 45° or greater, the reduction in pressure loss is very significant with vanes in place. For more gradual bends, however, the improvement is limited because the increase in skin friction and decrease in flow area due to the vanes offset the benefit of the improved flow patterns.

Among the different types of vanes, thin concentric splitters (Figure 11.11*a*) are usually spaced so that all the vane channels have the same ratio of radius of curvature to duct width. This arrangement can be achieved if the radius of the individual splitters (r_n) is chosen so that

$$\frac{r_n}{r_{n+1}} = \left(\frac{R_i}{R_i + b}\right)^{1/(n+1)} \qquad n = 0, 1, 2, \ldots \tag{11.24}$$

where n is the number of concentric splitters, $r_0 = R_i$, $r_{n+1} = R_i + b$, and R_i and b are the inner radius of the bend and the duct width, respectively. Concentric

SEC et al. v. MRI
SEC Exhibit 1018.0092
IPR2023-00254

Table 11.1 Loss Coefficients for Various Physical Configurations

Configuration	Loss coefficient k
Entrance flush with wall at right angle: 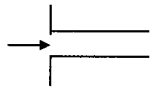	$k = 0.5$
Entrance flush with wall at arbitrary angle: 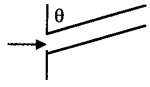	$k = 0.5 + 0.3 \cos\theta + 0.2 \cos^2\theta$
Round entrance in wall: 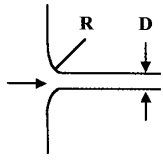	*R/D*: 0 — *k*: 0.5 *R/D*: 0.02 — *k*: 0.36 *R/D*: 0.04 — *k*: 0.26 *R/D*: 0.06 — *k*: 0.20 *R/D*: 0.08 — *k*: 0.15 *R/D*: 0.12 — *k*: 0.09 *R/D*: 0.16 — *k*: 0.06 *R/D*: > 0.16 — *k*: 0.03
Round entrance in wall with neighboring wall: 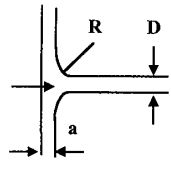	Values of *k* for various combinations of *R/D* and *a/D*:

a/D	*R/D* = 0	0.10	0.25	0.50	0.200	0.300	0.500	0.800
0.2	—	0.800	0.400	0.190	0.090	0.050	0.050	
0.3	—	0.500	0.300	0.170	0.070	0.040	0.040	
0.5	0.650	0.300	0.200	0.100	0.050	0.030	0.030	

Abrupt contraction: 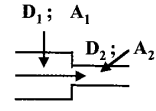	$k = 0.5(1 - A_2/A_1)$; $A_2 < A_1$
Abrupt expansion: 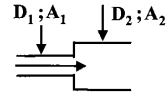	$k = (1 - A_1/A_2)^2$; $A_1 < A_2$
Exit:	$k = 1.0$

SEC et al. v. MRI
SEC Exhibit 1018.0093
IPR2023-00254

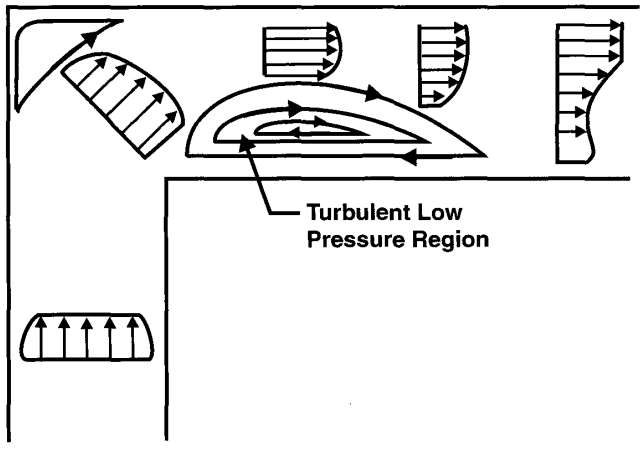

FIGURE 11.10 Turbulent flow pattern over a sharp bend.

splitters are generally made of thin sheet metal with the thickness less than 1/40 of the inner bend radius.

In the case of a sharp turn, short vanes such as circular arc and airfoil vanes (Figure 11.11*b* and *c*) can be used. The core length of the vane from the leading to the trailing edge is chosen so that

$$c = 2R_i \sin\frac{\theta}{2} \tag{11.25}$$

where θ is the bend angle. For example, $c = 2^{1/2}R_i$ for $\theta = 90°$.

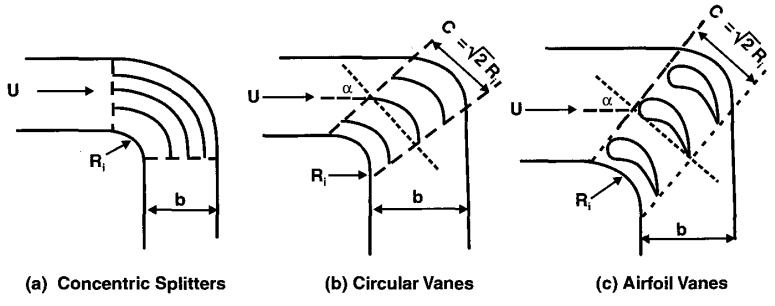

FIGURE 11.11 Flow in sharp bends with various types of vanes installed: (*a*) concentric splitters; (*b*) circular vanes; (*c*) airfoil vanes.

SEC et al. v. MRI
SEC Exhibit 1018.0094
IPR2023-00254

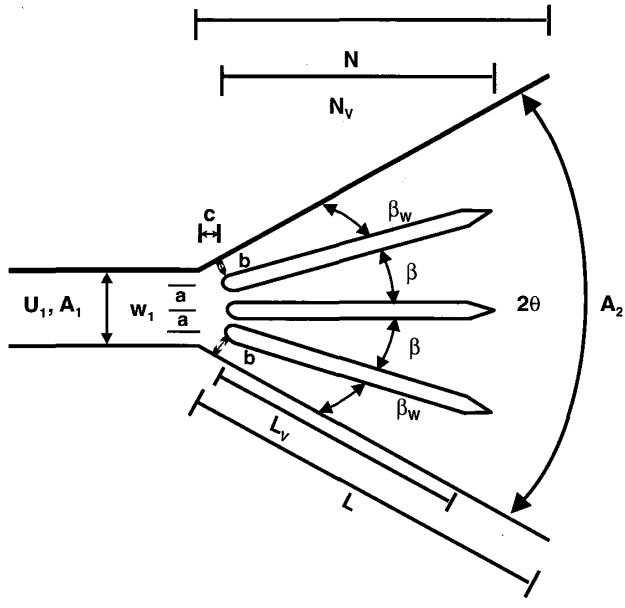

FIGURE 11.12 Vanes in a diffuser.

For uniform spacing between short vanes, the recommended maximum number of vanes is

$$n = m\left(\frac{b}{R_i}\right) - 1 \tag{11.26}$$

where the value of m is between 2.1 and 2.5. Increasing the number of vanes beyond this recommended value may result in an increase in pressure loss because of the increased skin friction resistance.

Flow separation can also occur in a diffuser. To minimize the pressure loss in the diffuser, the expansion angle between the diffuser walls should be limited to about 12° ($2\theta < 12°$), as shown in Figure 11.12. Vanes should be applied to reduce the pressure drop in short, wide-angle diffusers when the expansion angles are greater than 12°. The design method is described as follows [13]:

1. The number of vanes is chosen so that the included angle of passage between vanes is between 7 and 10°, that is, $\beta = 2\theta/(n + 1) = 7$ to 10°, where n is the number of vanes. The included angle of the wall passage, β_w, is usually slightly larger than β.

SEC et al. v. MRI
SEC Exhibit 1018.0095
IPR2023-00254

2. Equal spacing is used between the vanes so that $a = w_1/(n + 1)$, where a is the spacing between leading edges of the vanes and is measured perpendicular to the diffuser axis.
3. The leading edge of the vanes is set back slightly from the beginning of the diffuser divergence as $1 < b/a \leq 1.2$ or $0.1 < c/w_1 \leq 0.15$.
4. The length of the vane can be shorter than the full length of the diffuser. Vanes with $0.25 < L_v/L < 0.6$ have yielded very good performance (L_v and L are the length of the vane and diffuser, respectively).
5. The vanes are straight. The leading edges of the vanes are rounded and the trailing edges are tapered in at least a 5 to 1 taper to minimize the exit losses.
6. The thickness of the vanes is generally between $0.06w_1$ and $0.1w_1$. The thicker vanes require careful contouring of their leading and trailing edges.

Further improvements can also be made for two-dimensional diffusers having curved leading edges, as shown in Figure 11.13 [13]. The radius r is chosen so that

$$r = \frac{3w_i}{4\theta^*} \tag{11.27a}$$

where θ^* is measured in radians. $2\theta^*$ is the sum of the diffuser included angle and a correction angle which depends only on the diffuser area ratio:

$$2\theta^* = 2\theta + 2\Delta\theta \tag{11.27b}$$

where $\Delta\theta$ in degrees is listed as follows for various values of A_2/A_1:

A_2/A_1:	3.0	3.5	4.0	4.5	5.0
$\Delta\theta$ (degrees):	4.5	6.0	6.7	7.3	7.5

The number of vanes is chosen so that $\beta = 2\theta^*/(n + 1)$ is between 7 and 10° and the spacing between vanes is $a = w_1/(n + 1)$.

In a flow system, manifolds are frequently employed to provide proper flow rates to various branches. There are four types of manifolds, as shown in Figure 11.14. Two important factors involved in determining the pressure drop along the flow direction in a manifold are the inertia and friction terms as given in the following equation:

$$dP = -\frac{\rho d(v^2)}{2g} + \frac{f\rho v^2(ds)}{D} \tag{11.28}$$

where s is measured from the dead end and D is the manifold diameter. The differential ("d") term can be replaced by a "Δ" term in a numerical analysis. The sign of the first term that represents the change of velocity head is negative because an increase of pressure corresponds to a decrease of velocity. The

SEC et al. v. MRI
SEC Exhibit 1018.0096
IPR2023-00254

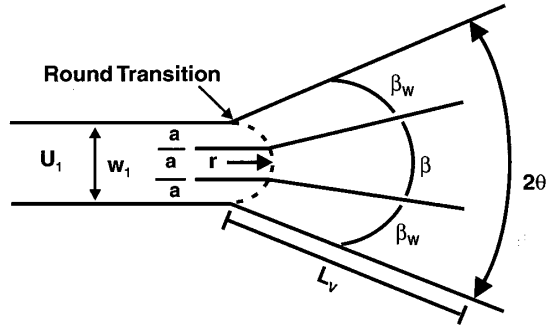

FIGURE 11.13 Improvement on vanes in a diffuser.

friction loss represented by the second term of the equation, on the other hand, is always positive because of loss of fluid pressure along the length. Therefore, the relative magnitudes of the pressure regain due to the deceleration and the pressure loss due to friction determine whether the pressure rises or falls from the inlet end to the closed (or dead) end of the manifolds as illustrated in Figure 11.15. The branch flow rates are determined by the net pressure difference between the combined and divided manifold.

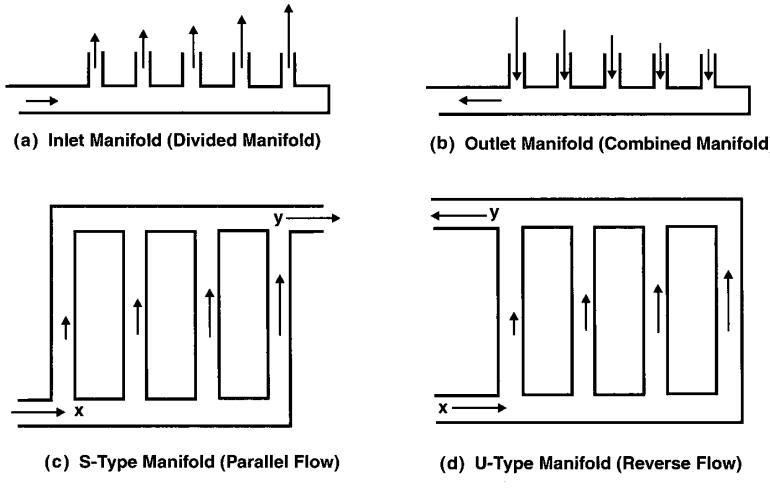

FIGURE 11.14 Four types of manifolds: (*a*) inlet manifold (divided manifold), (*b*) outlet manifold (combined manifold), (*c*) S-type manifold (parallel flow), and (*d*) U-type manifold (reverse flow).

SEC et al. v. MRI
SEC Exhibit 1018.0097
IPR2023-00254

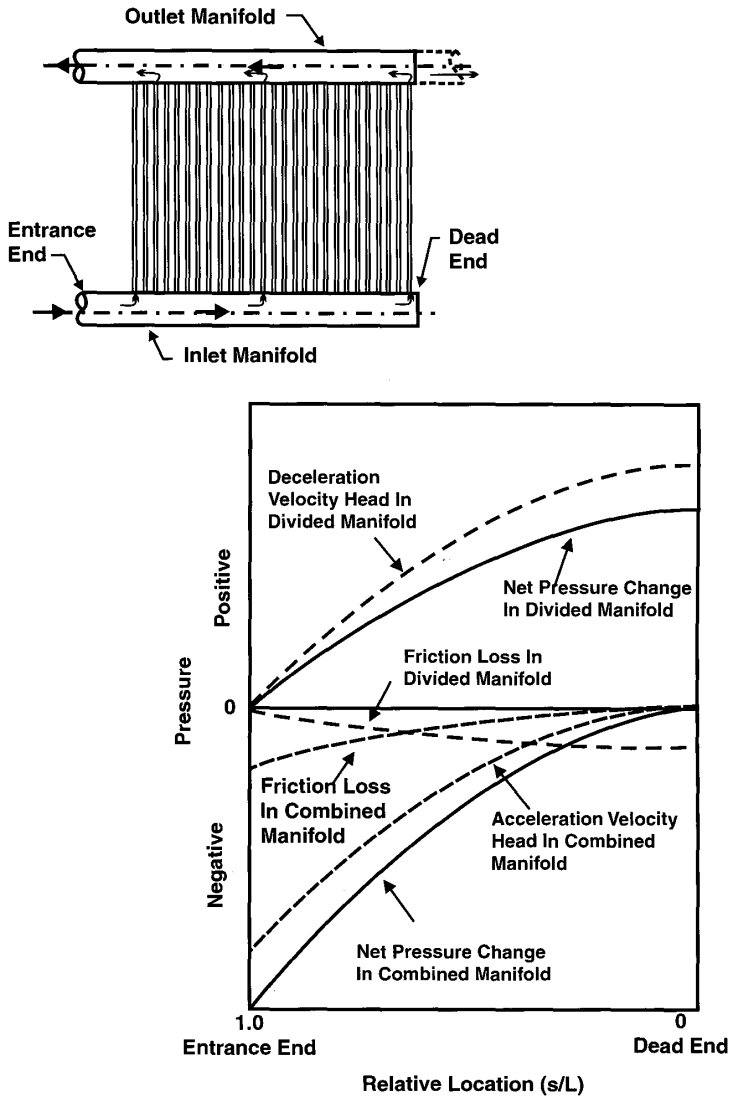

FIGURE 11.15 Pressure distribution in manifolds.

SEC et al. v. MRI
SEC Exhibit 1018.0098
IPR2023-00254

No detailed analysis will be provided here. The reader should refer to Singhal et al. [14] for a detailed analysis. General features and characteristics of manifolds are described as follows:

1. The ratio of total lateral (branch) cross-sectional area to header (manifold) cross-sectional area should be less than 1 (as small as possible) in order to obtain a better uniform flow distribution in branches.
2. Large lateral (branch) resistance is desirable for uniform flow distribution in branches.
3. The effect of friction in the manifold may be neglected for small manifold length-to-diameter ratio.
4. The fully developed friction factor may be used if the spacing between laterals (branches) is large; however, the friction factor for developing flow should be considered when the spacing between the laterals is small.
5. Uniform flow distribution in the laterals is attained when the manifolds are large enough to act as infinite reservoirs.
6. A reverse (U-type) flow system has a better flow distribution than a parallel (S-type) flow system if other parameters remain the same. The total pressure in the former is also less than that in the latter.

Orifice plates of different sizes can be installed in the branches to regulate individual flows in order to achieve any desired flow distribution to each branch. In addition, the diameter or cross section of a manifold can also be varied to obtain the proper flow pattern.

REFERENCES

1. E. M. Sparrow, J. E. Niethammer, and A. Chaboki, "Heat Transfer and Pressure Drop Characteristics of Arrays of Rectangular Modules Encountered in Electronic Equipment," *Int. J. Heat and Mass Transfer* 25(7), 1982.
2. E. M. Sparrow, A. A. Yanezmoreno, and D. R. Ottis, Jr., "Convective Heat Transfer Response to Height Differences in an Array of Blocks-Like Electronic Components," *Int. J. Heat and Mass Transfer* 27(3), 1984.
3. P. R. Souza Mendes and W. F. N. Santos, "Heat Transfer and Pressure Drop Experiments in Air-Cooled Electronic Component Arrays," *J. Thermophysics* 1(4), 1987.
4. Y. P Gan, Q. J. Peng, C. F. Ma, Z. Y. Zhou, and D. Y. Cai, "Forced Convective Air Cooled from Electronic Component Arrays in a Parallel Channel," in R. K Shah and A. Hashemi, eds., *Aerospace Heat Exchanger Technology,* Elsevier Science Publishers, Amsterdam, 1993.
5. M. Wills, "Thermal Analysis of Air-Cooled PCBs" (4 parts), *Electronic Production,* May–August, 1983.
6. F. E. Altoz, "Thermal Management," Chapter 2 in C. A. Harper, ed., *Electronic Packaging and Interconnection Handbook,* McGraw-Hill, New York, 1991.
7. W. M. Kays and M. E. Crawford, *Convective Heat and Mass Transfer,* 2nd ed., McGraw-Hill, New York, 1980.

SEC et al. v. MRI
SEC Exhibit 1018.0099
IPR2023-00254

8. R. J. Moffat and A. Ortega, "Direct Air-Cooling of Electronic Components," in A. Bar-Cohen and A. D. Kraus, eds., *Advances in Thermal Modeling of Electronic Components and Systems*, Vol. 1, Hemisphere, New York, 1988.
9. R. Hannemann, L. R. Fox, and M. Mahalingham, "Heat Transfer in Microelectronic Components," keynote paper, *Proc. Int. Symp. Cooling Technol. Electronic Equipment*, Honolulu, March 17–21, 1987.
10. K. S. Lau and R. P. Mahajan, "Effects of Tip Clearance and Fin Density on the Performance of Heat Sinks for VLSI Packages," *IEEE Trans. Components, Hybrids, and Manufacturing Technol.* 12(4), 1989.
11. R. S. Lee, H. C. Huang, and W. Y. Chen, "A Thermal Characteristic Study of Extruded Type Heat Sinks in Considering Air Flow Bypass Phenomenon," *Proc. 6th Ann. IEEE Semiconductor Thermal and Temperature Measurement Symp.*, 1990.
12. C. L. Chapman, S. Lee, and B. L. Schmidt, "Thermal Performance of an Elliptical Pin Fin Heat Sink," *Proc. 10th Ann. IEEE Semiconductor Thermal and Temperature Measurement Symp.*, 1994.
13. R. D. Blevins, *Applied Fluid Dynamics Handbook*, Van Nostrand Reinhold, New York, 1984.
14. A. K. Singhal, L. W. Keeton, A. K. Majundar, T. Mukerjee, and R. S. Johnson, "An Improved Mathematical Formulation for the Computations of Flow Distributions in Manifolds for Compact Heat Exchangers," *Adv. Heat Exchanger Des.*, ASME HTD 66, 1986.

SEC et al. v. MRI
SEC Exhibit 1018.0100
IPR2023-00254

Chapter 12

NATURAL AND MIXED CONVECTION

The basic theory of natural convection was discussed in Chapter 3. This chapter will focus on natural convection for special configurations such as in parallel plates, U-channels, pin fins, and enclosures. In addition, the problems of mixed convection in parallel plates will also be discussed here.

For laminar flow with a moderate temperature gradient, the following simple correlation for natural convection with air over a vertical plate can be used:

$$\mathrm{Nu} = 0.59\,\mathrm{Ra}_H^{0.25} \tag{12.1a}$$

where

Nu = Nusselt number, $\dfrac{hH}{k}$
Ra_H = Rayleigh number, GrPr
Pr = Prandtl number, $\dfrac{c_p\mu}{k}$
Gr = Grashof number, $\dfrac{\beta\rho^2 g H^3\,\Delta T}{\mu^2} = BH^3\,\Delta T$
H = plate height
ΔT = temperature difference between wall and ambient
B = parameter from Table C.1 of Appendix C

This equation is often used as a base to develop other general correlations for more complicated configurations.

For horizontal plates, the following equations can be applied:

Heated plate facing upward:

$$\mathrm{Nu} = 0.54\,\mathrm{Ra}_L^{0.25} \qquad 10^5 < \mathrm{Ra}_L < 4\times10^7 \ \text{(laminar)} \tag{12.1b}$$

$$\mathrm{Nu} = 0.162\,\mathrm{Ra}_L^{1/3} \qquad 4\times10^7 < \mathrm{Ra}_L \ \text{(turbulent)} \tag{12.1c}$$

Heated plate facing downward:

$$\mathrm{Nu} = 0.27\,\mathrm{Ra}_L^{0.25} \qquad 3\times10^5 < \mathrm{Ra}_L < 3\times10^{10} \tag{12.1d}$$

SEC et al. v. MRI
SEC Exhibit 1018.0101
IPR2023-00254

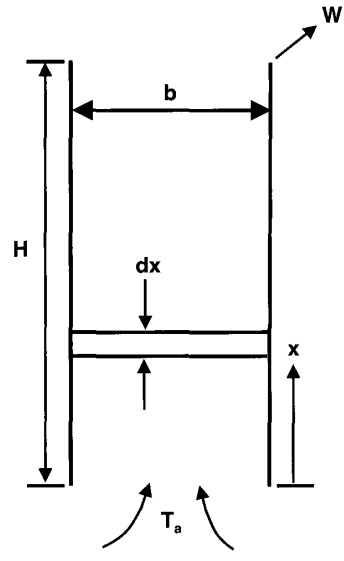

FIGURE 12.1 Flow between parallel plates.

For a horizontal plate, the characteristic length L for a square plate is taken as the length of the side of the square; for a finite rectangular plate, as the arithmetic mean of the lengths of two sides; and for a circular disk, as $0.9 \times$ disk diameter. For other shaped plates, L is defined as A/P, where A is the surface area and P is the perimeter.

12.1 PARALLEL PLATES

Flow between parallel plates as illustrated in Figure 12.1 is frequently considered in heat transfer. For fully developed laminar flow, the pressure losses due to friction and due to buoyancy can be expressed by the following equations, respectively:

$$\left(\frac{dp}{dx}\right)_F = -\frac{12\mu m}{\rho b^3 w} \tag{12.2a}$$

and

$$\left(\frac{dp}{dx}\right)_B = (\rho' - \rho_a)g = -\rho'\beta g(T_f' - T_a) \tag{12.2b}$$

SEC et al. v. MRI
SEC Exhibit 1018.0102
IPR2023-00254

where m is the mass flow rate, w is the width of plate, ρ' the average fluid density, β the coefficient of thermal expansion, and T'_f and T_a the average fluid temperature and the ambient temperature, respectively.

The mass flow rate m can be determined by relating Equations 12.2*a* and *b* as follows:

$$\frac{m}{w} = \frac{\rho'^2 g\beta b^3 (T'_f - T_a)}{12\mu} \tag{12.3}$$

For uniform heating on two plates, the local fluid temperature is found from:

$$\frac{dT_f}{dx} = \frac{2q''w}{mc_p} \tag{12.4a}$$

or

$$T_f = T_a + \frac{2q''xw}{mc_p} \tag{12.4b}$$

where c_p is the specific heat of the fluid and q'' is the constant heat flux. The average fluid temperature can be obtained by integration over the height of the plate and leads to

$$T'_f = T_a + \frac{q''H}{mc_p} \tag{12.5}$$

Combining Equations 12.3 and 12.5, one obtains

$$\frac{m}{w} = \left(\frac{\rho'^2 g\beta b^3 q''H}{12\mu c_p} \right)^{1/2} \tag{12.6}$$

Natural convection between vertical parallel plates was first studied experimentally by Elenbaas [1] in 1942, and the correlation for isothermal plates is as follows:

$$\mathrm{Nu} = \frac{1}{24}\left(\frac{b}{H}\right)\mathrm{Ra}[1 - e^{-35H/(b\,\mathrm{Ra})}]^{3/4} \tag{12.7}$$

where the Nusselt and Grashof numbers are based on the plate spacing b. All properties are evaluated at the wall temperature T_w, except that β is computed at the ambient (or free-stream) temperature T_a. Later, Sparrow and Bahrami [2] performed similar tests but extended the study to the cases with blockage along either one or both of the two edges. Comparisons between Elenbaas' and

SEC et al. v. MRI
SEC Exhibit 1018.0103
IPR2023-00254

Sparrow and Bahrami's results are given in Figure 12.2. The differences as explained by Sparrow and Bahrami [2] are attributed to the following factors:

1. Some doubts persist about the appropriate property values used by Elenbaas in developing the correlation because of a large temperature difference (up to 330°C) in Elenbaas' tests.
2. Elenbaas seemed to overestimate the experimental losses at the lower values of $(b/H)\ \mathrm{Ra}^*$.

In addition, one should also note that the plate sizes used in the tests in the two sources are different. Elenbaas used a larger plate (4.72 in × 4.72 in) as compared with a plate 3 in × 3 in used by Sparrow and Bahrami. As should be expected, better heat transfer occurs from the smaller plate.

The results for blockage along the edges [2] are given in Figure 12.3. The results from Sparrow and Bahrami can be summarized as follows:

3. For $(b/H)\ \mathrm{Ra}^* > 20$, the results agree with Elenbaas' data.
4. For $(b/H)\ \mathrm{Ra}^* > 4$, the results for edge blockage of one side are identical to those for the unblocked case.
5. For $(b/H)\ \mathrm{Ra}^* > 10$, the heat transfer results are independent of whether the edges are fully open or blocked along one or two lateral edges.

The curve fits for the data from Sparrow and Bahrami [2], as indicated in Figure 12.2*a*, are as follows:

$$\mathrm{Nu} = \begin{cases} 0.24y^{0.35} & y < 10 \qquad (12.8a) \\ 2.04y^{-0.135}(1-e^{-35/y})^{3/4} & 10 \le y \le 100 \qquad (12.8b) \\ \frac{1}{24}(1-e^{-35/y})^{3/4} & y > 100 \qquad (12.8c) \end{cases}$$

where $y = (b/H)(\mathrm{Ra})$.

Examining Figure 12.2*b* reveals that the heat transfer coefficient increases as the temperature difference $T_w - T_a$ increases. For large plate spacing, data from both sources [1, 2] approach the results obtained from Equation 12.1.

For vertical parallel-plate channels, the heat transfer rate from each plate decreases when the plate spacing is reduced. For a given envelope space, however, the number of plates, or total heat transfer surface area, is increased as the plate spacing decreases. Therefore, achieving the optimum plate spacing—the spacing at which the product of the heat transfer coefficient and the total heat transfer surface area is maximum—may maximize the total heat transfer rate. Elenbaas found that the optimum spacing between two vertical plates for laminar natural convection is

$$\frac{b}{H}\ \mathrm{GrPr} \approx 46 \qquad (12.9)$$

This equation represents the case where optimum spacing refers to the spacing that permits the greatest convection heat transfer rate for a given plate temperature.

SEC et al. v. MRI
SEC Exhibit 1018.0104
IPR2023-00254

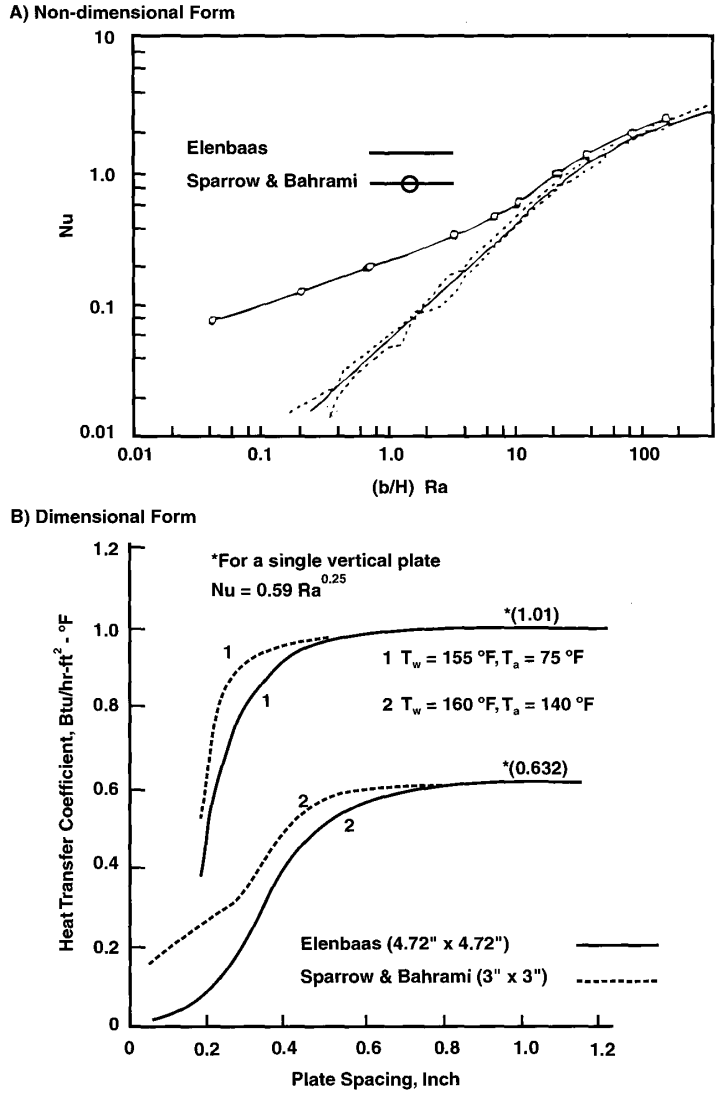

FIGURE 12.2 Natural convection between vertical parallel plates: (*a*) nondimensional form; (*b*) dimensional form.

SEC et al. v. MRI
SEC Exhibit 1018.0105
IPR2023-00254

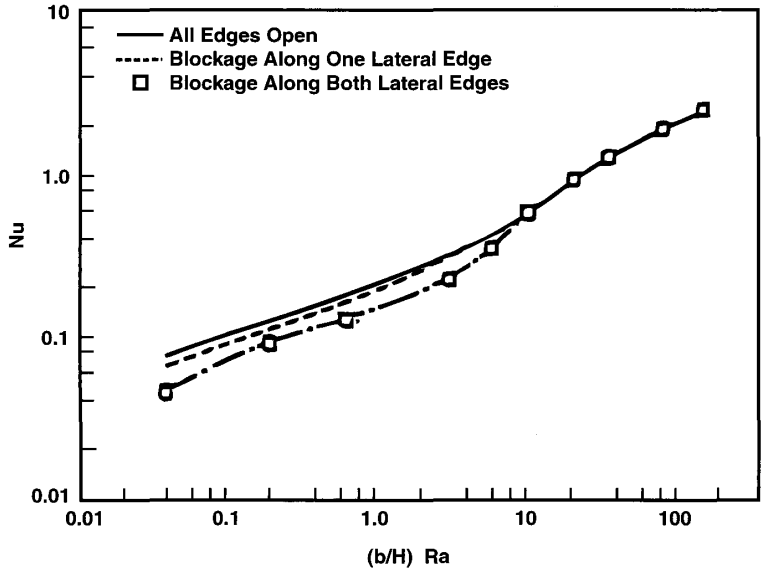

FIGURE 12.3 Effects of edge blockage on heat transfer in parallel plates.

On the other hand, the spacing which minimizes the plate temperature for a given convection heat transfer rate can be determined from the following equation [3]:

$$\frac{b}{H}\,\mathrm{GrPr} \approx 600 \tag{12.10}$$

Here, optimum spacing means the spacing that allows the maximum heat transfer coefficient from each plate. Basically, achieving this optimization means separating the plates so that no boundary-layer interference occurs between plates.

If the spacing between two plates is large enough as compared with the plate height, the pair can be treated as an isolated plate because the boundary layers associated with the individual plates do not interfere with each other. On the other hand, for very long plates, or small plate spacing, the boundary layers merge together near the entrance, and fully developed flow prevails along much of the channel. Based on these two limiting solutions, Bar-Cohen and Rohsenow [4] developed an analytical solution for each type of thermal boundary condition. A summary of their results is given in Table 12.1

Sparrow and Prakash [5, 6] proposed methods to improve heat transfer from vertical continuous-plate arrays by using discrete plates as shown in Figure 12.4.

SEC et al. v. MRI
SEC Exhibit 1018.0106
IPR2023-00254

Table 12.1 Heat Transfer Correlations for Parallel Plates

Condition	Nu	Optimum Spacing, b_o	Optimum $(Nu)_o$
Isothermal plates			
Symmetric	$Nu = \left[\frac{576}{(Ra')^2} + \frac{2.873}{(Ra')^{0.5}}\right]^{-0.5}$	$b_o = 2.714P^{-0.25}$	$(Nu)_o = 1.31$
Asymmetric	$Nu = \left[\frac{144}{(Ra')^2} + \frac{2.873}{(Ra')^{0.5}}\right]^{-0.5}$	$b_o = 2.154P^{-0.25}$	$(Nu)_o = 1.04$
Isoflux plates			
Symmetric	$(Nu)_{H/2} = \left[\frac{12}{Ra''} + \frac{1.88}{(Ra')^{0.4}}\right]^{-0.5}$	$b_o = 1.472R^{-0.2}$	$(Nu)_{o,\,H/2} = 0.62$
Asymmetric	$(Nu)_{H/2} = \left[\frac{6}{Ra''} + \frac{1.88}{(Ra')^{0.4}}\right]^{-0.5}$	$b_o = 1.169R^{-0.2}$	$(Nu)_{o,\,H/2} = 0.49$

where

$$Nu = \frac{q''b}{k(T_w - T_a)} \qquad Ra = \frac{c_p\rho^2 g\beta H^3 \Delta T}{\mu k}$$

$$P = \frac{c_p\rho^2 g\beta \Delta T}{H\mu k} \qquad Ra' = \frac{c_p\rho^2 g\beta b^4 \Delta T}{H\mu k}$$

$$R = \frac{c_p\rho^2 g\beta b^5 q''}{H\mu k} \qquad Ra'' = \frac{c_p\rho^2 g\beta b^5 q''}{H\mu k^2}$$

Replacing continuous plates with discrete plates breaks up the boundary layer, resulting in an increased heat transfer rate; however, this enhancement technique will also increase the pressure drop and pumping power. For the case of forced convection, the heat transfer coefficient will always increase as long as the fan or pump can overcome the increased system pressure. The pumping power (or driving force) in natural convection is limited by the system height and the difference in densities, which is limited by the temperature gradient. An increase in the system pressure drop caused by heat transfer enhancement will reduce the mass flow rate. Under certain conditions, the heat transfer from discrete plates will actually be less than that for continuous plates because of a significant reduction in mass flow due to an increased system pressure drop. Comparisons between staggered discrete and continuous vertical plates are given in Figure 12.5*a* and *b* for heat transfer rate and inlet velocity, respectively.

Sparrow and Prakash [5, 6] made three types of performance comparisons in their work. The first case was to maximize the heat transfer rate at fixed values of the temperature difference and surface area. The second case was to minimize the temperature difference for a fixed heat transfer rate and surface area. The final case was to minimize the array height for a fixed heat load and temperature difference. The results are presented in Figures 12.6 through 12.8.

SEC et al. v. MRI
SEC Exhibit 1018.0107
IPR2023-00254

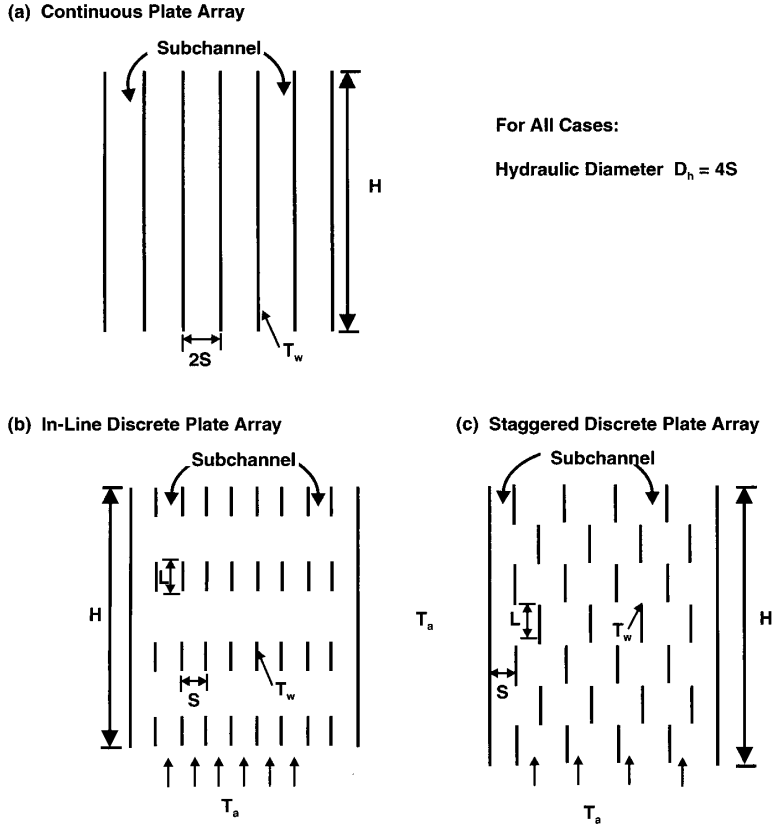

FIGURE 12.4 Continuous and discrete vertical plates: (*a*) continuous-plate array; (*b*) in-line discrete-plate array; (*c*) staggered discrete-plate array.

12.2 STRAIGHT-FIN ARRAYS

The straight-fin array as shown in Figure 12.9 consists of a number of U-shaped channels. The correlations for vertical parallel plates cannot be directly applied to a U-shaped channel because of the base involved. Aibara [7] indicated that U-shaped channels may be approximated by parallel plates within an error of 5% in the heat transfer rate only if the ratio of channel depth to channel width (L/S) is greater than 5. For many heat sinks in practical applications, however, the ratio L/S is often less than 5. In these cases, the base plate of the heat sink creates

SEC et al. v. MRI
SEC Exhibit 1018.0108
IPR2023-00254

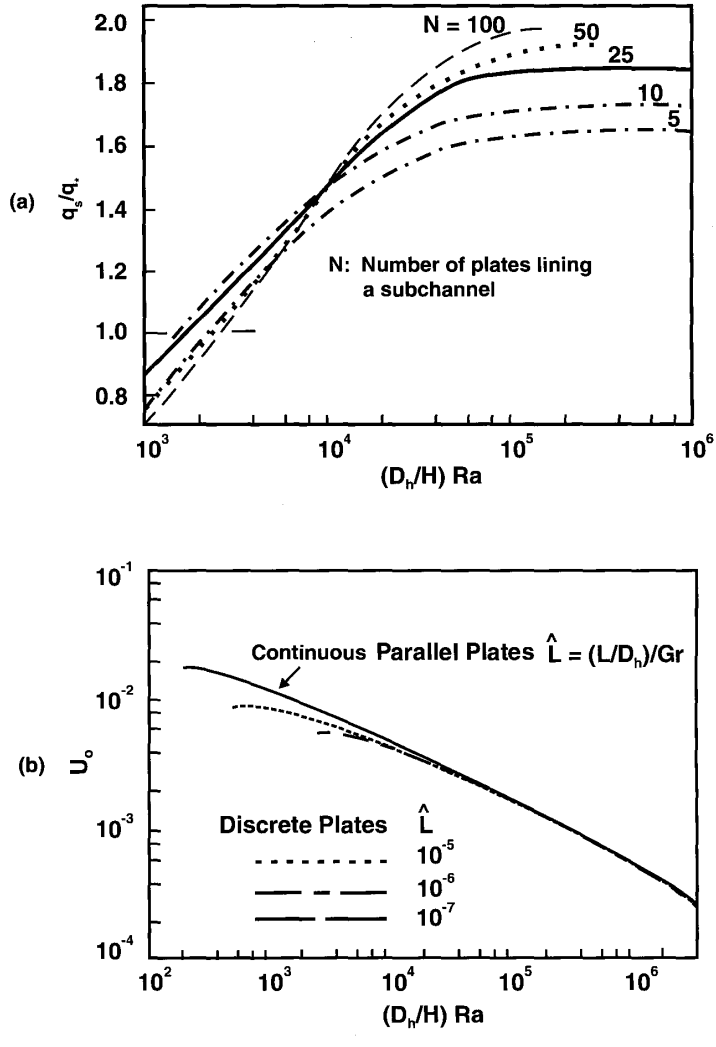

FIGURE 12.5 Comparisons between staggered discrete and continuous parallel plates: (*a*) ratio of heat transfer rates. Subscripts: *, continuous parallel-plate channel; *s*, staggered discrete plates.

SEC et al. v. MRI
SEC Exhibit 1018.0109
IPR2023-00254

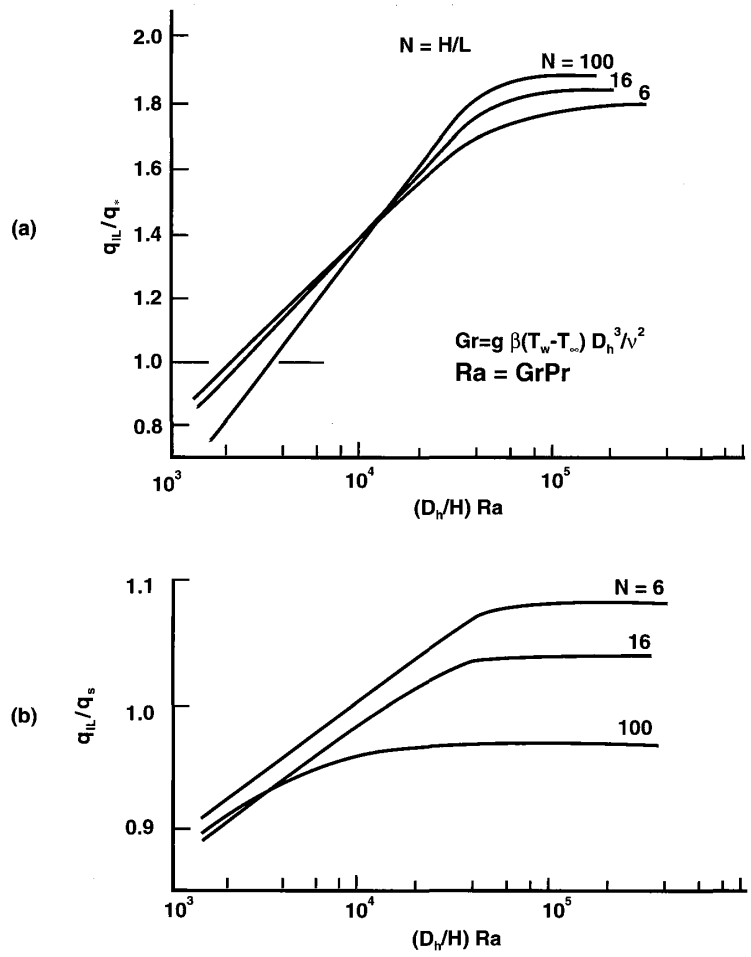

FIGURE 12.6 Comparisons of heat transfer rates at fixed ΔT and area: (*a*) q_{IL}/q_*; (*b*) q_{IL}/q_s. Subscripts: IL, in-line discrete plates; *, continuous parallel-plate channel; *s*, staggered discrete plates.

additional surface, where a third boundary layer is developed, and two corners that cause a significant reduction in the heat transfer.

For vertical-fin arrays, several experimental data [8–10] are available. Among them, Izume and Nakamura [10] developed a mathematical relationship describing heat transfer from fin arrays; however, their equation does not hold

SEC et al. v. MRI
SEC Exhibit 1018.0110
IPR2023-00254

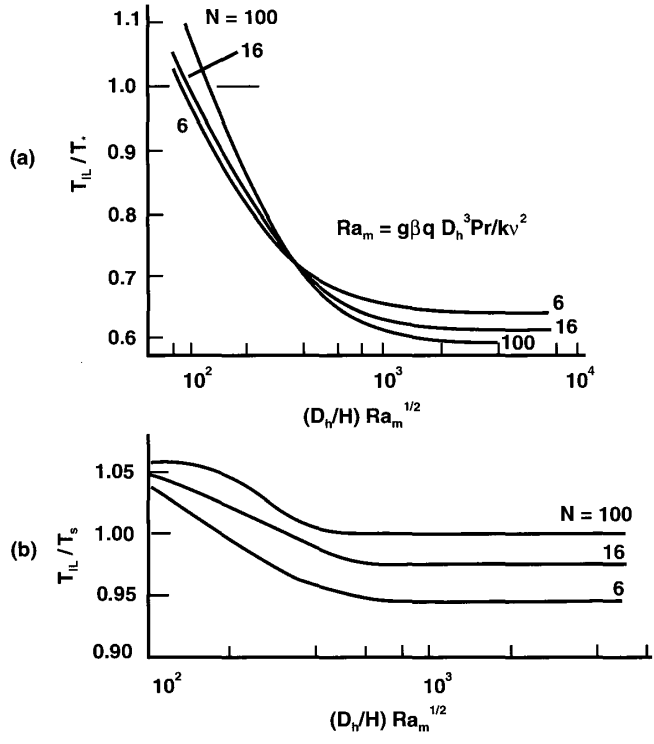

FIGURE 12.7 Comparison of temperature difference at fixed q and area: (*a*) T_{IL}/T_*; (*b*) T_{IL}/T_s. Subscripts: IL, in-line discrete plates; *, continuous parallel-plate channel; *s*, staggered discrete plates.

in the limiting cases of very large or very small ratios of channel depth to channel width. To overcome this problem, Van De Pol and Tierney [11] developed the following correlation applicable to any channel depth to width ratio:

$$\mathrm{Nu}_r = \frac{\mathrm{Ra}^*}{\psi}\left\{1 - \exp\left[-\psi\left(\frac{0.5}{\mathrm{Ra}^*}\right)^{3/4}\right]\right\} \tag{12.11}$$

where

$$\mathrm{Nu}_r = \frac{hr}{k}$$

SEC et al. v. MRI
SEC Exhibit 1018.0111
IPR2023-00254

FIGURE 12.8 Array height ratios vs. $\hat{q}$ at fixed q and ΔT: (*a*) H_{IL}/H_{S}; (*b*) H_{IL}/H_{∞}. Subscripts: IL, in-line discrete plates; *S*, staggered discrete plates; *, continuous parallel-plate channel.

SEC et al. v. MRI SEC
Exhibit 1018.0112
IPR2023-00254

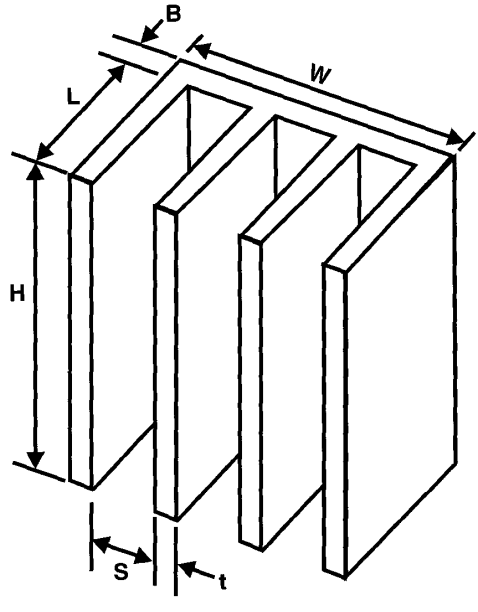

FIGURE 12.9 A vertical straight-fin array.

$$r = \frac{2LS}{2L + S}$$

$$\mathrm{Ra}^* = \frac{r}{H}\mathrm{Gr}_r\mathrm{Pr}$$

$$\mathrm{Gr}_r = g\beta\left(\frac{\rho}{\mu}\right)^2 (T_w - T_a)r^3$$

$$\psi = \frac{24(1 - 0.483e^{-0.17/a})}{\{(1 + 0.5a)[1 + (1 - e^{-0.83a})(9.14a^{0.5}e^{VS} - 0.61)]\}^3}$$

$$a = \frac{S}{L}$$

$$V = -11.8 \text{ in}^{-1}$$

When r approaches S as $L/S \to \infty$, the Nusselt number in Equation 12.11 is reduced to the Elenbaas equation (12.1) for parallel plates. On the other hand, when the ratio L/S approaches zero, the resulting heat transfer coefficient (Nusselt number) is reduced to Equation 12.1 for a single vertical plate. All physical properties are evaluated at the wall temperature, with the exception of β, which is computed at the fluid temperature.

SEC et al. v. MRI
SEC Exhibit 1018.0113
IPR2023-00254

As in any natural convection, thermal radiation always plays an important role. Rea and West [12] proposed a method to estimate thermal radiation from finned heat sinks (U-channels). The thermal radiation from one U-channel can be expressed as

$$q_r = \varepsilon_a \sigma S H (T_w^4 - T_a^4) \tag{12.12}$$

where ε_a is the U-channel apparent emittance, σ the Stefan-Boltzmann constant, and S and H sink dimensions in Figure 12.9. The U-channel apparent emittance is a function of heat sink dimensions and surface emittance ε of the heat sink, and this apparent emittance can be greater than 1. Typical results for the U-channel emittance are given in Figure 12.10.

Because the efficiency of a fin is generally less than 100%, the temperature of the fin at the tip is different from that at the base. Therefore, it is recommended that the average temperature be used to calculate the heat transfer rate from the heat sink to the ambient.

If the base plate of a straight-fin array is oriented horizontally as shown in Figure 12.11, the heat transfer coefficient for natural convection can be correlated [13] as follows:

$$\mathrm{Nu} = 5.22 \times 10^{-3} \left(\frac{\mathrm{GrPr}\, Sn}{H} \right)^{0.57} \left(\frac{H}{L} \right)^{0.656} \left(\frac{S}{L} \right)^{0.412} \tag{12.13a}$$

for

$$10^6 < \frac{\mathrm{GrPr}\, Sn}{H} < 2.5 \times 10^7$$

and

$$\mathrm{Nu} = 2.787 \times 10^{-3} \left(\frac{\mathrm{GrPr}\, Sn}{H} \right)^{0.745} \left(\frac{H}{L} \right)^{0.656} \left(\frac{S}{L} \right)^{0.412} \tag{12.13b}$$

for

$$2.5 \times 10^7 < \frac{\mathrm{GrPr}\, Sn}{H} < 1.5 \times 10^8$$

where n is the number of spacings, H is the height, and $2L$ is the length of the fin array. Also, Nu and Gr are based on L (half-length of the fin array). All thermal properties are evaluated at the wall temperature.

Example 12.1

Determine the total heat loss from a vertical straight-fin array as shown in Figure 12.8. The temperatures of the heat sink and ambient are T_w and T_a,

SEC et al. v. MRI
SEC Exhibit 1018.0114
IPR2023-00254

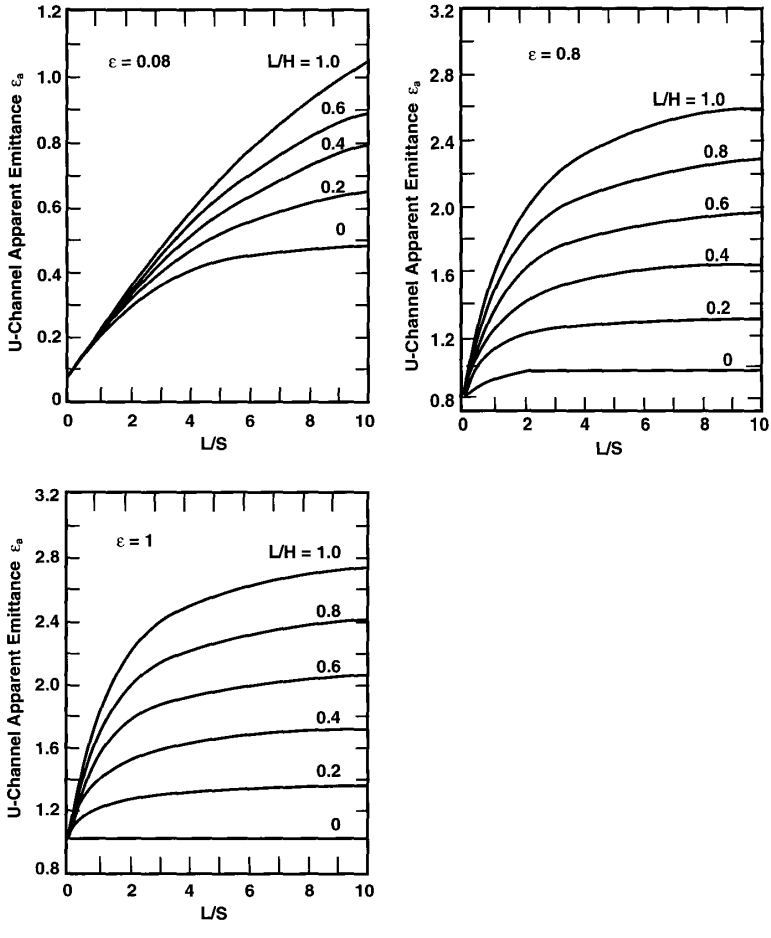

FIGURE 12.10 U-channel apparent emittance ϵ_a for different values of ϵ.

respectively. It is assumed that the fin efficiency is 100% and the total number of fins, including two end fins, is n.

Solution

In theory, there are four different heat transfer coefficients for natural convection:

SEC et al. v. MRI
SEC Exhibit 1018.0115
IPR2023-00254

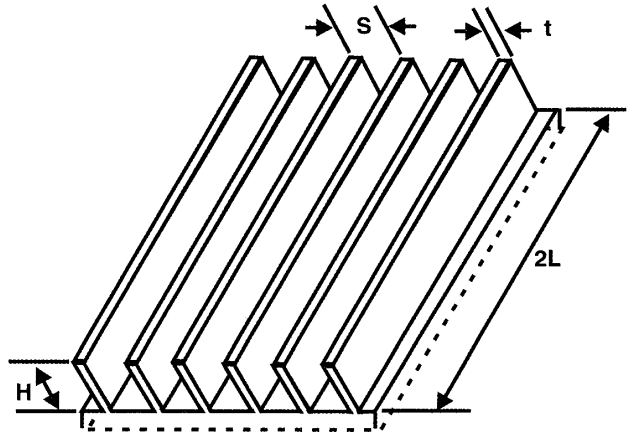

FIGURE 12.11 Horizontal fin array configuration.

h_u: heat transfer coefficient from a U-channel, from Equation 12.11
h_v: heat transfer coefficient from a vertical plate, from Equation 12.1*a*
h_t: heat transfer coefficient from a horizontal plate with heated surface facing up, from Equation 12.1*b* or 12.1*c*
h_b: heat transfer coefficient from a horizontal plate with heated surface facing down, from Equation 12.1*d*

Heat loss by natural convection is

$$q_c = [(n-1)(2LH + HS)h_u + 2(L+B)Hh_v + nHth_v + Bw(h_t + h_b) + ntL(h_t + h_b)](T_w - T_a)$$

The components of this heat loss, represented by the terms inside the brackets, are the respective heat losses from $(n - 1)$ U-channels, from the external surfaces of the two end fins, from n fin tips, and from the upward- and downward-facing surfaces of n base-plate thicknesses.

Similarly, heat loss by radiation is

$$q_r = [(n-1)HS\varepsilon_a + 2(L+B)H\varepsilon + nHt\varepsilon + 2Bw\varepsilon + 2ntL\varepsilon]\sigma(T_w^4 - T_a^4)$$

where ε_a and ε are apparent emissivity (from Figure 12.10) and surface emissivity of the fin array. The absolute temperature must be applied to radiation heat transfer.

SEC et al. v. MRI
SEC Exhibit 1018.0116
IPR2023-00254

In most practical design analyses, the heat losses from the tips, leading edges, and trailing edges of the fins might be ignored because the fin thickness t is generally small. The total heat loss from the array is the sum of the heat losses from natural convection and radiation. The dimension B as shown in Figure 12.9 is usually equal to zero because the base plate of the fin array is an integrated part of the chassis wall.

12.3 PIN-FIN ARRAYS

Pin-fin arrays that consist of many solid pins on a common base plate are frequently used to cool electronic equipment. The cross-section of individual fins can be any shape. Because of the difficulty of separating the radiation loss from the total heat loss of a pin-fin array, the heat loss is typically expressed by the combined natural convection and radiation. Sparrow and Vemuri [14, 15] performed experimental studies on a small pin-fin array (3 in × 3 in) with circular pins. Later Alessio and Kaminski [16] correlated all existing data, including their own results, into the following equation:

$$\mathrm{Nu}_d = 1.035(\mathrm{Ra}_d)^{0.24}\left[\frac{(a-D)\cos\theta}{D}\right]^{1.3}\left(\frac{H\cos\theta}{D}\right)^{-0.37} \tag{12.14}$$

where

a = fin pitch
$d = a\cos\theta$
D = fin diameter
H = fin length or height
θ = angle of inclination from the horizontal

$$\mathrm{Nu}_d = \frac{hd}{k}$$

$$\mathrm{Ra}_d = \frac{g\beta\rho^2 c_p \Delta T\, d^3}{\mu k}$$

$$h = \frac{q}{A\,\Delta T}$$

In the equation defining h, A is the total surface area of the array, including the sides of the fins, the tips of the fins, and the exposed area of the base plate. The surface emissivity is about 0.82 for the above test data.

Since most of the data were based on the tests performed on a 3-in square base plate, the ratio of the edge fins to the total number of fins is very high. Because the edge fins have higher heat transfer rates as compared with inner fins, and also because they comprise a significant portion of the total number of fins, the results from Equation 12.14 will overestimate the heat transfer coefficient for larger pin-fin arrays. Conversely, smaller pin-fin arrays should perform better, and the results presented here would be underestimates.

SEC et al. v. MRI
SEC Exhibit 1018.0117
IPR2023-00254

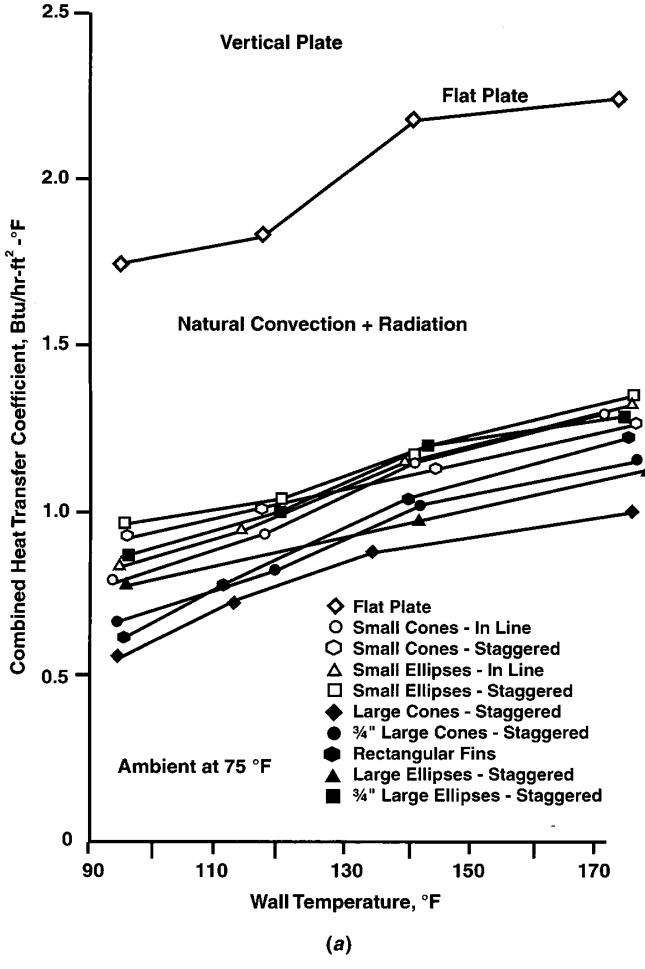

(*a*)

FIGURE 12.12 Heat transfer coefficients for pin-fin arrays: (*a*) arrays with vertical base plate; (*b*) arrays facing up; (*c*) arrays facing down.

It is difficult to correct the results from Equation 12.14 for various sizes of the array, because of a lack of available data. The only data available are the results of Taylor [17] for a large array with a base plate of 10 in by 20 in as shown in Figure 12.12*a*. Based on these limited data, the following correction to Equation 12.14 is suggested:

SEC et al. v. MRI
SEC Exhibit 1018.0118
IPR2023-00254

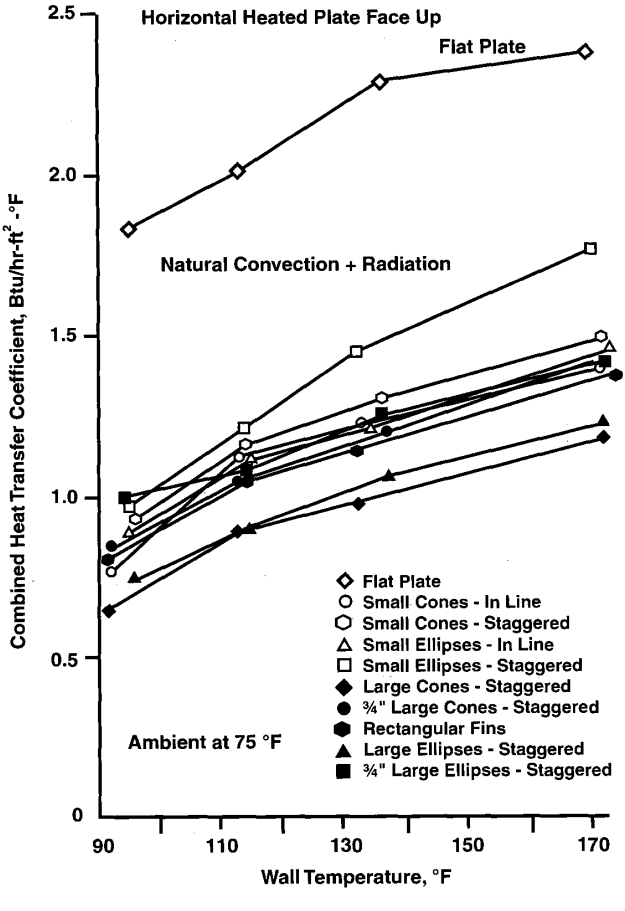

(*b*)

FIGURE 12.12 ***(Continued).***

$$h' = h\left(\frac{R}{0.4}\right)^{0.8} \tag{12.15}$$

where h is computed from Equation 12.14 and R is the ratio of edge fins to the total number of fins in an array under consideration.

Fins used for comparison from Taylor [17] are small cones in a staggered arrangement with a fin pitch of 0.5 in. The fin major and minor diameters are

SEC et al. v. MRI
SEC Exhibit 1018.0119
IPR2023-00254

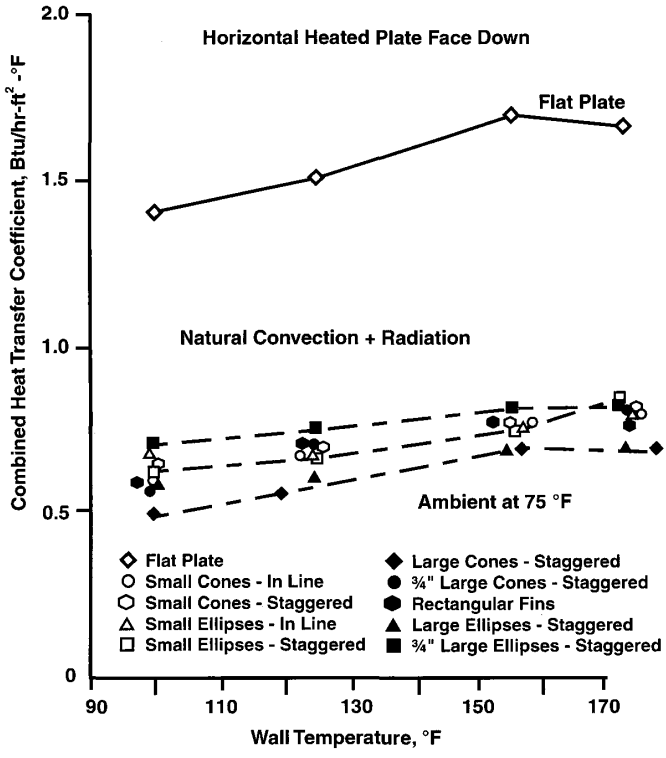

(*c*)

FIGURE 12.12 ***(Continued).***

0.25 and 0.12 in, respectively. The height of the fin is 1 in. The results for the pin-fin array facing up or down are also included in the same reference, and they are shown in Figure 12.12*b* and *c*, respectively.

A pin-fin array is often made by the casting method. One should consult with the casting vendor about fin design limits. However, the following are basic design guidelines for casting pin fins with the configurations given in Figure 12.13:

Pin fins should be tapered at 0.25 inches per foot.
The major diameter of a pin fin should not exceed its supporting wall thickness.
The dimensional limits are $S_t/D > 2$, $S_l/D > 2$, and $H/D \leq 7$.
The minimum diameter D is 0.06 inches. H/D is limited to 2.5 when D is 0.06 inches.

SEC et al. v. MRI
SEC Exhibit 1018.0120
IPR2023-00254

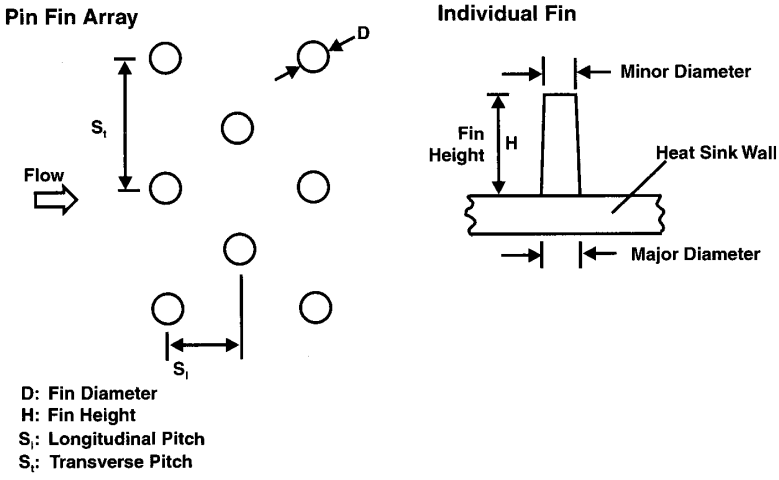

FIGURE 12.13 Pin-fin configurations.

Example 12.2

A pin fin array consists of 449 horizontal fins arrange in an equilateral configuration with 0.5 inch pitch. Determine the heat transfer coefficient of a pin-fin array with the following dimensions:

$$H = 0.65 \text{ in} \qquad D = 0.25 \text{ in} \qquad a = 0.5 \text{ in}$$

and

$\theta = 0$ (horizontal fins)
$R = 0.25$ (ratio of number of edge fins to total fins)

Solution

Assume the ambient and the base-plate temperatures are 75 and 115°F, respectively. Then all properties are calculated at the average temperature of 95°F [= (75 + 115)/2]:

$$\rho = 0.0725 \text{ lb}_m/\text{ft}^3$$
$$\beta = 0.001822 \text{ °F}^{-1}$$
$$\mu = 0.04595 \text{ lb}_m/(\text{ft} \cdot \text{hr})$$
$$k = 0.0153 \text{ Btu}/(\text{hr} \cdot \text{ft} \cdot \text{°F})$$
$$c_p = 0.24 \text{ Btu}/(\text{lb}_m \cdot \text{°F})$$
$$d = 0.5 \text{ in}$$
$$\Delta T = 40\text{°F}$$

SEC et al. v. MRI
SEC Exhibit 1018.0121
IPR2023-00254

Finally, from Equation (12.14)

$$\mathrm{Ra}_d = 3931.3 \Rightarrow \mathrm{Nu}_d = 5.298$$

further implying

$$h = 1.945 \text{ Btu/(hr} \cdot \text{ft}^2 \cdot {}^\circ\text{F)}$$

and

$$h' = 1.945\left(\frac{0.25}{0.4}\right)^{0.8} = 1.335 \text{ Btu/(hr} \cdot \text{ft}^2 \cdot {}^\circ\text{F)}$$

12.4 ENCLOSURES

The following discussion deals with natural convection heat transfer between concentrically located isothermal spherical, cylindrical, and cubical inner bodies and their spherical and cubical enclosures [18, 19]. Typically, three possible heat transfer regimes can occur within the enclosure: (1) convection without the effect of enclosure—infinite-atmosphere solution for large gap (L/R_i); (2) convection with the effect of enclosure—enclosure solution for moderate gap (L/R_i); and (3) pure conduction—conduction solution for small gap (L/R_i).

The following steps are used to determine the range of each regime so that a proper correlation can be applied:

1. The hypothetical radii for inner and outer bodies for spheres, cylinders, and cubes are defined as the corresponding radii of a sphere having the same volume as the body in question.
   a. Sphere:

$$R_i = 0.5D_i \quad R_o = 0.5D_o$$

   where D_i and D_o are actual diameters of inner and outer bodies, respectively.
   b. Cylinder:

$$R_i = \left(\frac{3D_i^2 H_i}{16}\right)^{1/3} \quad R_o = \left(\frac{3D_o^2 H_o}{16}\right)^{1/3}$$

   where H is the height of the cylinder.
   c. Cube:

$$R_i = \left(\frac{3H_i^3}{4\pi}\right)^{1/3} \quad R_o = \left(\frac{3H_o^3}{4\pi}\right)^{1/3}$$

   where H is the side length of the cube.

SEC et al. v. MRI
SEC Exhibit 1018.0122
IPR2023-00254

d. Rectangular block:

$$R_i = \left(\frac{3x_i y_i z_i}{4\pi}\right)^{1/3} \quad R_o = \left(\frac{3x_o y_o z_o}{4\pi}\right)^{1/3}$$

where x, y, and z are the sides of the rectangular block.

2. Gap width: $L = R_o - R_i$.
3. Boundary-layer length on the inner body:
   a. Sphere: $b = 0.5\pi D_i$.
   b. Cylinder: $b = H_i + D_i(0.5\pi - 1)$.
   c. Cube: $b = 2H_i$.
   d. Rectangular block: $b = 2Y_i$ where $Y_i = (x_i y_i z_i)^{1/3}$.
4. $\mathrm{Ra}_b = \mathrm{Gr}_b \mathrm{Pr}$ and $\mathrm{Ra}_b^* = \mathrm{Ra}_b\left(\frac{L}{R_i}\right)$

where b is used as the characteristic length for Gr_b and Ra_b.

5. The lower limit for an infinite region can be obtained by setting the solutions equal for regimes 1 (infinite region with no enclosure effect) and 2 (region with enclosure effect).
   a. Sphere: $\left(\frac{L}{R_i}\right)_1 = 0.978\,\mathrm{Ra}_b^{0.0593}$
   b. Cylinder: $\left(\frac{L}{R_i}\right)_1 = \left\{\frac{[D_i/(H + 0.571D_i)]^{-0.25}}{0.585}\right\}^{1/0.236} \mathrm{Ra}_b^{0.0593}$
   c. Cube: $\left(\frac{L}{R_i}\right)_1 = 1.26\,\mathrm{Ra}_b^{0.0593}$
6. Checking limits:
   a. If $L/R_i > (L/R_i)_1$ (convection over a single inner body—no enclosure effect), then

$$\mathrm{Nu}_D = \frac{hD_i}{k} = 0.52\,\mathrm{Ra}_D^{0.25} \tag{12.16a}$$

where D_i is the inner diameter for spheres and cylinders, and the side length for cubes.

   b. If $L/Ri < (L/R_i)_1$ (convection in enclosures—with enclosure effect), then

$$\mathrm{Nu}_b = \frac{hb}{k} = 0.585(\mathrm{Ra}_b^*)^{0.236} \tag{12.16b}$$

   c. If $L/R_i < 0.45$ (conduction may be important), then

$$\frac{q_{\mathrm{conv}}}{q_{\mathrm{cond}}} = 0.2(\mathrm{Ra}_L^*)^{0.239} \tag{12.17}$$

SEC et al. v. MRI
SEC Exhibit 1018.0123
IPR2023-00254

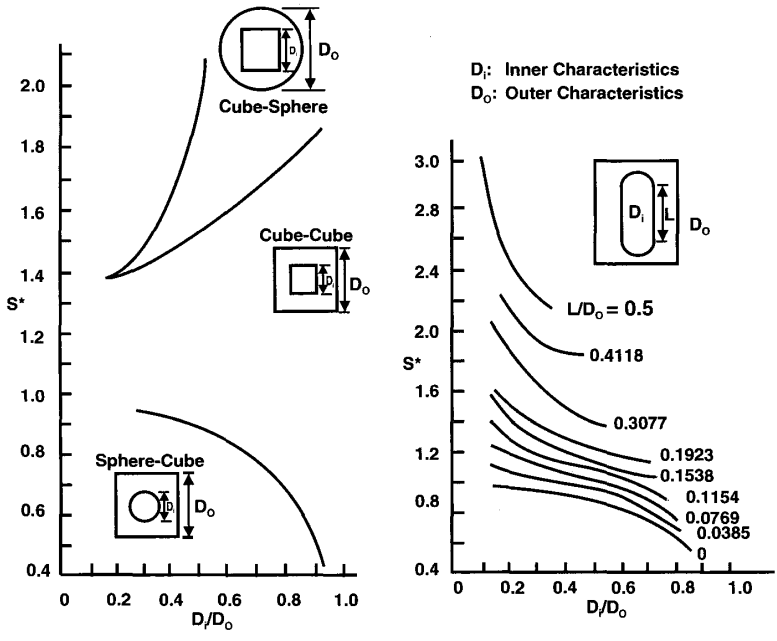

FIGURE 12.14 Dimensionless shape factors for conduction.

where q_{conv} and q_{cond} are the heat transfer rates due to convection and conduction, respectively, and

$$\mathrm{Ra}_L^* = \left(\frac{L}{b}\right)^3 \mathrm{Ra}_b^* \quad \text{or} \quad \mathrm{Ra}_L^* = \mathrm{Ra}_L\left(\frac{L}{R_i}\right)$$

For very small values of L/R_i, heat transfer could be primarily due to conduction rather than convection. It is recommended that one use whichever predicts the higher value—convection or conduction—for heat transfer.

For heat conduction in three-dimensional shells, Warrington et al. [20] provide graphical *shape factors* between two surfaces, defined as heat transfer divided by thermal conductivity and by temperature difference. Figure 12.14 charts for various configurations the nondimensional shape factor S^* defined as follows:

$$S^* = \frac{S}{S_i} \tag{12.18}$$

SEC et al. v. MRI
SEC Exhibit 1018.0124
IPR2023-00254

where $S_i = 2\pi D_i D_o/(D_o - D_i)$ and where D_i and D_o are equivalent diameters of the outer and inner surfaces, respectively. The equivalent diameter of a cube is its edge length, and the equivalent diameter of a cylinder or sphere is equal to its diameter. The heat transfer rate for conduction becomes as follows:

$$q = kS\,\Delta T \tag{12.19}$$

12.5 MIXED CONVECTION IN VERTICAL PLATES

In theory, natural and forced convection always occur together; however, in some cases, one may neglect either component depending on the flow condition. The following guideline can be applied to determine the nature of the problem:

Natural convection alone: $\text{Gr} >> \text{Re}^2$
Forced convection alone: $\text{Gr} << \text{Re}^2$
Mixed convection: $\text{Gr} \approx \text{Re}^2$

For mixed convection, the experimental data have revealed the existence of flow reversal in the fully developed region at a low Reynolds number, i.e., low forced-flow velocity. Mixed convection can take the form of either buoyancy-assisted (or aided) flow or buoyancy-resisted (or opposed) flow.

12.5.1 Buoyancy-Assisted Flow

Buoyancy-assisted flow refers to forced flow in the direction of buoyancy as shown in Figure 12.15. Cheng et al. [21] presented the solutions for three fundamental combinations of thermal boundary conditions on the respective wall surfaces, namely, isoflux-isoflux, isoflux-isothermal, and isothermal-isothermal. The flow reversal regions are given in graphical form in Figure 12.16.

The expression of the Nusselt number for the isoflux-isoflux case is somewhat complicated, but the equations for the other two cases are relatively simple. For the isoflux-isothermal boundary condition,

$$\text{Nu}_1 = \frac{720(\text{Re}/\text{Gr})}{360(\text{Re}/\text{Gr}) - Q_1} \tag{12.20a}$$

and

$$\text{Nu}_2 = \frac{720(\text{Re}/\text{Gr})}{360(\text{Re}/\text{Gr}) + Q_1} \tag{12.20b}$$

where $Q_1 = q_1 b[k(T_2 - T_0)]$ and T_0 is the ambient temperature. Equations 12.20*a* and *b* are valid only for cases where $Q_1 \neq 0$. For $Q_1 = 0$, the Nusselt numbers at wall 1 and wall 2 become

SEC et al. v. MRI
SEC Exhibit 1018.0125
IPR2023-00254

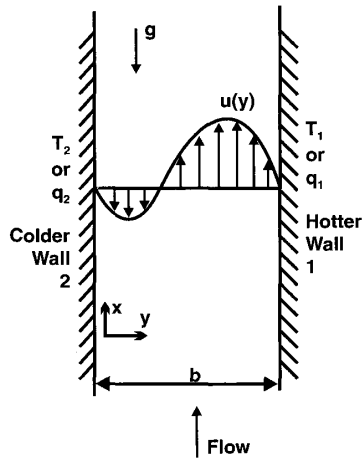

FIGURE 12.15 Flow reversal of buoyancy-assisted flow in vertical plates.

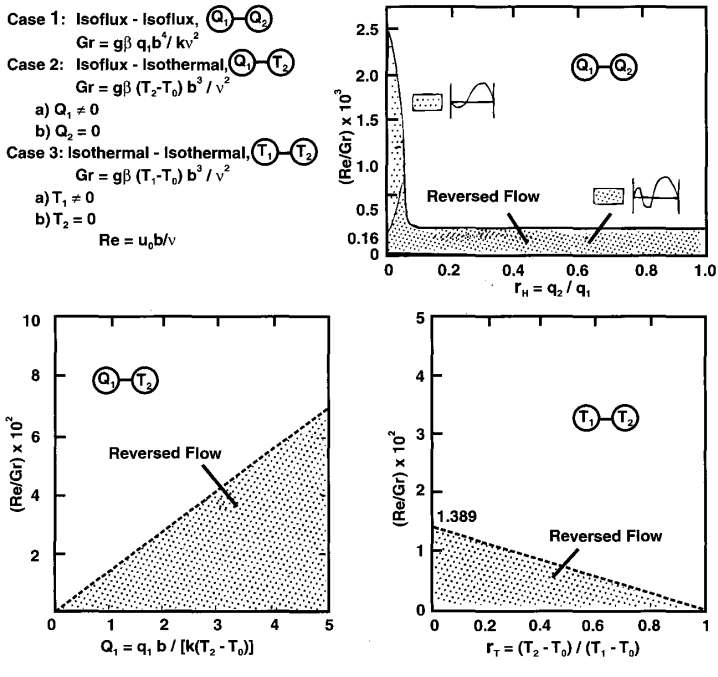

FIGURE 12.16 Reversed-flow zone in buoyancy-assisted flow.

SEC et al. v. MRI
SEC Exhibit 1018.0126
IPR2023-00254

Table 12.2 Nusselt Numbers for Isoflux-Isoflux

$r_H = q_2/q_1$

	0		0.4		0.5		0.6		1.0	
Re/Gr	Nu_1	Nu_2	Nu_1	Nu_2	Nu_1	Nu_2	Nu_1	Nu_2	Nu_1	Nu_2
0.001	5.312	0	5.319	9.026	5.403	7.371	5.506	6.695	6.081	6.081
0.01	3.176	0	3.534	13.984	3.644	7.746	3.764	6.034	4.353	4.353
0.1	2.745	0	3.172	19.078	3.300	8.611	3.440	6.315	4.141	4.141
1.0	2.698	0	3.130	19.903	3.260	8.736	3.402	6.359	4.120	4.120
∞*	2.692	0	3.125	20.000	3.256	8.750	3.398	6.364	4.118	4.118

*Approach to pure forced convection.

$$Nu_1 = 0 \tag{12.21a}$$

and

$$Nu_2 = 2.43 \tag{12.21b}$$

For the isothermal-isothermal boundary condition with $T_1 \neq T_2$,

$$Nu_1 = \frac{720(Re/Gr)}{360(Re/Gr) + r_T - 1} \tag{12.22a}$$

and

$$Nu_2 = \frac{720(Re/Gr)}{360(Re/Gr) - r_T + 1} \tag{12.22b}$$

where $r_T = (T_2 - T_0)/(T_1 - T_0)$. For symmetric heating ($T_1 = T_2$),

$$Nu_1 = Nu_2 = 3.77 \tag{12.23}$$

Nusselt numbers for the isoflux-isoflux case are given in Table 12.2.

It should be noted that the Nusselt and Reynolds numbers are based on the spacing between two plates, which is one-half of the hydraulic diameter. Figure 12.16 reveals that there are two possible patterns of reversed-flow velocity profile for the isoflux-isoflux boundary condition. For the other two cases, only the single-peak pattern with a negative-velocity area adjacent to the colder wall could be found.

12.5.2 Buoyancy-Resisted Flow

Buoyancy-resisted (or opposed) flow refers to forced flow in the direction opposite to the buoyancy—e.g., the flow resulting when an upflow is cooled or a

SEC et al. v. MRI
SEC Exhibit 1018.0127
IPR2023-00254

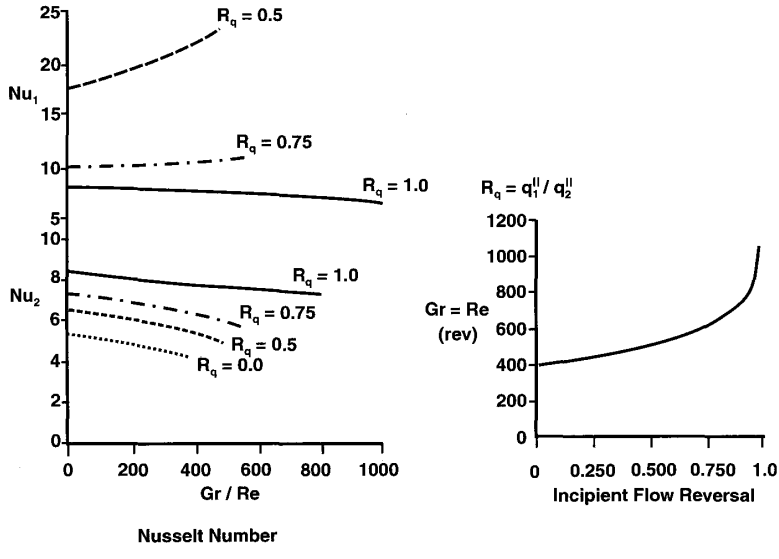

FIGURE 12.17 Nusselt numbers and flow reversal for isoflux-isoflux.

downflow is heated. Hamadah and Wirtz [22] obtained closed-form solutions for the fully developed flow with the following boundary conditions:

1. Both walls isothermal, with the right wall ($Y = 1$) at T_2 and the left wall ($Y = 0$) at T_1 where $T_2 > T_1$
2. Both walls isoflux, with the right wall at $(q_2)''$ and the left wall at $(q_1)''$ where $(q_2)'' > (q_1)''$
3. Isoflux-isothermal, with the right wall at $(q_2)''$ and the left wall at $T_1 = T_0$ (the fluid inlet temperature)

For case 2, the flow reversal and the Nusselt number are given in Figure 12.17. On the other hand, simple equations are available for the other two cases:

Case 1: *Isothermal-isothermal*

$$\mathrm{Nu}_1 = \frac{4}{1 - \mathrm{Gr}(1 - R_T)/(1440\,\mathrm{Re})} \qquad R_T < 1 \tag{12.24a}$$

$$\mathrm{Nu}_2 = \frac{4}{1 + \mathrm{Gr}(1 - R_T)/(1440\,\mathrm{Re})} \qquad R_T < 1 \tag{12.24b}$$

SEC et al. v. MRI
SEC Exhibit 1018.0128
IPR2023-00254

and the flow reversal occurs for

$$\frac{\text{Gr}}{\text{Re}} > \frac{288}{1-R_T} \tag{12.25}$$

where the Nusselt, Reynolds, and Grashof numbers are based on the hydraulic diameter (= $2b$) and R_T is defined as $(T_1 - T_0)/(T_2 - T_0)$.

Case 3: *Isoflux-isothermal*

$$\text{Nu}_1 = \frac{4}{1-\text{Gr}/(2880\,\text{Re})} \tag{12.26a}$$

$$\text{Nu}_2 = \frac{4}{1+\text{Gr}/(2880\,\text{Re})} \tag{12.26b}$$

and the flow reversal occurs for

$$\frac{\text{Gr}}{\text{Re}} > 576 \tag{12.27}$$

It should be noted that the heat transfer coefficients or Nusselt numbers in Equations 12.20 through 12.26 for both buoyancy-assisted and buoyancy-opposed flow are reduced to the values for fully developed forced convection if Gr/Re is zero.

REFERENCES

1. W. Elenbaas, "Heat Dissipation of Parallel Plates by Convection," *Physica* 9(1), 1942.
2. E. M. Sparrow and P. A. Bahrami, "Experiments on Natural Convection from Vertical Parallel Plates with Either Open or Closed Edges," *J. Heat Transfer* 102, 1980.
3. E. K. Levy, "Optimum Plate Spacing for Laminar Natural Convection from Vertical Isothermal Flat Plates," *J. Heat Transfer* 93, 1971.
4. A. Bar-Cohen and W. M. Rohsenow, "Thermally Optimum Spacing of Vertical, Natural Convection Cooled Parallel Plates," *J. Heat Transfer* 106, 1984.
5. E. M. Sparrow and C. Prakash, "Enhancement of Natural Convection Heat Transfer by a Staggered Array of Discrete Vertical Plates," *J. Heat Transfer* 102, 1980.
6. E. M. Sparrow and C. Prakash, "Natural Convection Heat Transfer Performance Evaluation for Discrete- (In-Line or Staggered) and Continuous-Plate Arrays, *Numerical Heat Transfer* 3, 1980.
7. T. Aibara, "Natural Convective Heat Transfer in Vertical Parallel Fins of Rectangular Profiles," *Jap. Soc. Mech. Eng.* 34, 1968.

SEC et al. v. MRI
SEC Exhibit 1018.0129
IPR2023-00254

8. K. E. Starner and H. N. McManus, "An Experimental Investigation of Free Convection Heat Transfer from Rectangular Fin Arrays," *J. Heat Transfer* 85, 1963.
9. J. R. Welling and C. B. Wooldridge, "Free Convection Heat Transfer Coefficients from Rectangular Vertical Fins," *J. Heat Transfer* 87, 1965.
10. K. Izume and H. Nakamura, "Heat Transfer by Convection on the Heated Surface with Parallel Fins," *Jap. Soc. Mech. Eng.* 34, 1968.
11. D. W. Van De Pol and J. K. Tierney, "Free Convection Nusselt Number for Vertical U-Shaped Channels," *J. Heat Transfer* 95, 1973.
12. S. N. Rea and S. E. West, "Thermal Radiation from Finned Heat Sinks," *IEEE Trans. Parts, Hybrids, and Packaging* PHP-12(2), 1976.
13. F. Harahap and H. N. McManus Jr., "Natural Convection Heat Transfer from Horizontal Rectangular Fin Arrays," *J. Heat Transfer* 89, 1967.
14. E. M. Sparrow and S. B. Vemuri, "Natural Convection/Radiation Heat Transfer from Highly Populated Pin Fin Arrays," *J. Heat Transfer* 107, 1985.
15. E. M. Sparrow and S. B. Vemuri, "Orientation Effects on Natural Convection/Radiation Heat Transfer from Pin Fin Arrays," *Int. J. Heat and Mass Transfer* 29, 1986.
16. M. E. Alessio and D. A. Kaminski, "Natural Convection and Radiation Heat Transfer from an Array of Inclined Pin Fins," *J. Heat Transfer* 111, 1989.
17. M. Taylor, "Experimental Comparison of Pin Fin Configurations for Extended Surface Heat Transfer in Space Applications," *Proc. 4th Int. Electronics Packaging Conf.*, 1984.
18. R. O. Warrington, S. Smith, R. E. Powe, and R. L. Mussulman, "Boundary Effects on Natural Convection Heat Transfer for Cylinders and Cubes," *Heat Transfer in Enclosures, ASME HTD-39*, 1984.
19. R. O. Warrington and R. E. Powe, "The Transfer of Heat by Natural Convection between Bodies and Their Enclosures," *Int. J. Heat and Mass Transfer* 28, 1985.
20. R. O. Warrington, R. E. Powe, and R. L. Mussulman, "Steady Conduction in Three Dimensional Shells," *J. Heat Transfer* 104, 1982.
21. C. H. Cheng, H. S. Kou, and W. H. Huang, "Flow Reversal and Heat Transfer of Fully Developed Mixed Convection in Vertical Channels," *J. Thermophysics* 4(3), 1990.
22. T. T. Hamadah and R. A. Wirtz, "Analysis of Laminar Fully Developed Mixed Convection in a Vertical Channel with Opposing Buoyancy," *J. Heat Transfer* 113, 1991.

SEC et al. v. MRI
SEC Exhibit 1018.0130
IPR2023-00254

Chapter 13

HEAT EXCHANGERS AND COLD PLATES

A heat exchanger is a device that is used to transfer thermal energy from one fluid to another. The process involves two fluids. On the other hand, a cold plate involves only one fluid that is used to cool (or heat) a system. The general analysis and design principles for a cold plate are identical to those for a heat exchanger. Therefore, all discussion in this chapter will be confined to heat exchangers. Heat exchangers are normally used to cool the circulating fluid in electronic equipment.

13.1 COMPACT HEAT EXCHANGERS

The term *compact heat exchanger (CHE)* does not necessarily imply small bulk and weight but instead refers to a heat exchanger with a high ratio of heat transfer surface area to volume. Typically, the ratio of heat transfer surface area to volume (or area density) for a compact heat exchanger is greater than 213 ft^2/ft^3 (or 700 m^2/m^3).

As compared with shell-and-tube heat exchangers, the distinguishing characteristics of compact heat exchangers are as follows:

1. They are very flexible, and it is easy to apply different area densities on the hot and cold sides separately as desired.
2. Fluids must be clean and relatively noncorrosive because of small flow passages used to achieve high surface area density, and one of the fluids is typically a gas.
3. Operating pressure and temperature are limited because of construction features of brazing joints.
4. The fluid pumping power (i.e., pressure drop) is often of equal importance to the heat transfer rate.
5. The header design of a compact heat exchanger is much more difficult and is also important for uniform flow distribution.

Compact heat exchanger design generally employs one of three fluid technologies: (1) gas to gas, (2) gas to liquid, and (3) gas to condensing or evaporating fluid.

SEC et al. v. MRI
SEC Exhibit 1018.0131
IPR2023-00254

The reader should refer to Kays and London [1] for an in-depth discussion and additional information about compact heat exchangers. This source also contains much experimental data on heat transfer and friction factor for various types of fin.

13.2 FLOW ARRANGEMENT OF HEAT EXCHANGERS

Generally, a heat exchanger is configured in one of the following flow arrangements:

1. *Parallel-flow heat exchanger.* Both fluids flow in the same direction. The final temperature of the colder fluid can never reach the exit temperature of the hot fluid.
2. *Counterflow heat exchanger.* Two fluids flow in opposite directions. The exit temperature of the colder fluid may exceed the outlet temperature of the hot fluid.
3. *Crossflow heat exchanger.* The flow directions are normal to each other. This is the most common flow arrangement in compact heat exchangers.

In any heat exchanger, the fluids in the two streams (hot and cold streams) can be either fully mixed or unmixed.

13.3 OVERALL HEAT TRANSFER COEFFICIENT

When heat is transferred from one fluid to another through the separating wall of a heat exchanger, heat transfer occurs through conduction across the wall thickness and convection from both solid surfaces to fluids. The heat transfer rate can be expressed by the following equation:

$$q = U\eta_o A(T_h - T_c) \tag{13.1}$$

where U is the overall heat transfer coefficient; A is the heat transfer surface area; T_h and T_c are temperatures for hot and cold fluids, respectively; and η_o is the surface efficiency, defined as follows:

$$\eta_o = 1 - \frac{A_f}{A}(1 - \eta_f) \tag{13.2}$$

where A is the total surface area and A_f and η_f are the surface area and efficiency of the fins under consideration. For a rectangular fin, η_f is approximately equal to $(\tanh ml)/ml$, where the parameter m is $(2h/k\delta)^{0.5}$ and δ and l are fin thickness and height, respectively. (See Chapter 8 for details.)

Various fin configurations result in different surface areas and efficiencies for the hot and cold sides of the heat exchanger; therefore, the overall heat transfer coefficient can be written based either on the hot side or on the cold side as follows. For the hot side,

SEC et al. v. MRI
SEC Exhibit 1018.0132
IPR2023-00254

Table 13.1 Fouling Factors for Some Fluids

Fluids	F, hr·ft²·°F/Btu
Seawater below 125°F	0.0005
Seawater above 125°F	0.001
Treated boiler feedwater above 125°F	0.001
Fuel oil	0.005
Quenching oil	0.004
Alcohol	0.0005
Steam	0.0005
Industrial air	0.002
Refrigerating liquid	0.001

$$U_h = \frac{1}{\dfrac{1}{\eta_{o,h} h_h} + \dfrac{a}{A_w/A_h} + \dfrac{1}{\eta_{o,c}(A_c/A_h)h_c} + F} \tag{13.3a}$$

and for the cold side,

$$U_c = \frac{1}{\dfrac{1}{\eta_{o,c} h_c} + \dfrac{a}{A_w/A_c} + \dfrac{1}{\eta_{o,h}(A_h/A_c)h_h} + F} \tag{13.3b}$$

where a is the thickness of the plate separating the hot and cold fluids; the subscripts h and c represent the hot and cold fluids, respectively; A_w, A_h, and A_c are the heat transfer areas of the separating plate for conduction and of the finned surface areas for convection on the hot and cold sides of the heat exchanger, respectively; and F is the fouling factor (or resistance), defined as

$$F = \frac{1}{U_{\text{dirty}}} - \frac{1}{U_{\text{clean}}} \tag{13.4}$$

The fouling factor represents the degree to which the heat transfer surfaces are corroded or coated with various deposits after some period of operation. The deposits on the surface create an additional thermal resistance. The average values of the fouling factors for some fluids are listed in Table 13.1 [2].

13.4 HEAT EXCHANGER EFFECTIVENESS

Heat exchanger effectiveness is defined as the ratio of the actual heat transfer rate to the maximum possible heat transfer rate under the second law of thermodynamics:

$$\varepsilon = \frac{q}{q_{\max}} \tag{13.5}$$

SEC et al. v. MRI
SEC Exhibit 1018.0133
IPR2023-00254

where

$$q = (mc_p)_h(T_{h,i} - T_{h,o}) = C_h(T_{h,i} - T_{h,o}) \quad (13.6a)$$
$$= (mc_p)_c(T_{c,o} - T_{c,i}) = C_c(T_{c,o} - T_{c,i}) \quad (13.6b)$$

C_h and C_c are heat capacities for the hot and cold sides, respectively. q_{max} occurs in a counterflow heat exchanger with an infinite heat transfer area. In other words, if there is no external loss, the outlet temperature of the cold fluid equals the inlet temperature of the hot fluid when $C_c < C_h$. On the other hand, the temperature at the exit of the hot fluid is equal to the inlet temperature of the cold fluid when $C_h < C_c$. Thus,

$$q_{max} = C_{min}(T_{h,i} - T_{c,i}) \quad (13.6c)$$

where C_{min} is the minimum value of C_h and C_c.

Combining Equations 13.5 and 13.6, one obtains

$$\varepsilon = \frac{C_h(T_{h,i} - T_{h,o})}{C_{min}(T_{h,i} - T_{c,i})} \quad (13.7a)$$
$$= \frac{C_c(T_{c,o} - T_{c,i})}{C_{min}(T_{h,i} - T_{c,i})} \quad (13.7b)$$

The effectiveness ε is typically expressed by tabular or graphical values as a function of the following parameters:

$$\varepsilon = \varepsilon\left\{\text{NTU}, \frac{C_{min}}{C_{max}}, \text{flow arrangement}\right\} \quad (13.8)$$

where NTU is the number of heat transfer units and is defined as AU/C_{min}. As described previously, the flow arrangement in a heat exchanger may be parallel flow, counterflow, or crossflow.

13.5 HEAT EXCHANGER ANALYSIS

Thermal analysis of a heat exchanger can be performed by either using the logarithmic mean temperature difference (LMTD) method or employing the heat exchanger effectiveness (ε-NTU) method. The former requires that the inlet and exit conditions of both fluids be specified. This approach is widely employed in the design of heat exchangers to given specifications. On the other hand, in many cases, the performance of a heat exchanger (i.e., U) is known, or can at least be estimated, but the fluid exit temperatures are unknown. This type of problem is often encountered in the selection of a heat exchanger or when the heat exchanger is tested at one flow rate while service conditions require different flow rates.

SEC et al. v. MRI
SEC Exhibit 1018.0134
IPR2023-00254

The detailed derivations of both methods are available in References 1 through 4 and will not be repeated here. The heat transfer rate of a heat exchanger found by the LMTD method is

$$q = UA\,\Delta T_m \tag{13.9}$$

where

$$\Delta T_m = \frac{\Delta T_a - \Delta T_b}{\ln(\Delta T_a/\Delta T_b)}$$

The subscripts a and b refer to the respective ends of the heat exchanger.

As indicated previously, the effectiveness depends on the flow arrangement. For a parallel-flow system, the effectiveness is

$$\varepsilon = \frac{1 - e^{-\text{NTU}(1+R)}}{1+R} \tag{13.10}$$

where R is the capacity ratio $C_{\min}/C_{\max}$.

Figure 13.1 shows the effectiveness as a function of NTU and of the capacity ratio for both parallel-flow and counterflow systems. The most common and most effective flow arrangement for a heat exchanger is the counterflow system, and its effectiveness is

$$\varepsilon = \frac{1 - e^{-\text{NTU}(1-R)}}{1 - Re^{-\text{NTU}(1-R)}} \tag{13.11}$$

Equation 13.11 can be reduced to two special cases where R is equal to 0 and 1, respectively. When an exchanger serves as a condenser or boiler, the fluid temperature on the side where the boiling or condensation takes place is nearly constant. This case implies that the flow rate in the condenser or boiler is very large as compared with the fluid on the other side of the heat exchanger. In other words, R approaches zero because $C_{\max} >> C_{\min}$. Under this condition, Equation 13.11 becomes

$$\varepsilon = 1 - e^{-\text{NTU}} \tag{13.12a}$$

On the other hand, Equation 13.11 is reduced to the following expression when $R = 1$:

$$\varepsilon = \frac{\text{NTU}}{1+\text{NTU}} \tag{13.12b}$$

This case frequently occurs in the regenerative process of the thermodynamics cycle where the same flow rate is used. From Equations 13.11 and 13.12*a* and *b*, the effectiveness of a counterflow heat exchanger reaches 1 when NTU approaches infinity.

SEC et al. v. MRI
SEC Exhibit 1018.0135
IPR2023-00254

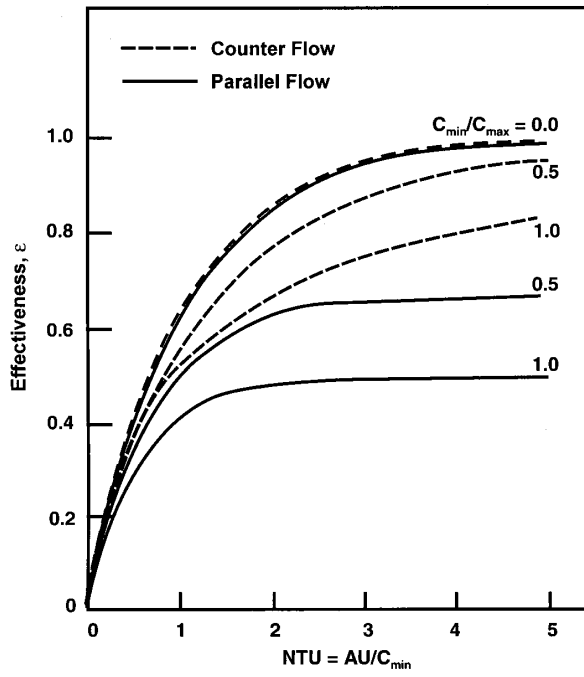

FIGURE 13.1 Effectiveness of parallel- and counterflow heat exchangers.

The effectiveness of a crossflow exchanger with the two fluids unmixed is available in References 4 and 5 and is expressed by the following equation:

$$\varepsilon = \frac{\sum_{n=0}^{\infty}\left[1-e^{-\mathrm{NTU}}\sum_{m=0}^{n}\frac{(\mathrm{NTU})^m}{m!}\right]\left[1-e^{-R\times\mathrm{NTU}}\sum_{m=0}^{n}\frac{(R\times\mathrm{NTU})^m}{m!}\right]}{R\times\mathrm{NTU}} \tag{13.13}$$

This equation reduces to Equation 13.12*a* for $R = 0$.

The greatest difference in performance among various flow systems occurs when the heat capacity ratio is equal to 1, i.e., when $C_{min}/C_{max} = 1$. A comparison of various flow arrangements' effectiveness under this condition is given in Figure 13.2.

13.6 HEAT TRANSFER AND PRESSURE DROP

The heat transfer coefficient is typically expressed by a Colburn-type correlation, i.e.,

SEC et al. v. MRI
SEC Exhibit 1018.0136
IPR2023-00254

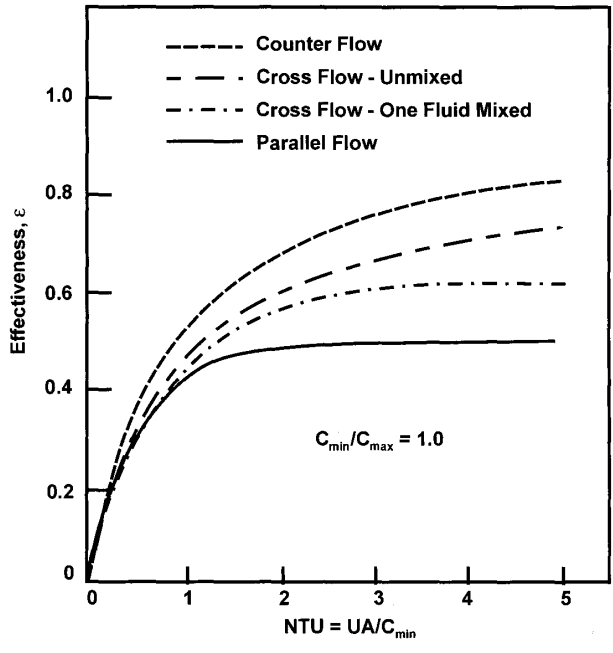

FIGURE 13.2 Effectiveness of various flow arrangements at $C_{min}/C_{max} = 1$.

$$\mathrm{St} = C\,\mathrm{Re}^{m}\,\mathrm{Pr}^{n} \tag{13.14}$$

where C is a constant and the dimensionless variables are defined as follows:

$$\mathrm{St} = \text{Stanton number} = \frac{h}{Gc_p}$$

$$\mathrm{Re} = \text{Reynolds number} = \frac{D_h G}{\mu}$$

$$\mathrm{Pr} = \text{Prandtl number} = \frac{c_p \mu}{k}$$

where D_h is the hydraulic diameter and G is the mass velocity. All properties should be evaluated at the average fluid temperature of each stream (hot and cold fluids, respectively).

Data are provided in Kays and London [1] for various types of fins in the form of the Colburn factor ($j = \mathrm{St}\,\mathrm{Pr}^{2/3}$) versus the Reynolds numbers. The values of the

SEC et al. v. MRI
SEC Exhibit 1018.0137
IPR2023-00254

friction factor are included in the database. The same reference also presents the following equation to calculate the pressure drop across a heat exchanger:

$$\Delta p = \frac{G}{2g_c\rho_1}\left[\underbrace{(K_c+1-\sigma^2)}_{\substack{\text{entrance}\\\text{effect}}}+\underbrace{2\left(\frac{\rho_1}{\rho_2}-1\right)}_{\substack{\text{flow}\\\text{acceleration}}}+\underbrace{f\frac{\rho_1}{\rho_m}\frac{A}{A_c}}_{\substack{\text{core}\\\text{friction}}}-\underbrace{(1-\sigma^2-K_e)\frac{\rho_1}{\rho_2}}_{\substack{\text{exit}\\\text{effect}}}\right] \tag{13.15}$$

where

A = total heat transfer area on one side
A_c = minimum free flow area on one side
$\frac{A}{A_c} = \frac{L}{r_h}$
f = friction factor
K_c = contraction loss coefficient
K_e = expansion loss coefficient
L = flow length
r_h = hydraulic radius = $\frac{1}{4}$ hydraulic diameter D_h
ρ_m = mean density between "1" (inlet) and "2" (exit)
$= \frac{1}{A}\int \rho\, dA \approx \frac{\rho_1+\rho_2}{2}$
σ = ratio of free flow area to frontal area

Generally, in the design of liquid-to-liquid heat exchangers, accurate knowledge of friction characteristics of the heat transfer surface is relatively unimportant because of the low power requirement for pumping high-density liquids (the ratio of pressure drop to heat transfer is low). On the other hand, the low gas density causes the friction power per unit mass flow rate to be relatively large in the case of gases.

13.7 GEOMETRIC FACTORS

Each heat exchanger includes two sides (fluids). Referring to Figure 13.3, the following relationships between geometric factors can be established.

Height:	$H = n_1(b_1 + a) + n_2(b_2 + a) + a$	(13.16*a*)
Volume:	$V = HWD$	(13.16*b*)
Frontal areas:	$A_{fr,1} = HW$ and $A_{fr,2} = HD$	(13.16*c*)
Free flow areas:	$A_{c,j} = \sigma_j A_{fr,j}$ $j = 1$ or 2	(13.16*d*)
Surface per unit volume:	$\alpha_j = \frac{b_j\beta_j}{b_1+b_2+2a}$ $j = 1$ or 2	(13.16*e*)
Heat transfer area:	$A_j = \alpha_j V$ $j = 1$ or 2	(13.16*f*)

SEC et al. v. MRI
SEC Exhibit 1018.0138
IPR2023-00254

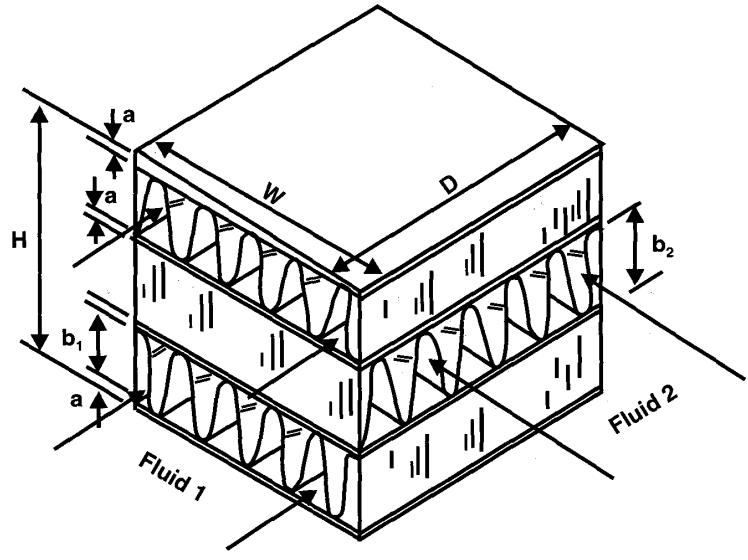

FIGURE 13.3 Sketch of a heat exchanger.

where

n_j = number of layers on side j $\quad j = 1$ or 2
a = separation plate thickness
b_j = spacing between plates on side j $\quad j = 1$ or 2
σ_j = ratio of free flow area to frontal area
$= \alpha_j r_{h,j}$
β_j = ratio of total surface area on one side to volume between plates of that side

The values of b, D_h, β, A_f/A, and δ (fin thickness) for several types of fin are presented in Reference 1.

13.8 COLD-PLATE ANALYSIS

A finned cold plate as shown in Figure 13.4 cools electronic components. In this case, the coolant can be gases or liquids, depending on the heat load and other requirements. The following is a step-by-step analysis approach:

SEC et al. v. MRI
SEC Exhibit 1018.0139
IPR2023-00254

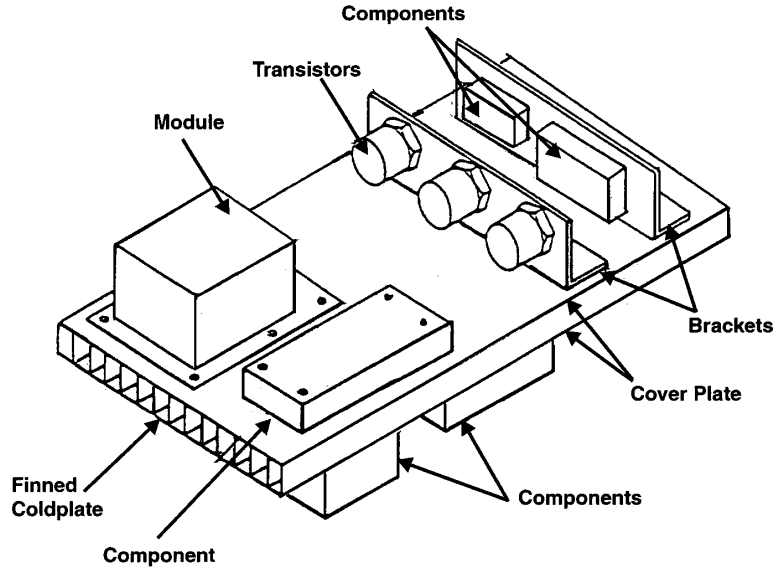

FIGURE 13.4 Electronics on a finned cold plate.

1. Coolant temperature rise ΔT_c:

$$\Delta T_c = \frac{q_e}{mc_p} \tag{13.17a}$$

where

q_e = total heat load
m = mass flow rate (either known or assumed initially)
c_p = specific heat of coolant

2. Average coolant temperature $(T_f)_{\text{ave}}$:

$$(T_f)_{\text{ave}} = T_{\text{in}} + \frac{\Delta T_c}{2} \tag{13.17b}$$

All fluid properties are evaluated at this temperature.

SEC et al. v. MRI
SEC Exhibit 1018.0140
IPR2023-00254

3. Convection temperature rise ΔT_f:

$$\Delta T_f = \frac{q_e}{hA\eta_o} \tag{13.17c}$$

The group of terms $hA\eta_o$ is often referred to as the *cold-plate conductance*. Each value is determined as described in the following paragraphs:

a. Frontal area of the cold plate:

$$A_{\text{fr}} = WH \tag{13.18a}$$

where

W = width of cold plate
H = height of cold plate

b. Free flow area:

$$A_c = A_{\text{fr}} - A_{\text{fin}} - A_w \tag{13.18b}$$

where

$A_{fin} = N_f H\delta$
N_f = number of fins
δ = fin thickness

A_c can also be determined from Equation 13.16*d* if the surface geometry of the fin is known (from Reference 1 for several types of fin stock). A_w is the cross-sectional area due to the wall thickness. This item is required when the wall thickness is included in Equation 13.18*a*.

c. Mass velocity:

$$G = \frac{m}{A_c} \tag{13.18c}$$

d. Hydraulic diameter:

$$D_h = 4r_h$$

The hydraulic diameter varies with the type of fin. This value is frequently provided in Reference 1; however, the hydraulic diameter can also be determined as follows:

$$D_h = \frac{2sH}{H+s} \tag{13.18d}$$

where s is the spacing between fins.

SEC et al. v. MRI
SEC Exhibit 1018.0141
IPR2023-00254

e. Reynolds number Re and Prandtl number Pr:

$$\mathrm{Re} = \frac{GD_h}{\mu}$$

and

$$\mathrm{Pr} = \frac{\mu c_p}{k}$$

The Prandtl number can also be found from the material property table or chart.

f. Heat transfer coefficient h. For a given Re, the value of the group $(h/Gc_p)\,\mathrm{Pr}^{2/3}$ can be found from Reference 1 or other sources for various types of fins; therefore, the heat transfer coefficient can be readily determined.

g. Fin and surface efficiency η_f and η_o. Once the heat transfer coefficient is known, the fin efficiency η_f can easily be calculated according to the equations described in the previous sections or Chapter 8. In calculating the efficiency, the fin length l should be set equal to the fin height for one side heating and to half the fin height for both sides heating.

The ratio of the fin area to the total heat transfer area (A_f/A) is constant for each fin configuration and is given in Reference 1; however, both areas can also be calculated. In addition, the ratio of the total heat transfer area to the volume of cold plate (β) is also provided in the same reference. Therefore, A and η_o can be calculated immediately. Consequently, the cold-plate conductance $hA\eta_o$ is known.

4. Cold-plate temperature T_c. The exit coolant temperature is

$$T_{\mathrm{out}} = T_{\mathrm{in}} + \Delta T_c \tag{13.18e}$$

and the cold-plate temperature is

$$T_c = T_f + \Delta T_f \tag{13.18f}$$

T_f is the local fluid temperature and is equal to T_{out} at the exit. For the uniformly heating case, the maximum cold-plate temperature occurs at the exit of the cold plate. To compute the actual (local) cold-plate temperature, heat conduction spreading must be included, and this often leads to a fully three-dimensional problem. In most cases, the calculated heat transfer coefficient and the surface efficiency are used as input to a thermal analyzer, which solves the temperature at various locations of the cold plate as well as electronic components.

5. Pressure drop Δp. Equation 13.15 can be used to compute the cold-plate pressure drop. K_c and K_e are functions of σ and are given in Reference 1. The friction factor f depends on the Reynolds number and is also available in the same reference.

SEC et al. v. MRI
SEC Exhibit 1018.0142
IPR2023-00254

At this point, the cold-plate temperature and the pressure drop are known. Additional iterations are usually required to design a cold plate that meets the performance requirements. For example, the following steps may be taken if the pressure drop is too high:

1. Increasing the minimum free flow area by increasing the width and/or height.
2. Reducing the flow path length. However, this also decreases the heat transfer area and thus reduces the cold-plate conductance. The better way, if possible, is to increase the width and/or height of the cold plate, and at the same time to reduce the length of the cold plate.
3. Using different types of fins which give a lower friction factor at the same mass flow rate.

On the other hand, if the calculated cold-plate conductance is too low, the possible improvements are as follows:

1. Increasing the fin thickness. This approach leads to an increase in fin (and surface) efficiency. In addition, the heat transfer coefficient is also increased due to a reduction in the free flow area.
2. Increasing the fin density. This method results in an increase of the heat transfer coefficient and surface area.
3. Replacing the straight fin with a wavy or interrupted fin. Wavy surfaces create a high heat transfer coefficient by interrupting the boundary-layer development on the fin.

Generally, the methods for increasing heat transfer also increase pressure drop. A good design provides a good balance between the heat transfer performance and pressure drop.

13.9 CORRELATIONS

Empirical data on heat transfer and friction factor in graphical form for various types of fins are included in Kays and London [1]. Wieting [6] provided the following empirical correlations of experimental heat transfer and flow friction data for rectangular offset plate fins:

For laminar flow ($Re \leq 1000$):

$$f = 7.661\left(\frac{x}{D_h}\right)^{-0.384} \alpha^{-0.092}\,\mathrm{Re}^{-0.712} \tag{13.19a}$$

$$j = 0.483\left(\frac{x}{D_h}\right)^{-0.162} \alpha^{-0.184}\,\mathrm{Re}^{-0.536} \tag{13.19b}$$

SEC et al. v. MRI
SEC Exhibit 1018.0143
IPR2023-00254

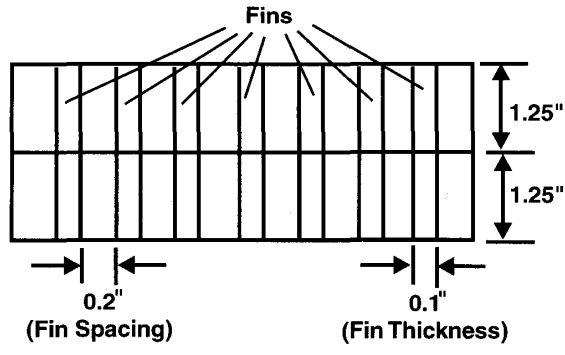

FIGURE 13.5 Cross-sectional view of the heat exchanger of Example 13.1.

For turbulent flow (Re ≥ 2000):

$$f = 1.136\left(\frac{x}{D_h}\right)^{-0.781}\left(\frac{t}{D_h}\right)^{-0.534}\mathrm{Re}^{-0.198} \tag{13.20a}$$

$$j = 0.242\left(\frac{x}{D_h}\right)^{-0.322}\left(\frac{t}{D_h}\right)^{-0.089}\mathrm{Re}^{-0.368} \tag{13.20b}$$

where

x = individual fin length in flow direction ≈ 0.125 in
α = aspect ratio $= \dfrac{w}{p}$
w = subchannel width
p = subchannel height
t = fin thickness

It should be noted that the empirical data listed in References 1 and 6 are limited to the case with air as the working fluid and they should not be used for liquid systems.

Example 13.1

The heat load for a counterflow air-to-air heat exchanger as shown in Figure 13.5 is 200 W. For simplicity, the same flow rate and fin configuration are assumed for both hot and cold sides. The fin thickness and height are 0.1 in and 1.25 in, respectively. The spacing between fins is 0.2 in, and there are 31 fins on each side. The depth (flow length) of the heat exchanger is 13 in. The flow rate is 400 lb_m/hr,

SEC et al. v. MRI
SEC Exhibit 1018.0144
IPR2023-00254

and the inlet temperature to the cold side is 120°F. Determine the exit temperatures for the hot and cold sides of the heat exchanger.

Solution

The thick fins basically subdivide each side of the heat exchanger into many (32) subchannels. One may assume that the flow to subchannels is uniform.

$$C_{max} = C_{min} = 400 \times 0.24 = 96 \text{ Btu/(hr·°F)}$$

Cold Side

Fluid temperature rise:

$$\Delta T_c = 200 \times \frac{3.414}{96} = 7.1°\text{F}$$

Fluid outlet temperature:

$$T_{c,o} = 120 + 7.1 = 127.1°\text{F}$$

Hydraulic diameter (subchannel):

$$D_h = \frac{2 \times 0.2 \times 1.25}{0.2 + 1.25} = 0.345 \text{ in} = 0.0287 \text{ ft}$$

Width:

$$W = 0.2 \times (31 + 1) + 31 \times 0.1 = 9.5 \text{ in}$$

Frontal area:

$$A_{fr} = 9.5 \times \frac{1.25}{144} = 0.0825 \text{ ft}^2$$

Free flow area:

$$A_c = (31+1) \times 0.2 \times \frac{1.25}{144} = 0.0556 \text{ ft}^2$$
$$\sigma = \frac{A_c}{A_{fr}} = \frac{0.0556}{0.0825} = 0.673$$
$$\sigma^2 = 0.453$$

Mass velocity:

$$G = \frac{400}{0.0556} = 7194 \text{ lb}_m/(\text{hr} \cdot \text{ft}^2)$$

SEC et al. v. MRI
SEC Exhibit 1018.0145
IPR2023-00254

Average fluid temperature:

$$T_f = \frac{120+127.1}{2} = 123.6°\text{F}$$

Fluid:

$\rho = 0.0695\ \text{lb}_\text{m}/\text{ft}^3$ $\mu = 0.0478\ \text{lb}_\text{m}/(\text{ft}\cdot\text{hr})$
$k = 0.0159\ \text{Btu}/(\text{hr}\cdot\text{ft}\cdot°\text{F})$ $\text{Pr} = 0.715$

Reynolds number:

$$\text{Re} = \frac{7194\times 0.0287}{0.0478}$$
$$= 4320 > 2300 \quad \text{(turbulent flow)}$$
$K_c = 0.37$ $K_e = 0$ (from Kays and London [1])

Nusselt number: (Index 6 of Table H.2 in Appendix H)

$$\text{Nu} = 5 + 0.012\ \text{Re}^{0.83}(\text{Pr} + 0.29) = 17.55$$

Heat transfer coefficient:

$$h = \frac{17.55\times 0.0159}{0.0287} = 9.72\ \text{Btu}/(\text{hr}\cdot\text{ft}^2\cdot°\text{F})$$

Friction factor:

$$f = 0.079\ \text{Re}^{-0.25} = 0.00974$$

Fin efficiency [assuming $k_{\text{fin}} = 100$ Btu/(hr·ft·°F) for Aluminum]:

$$ml = \left(\frac{2h}{\delta k_{\text{fin}}}\right)^{0.5} l$$
$$= \left(\frac{2\times 9.72}{0.1\times 100/12}\right)^{0.5}\frac{1.25}{12}$$
$$= 0.5 \Rightarrow \eta_f = 0.92$$

Surface Areas:

$$A_f = 31\times\frac{2\times 1.25\times 13}{144} = 6.997\ \text{ft}^2$$

$$A = \left[0.2\times(31+1)+31\times 2\times 1.25\right]\times\frac{13}{144} = 7.574\ \text{ft}^2$$

SEC et al. v. MRI
SEC Exhibit 1018.0146
IPR2023-00254

Surface efficiency:

$$\eta_o = 1 - \frac{A_f}{A}(1 - \eta_f) = 0.93$$

Pressure drop using Equation 13.15:

$$\begin{aligned}\Delta p &= \frac{7194^2}{2 \times 0.0695 \times 4.17 \times 10^8} \\ &\quad \times \left[4 \times 0.00974 \left(\frac{13}{0.345} \right) + (0.37 + 1 - 0.453) - (1 - 0.453 - 0) \right] \\ &= 0.8929(1.468 + 0.917 - 0.547) = 1.641 \text{ lb}_\text{f}/\text{ft}^2 = 0.0114 \text{ lb}_\text{f}/\text{in}^2 \\ &= 0.316 \text{ in of water}\end{aligned}$$

Hot Side

In theory, we should repeat the above calculations for the hot side. Since we assume the same flow rate and fin configuration for both sides, we expect the same results if the effect due to the fluid properties (except for density related to pressure drop) is negligibly small.

NTU

Neglecting fouling factors and heat conduction across the thickness of the separating plate, we find from Equation 13.3*a* or *b*:

$$\frac{1}{U} = \frac{1}{0.93 \times 9.72} + \frac{1}{0.93 \times 9.72} \Rightarrow U = 4.52 \text{ Btu}/(\text{h} \cdot \text{ft}^2 \cdot {}^\circ\text{F})$$

$$\text{NTU} = \frac{AU}{C_{\min}} = 7.574 \times \frac{4.52}{96} = 0.357$$

Effectiveness ϵ

The effectiveness can generally be found from the charts in Kays and London[1]. For the present case, it can be computed from Equation 13.12*b* as follows:

$$\varepsilon = \frac{0.357}{1 + 0.357} = 0.263 = \frac{C_c(T_{c,o} - T_{c,i})}{C_{\min}(T_{h,i} - T_{c,i})}$$

$$T_{h,i} = 120 + \frac{7.1}{0.263} = 147.0 \text{ °F} \qquad \text{and} \qquad T_{h,o} = 147.0 - 7.1 = 139.9 \text{ °F}$$

For the present example, the pressure drop can approximately be related to the pressure drop of the cold side as follows:

$$(\Delta p)_h = \frac{\rho_c}{\rho_h}(\Delta p)_c = \frac{0.0695}{0.0671} \times 0.316 = 0.327 \text{ in of water}$$

SEC et al. v. MRI
SEC Exhibit 1018.0147
IPR2023-00254

REFERENCES

1. W. M. Kays and A. L. London, *Compact Heat Exchangers,* 2nd ed., McGraw-Hill, New York, 1955.
2. J. H. Seely and R. C. Chu, *Heat Transfer in Microelectronic Equipment: A Practical Guide,* Chapter IV, Marcel Dekker, New York, 1972.
3. F. Kreith, Chapter 11, *Principles of Heat Transfer,* 7th ed., International Textbook, Scranton, PA, 1963.
4. A. D. Kraus and A. Bar-Cohen, Chapter 10, *Thermal Analysis and Control of Electronic Equipment,* Hemisphere, Washington, DC, 1983.
5. J. L. Mason, "Heat Transfer in Cross Flow," *Proc. 2nd U.S. Natl. Congr. Applied Mechanics,* ASME, Ann Arbor, MI, 1955.
6. A. R. Wieting, "Empirical Correlations for Heat Transfer and Flow Friction Characteristics of Rectangular Offset-Fin Plate-Fin Heat Exchangers," *J. Heat Transfer,* August 1975.

SEC et al. v. MRI
SEC Exhibit 1018.0148
IPR2023-00254